A RATIONAL APPROACH TO DESIGN NOVEL INHIBITORS OF

Mycobacterium tuberculosis ISOCITRATE LYASES

A Thesis

by

VIET TRUC PHAM

Submitted to the Office of Graduate and Professional Studies of
Texas A&M University
in partial fulfillment of the requirements for the degree of

DOCTOR OF PHILOSOPHY

Chair of Committee,	Thomas D. Meek
Committee Members,	Dorothy E. Shippen
	Frank M. Raushel
	James C. Sacchettini
Head of Department,	Dorothy E. Shippen

May 2019

Major Subject: Biochemistry

ABSTRACT

Isocitrate lyase 1 & 2 are essential enzymes for *Mycobacterium tuberculosis* pathogenicity and antibiotic resistance, and thereby, are appealing targets for the treatment of latent tuberculosis. Since high-throughput screening campaigns were unsuccessful in identifying suitable inhibitors, these enzymes present an opportunistic venture for a rational approach. Understanding the catalytic mechanism would assist in new strategies for inhibiting the isocitrate lyases (ICLs). The retro-aldol catalytic cleavage and the nucleophilic active-site cysteine inspired an adaptation of isocitrate analogs as ICL mechanism-based inactivators. Finally, a mechanistic comprehension of ICL inhibition by known inactivators and substrate analogs imparts essential structural-activity features of potential inhibitors.

This disseration assembled kinetic data and mutagenesis studies to explain the catalytic mechanism of ICL in depth. Besides the recapitulation on discussion of *M. tuberculosis* ICL1 rate limiting step(s), Lys189 was identified as a potential catalytic base involving the first deprotonation step during isocitrate cleavage. Hence, Lys189, along with Cys191, comprises another susceptible nucleophilic active-site residue for development of novel inactivators.

On the other hand, characterization of 2-vinyl-(2*R*,3*S*)-isocitrate revealed the first mechanism-based inactivator of ICLs. Catalysis of 2-vinyl-(2*R*,3*S*)-isocitrate unmasks 2-vinyl-glyoxylate which then forms a covalent Michael adduct with the conserved cysteine. However, the maximal inactivation rate is slow ($k_{inact} = 0.08$ min^{-1}) and 2-vinyl-glyoxylate is susceptible to reaction with thiols. Hence, substrate analogs were evaluated to find a more suitable scaffold for the next generation of ICL inactivators. *Cis*-di-carboxylate compounds

were found to be better replacements for succinate than their *trans*-isomers, prompting the investigation of *cis*-epoxy-succinate as a potential ICL inactivator.

Cis-epoxy-succinate, a succinate analog, rapidly inactivates both ICLs via formation of thioether adducts with active-site conserved cysteines. In comparison with 2-vinyl-(2*R*,3*S*)-isocitrate, ICL1 inactivation efficiency (k_{inact}/K_{inact}) is improved by 750-fold. Exogenous thiols did not interfere with the inactivation. Neither did *cis*-epoxy-succinate show any inhibition effects on all eight of the tricarboxylic cycle enzymes tested. *Cis*-epoxy-succinate also demonstrated anti-mycobacteria effects ($IC_{50} = 100\ \mu M$) under conditions in which ICL activity is indispensable. Differential gel electrophoresis of *E.coli* lysate, pre-treated with and without *cis*-epoxy-succinate, asserted that *cis*-epoxy-succinate has a notable selectivity for ICL.

ACKNOWLEDGEMENTS

I would like to thank Dr. Thomas D. Meek for his insightful advice and timely criticism, which steered me towards the completion of this dissertation. Dr. Meek has given me not only the opportunity to take part in this rewarding endeavor but also the autonomy to take charge of the research.

I also thank the committee members for their precious considerations and feedbacks over these years. Every meeting has been the constructive force driving my progress. My thanks to Dr. Dorothy Shippen for her candid counsel at the most important graduate career decisions. Dr. Frank M. Raushel has always provided precise elucidations for enzymology problems whereas Dr. James C. Sacchettini has continued to compel engaging discussion.

I am grateful to my parents and extended family to whom I owed it all. It was for your patience and encouragement that I could pursue my improbable dreams.

With a special mention to my mentors, peers and supporters at Texas A&M: Dr. Margaret E. Glasner, Dr. Vishal Gohil, Dr. Andrew Bigley, Dr. Stephanie Perez, Dr. Xiang Zhai, Demetrios Kostomiris, Drake Mellott, and many others. It was fantastic to be able to meet and work with you all.

Last, but by no means least, thanks to the university staffs, especially Edward Janousek and Rafael Almanzar, for their unfailing assistance.

Thank you all!

CONTRIBUTORS AND FUNDING SOURCES

Contributors

This work was supervised by a dissertation committee consisting of Professor Thomas D. Meek, Professor Dorothy E. Shippen, and Professor James C. Sacchettini of Department of Biochemistry and Biophysics, and Professor Frank M. Raushel of Department of Chemistry.

The work on X-ray crystallography and mass spectrometry (MS) of *Mycobacterium tuberculosis* isocitrate lyases (ICL) was made possible by the collaboration with Dr. James Sacchettini and the Argonne National Laboratory.

The synthesis of 2-vinyl-(2*R*,3*S*)-isocitrate (2-VIC) and *icl2* plasmid preparation was supported by GlaxoSmithKline Pharmaceuticals. Initial analysis of 2-VIC inactivation of ICL1 was under a collaboration with Dr. Andrew Murkin (University of Buffalo, NY).

Dr. Hsiao-Ling Huang set up the co-crystalization and analyzed the structure of ICL1 inactivated by 2-VIC in section 3. Other ligand-bound ICL1 structures, reported in section 4 and 5, were analyzed by Dr. Inna Krieger.

The student completed all other work conducted for the dissertation independently.

Funding Sources

TABLE OF CONTENTS

LIST OF FIGURES

LIST OF TABLES

1. INTRODUCTION

Tuberculosis (TB) remains a major concern for public health in spite of the $6.9 billion of global funding spent on prevention, diagnosis and treatment services in 2018[1]. Over one million deaths among HIV-negative patients, together with 0.3 million deaths among HIV-positive patients, were caused by tuberculosis, which placed the disease in the top ten causes of death in 2017[1]. Even though annual mortality rate has seen continuous decline from 2013, the rise of multiple-drug resistant strains highlights the disease burden on public health. Treatment outcome data showed a reduction in success rate from 86% in 2013 to 82% in 2016[1]. Available treatments and vaccines do not guarantee the elimination of this disease. In order to improve the quality of treatment, extensive research has been devoted to the discovery of new therapeutic agents, especially those for treating drug-resistant tuberculosis. In fact, drug-resistant tuberculosis cases have been rising slowly over the past 5 years while treatment success remains at 55% globally[1].

One of the major challenges in eradicating *M. tuberculosis* (*Mtb*), is the ability of the organism to persist in the harsh conditions of pulmonary phagocytes during extended drug treatment which increases the probability of acquiring drug resistance genes[2, 3]. The prolonged therapy is largely due to the fact that the current therapy while effective in killing growing bacilli is not as effective in killing persistent or dormant bacilli. Therefore, the phenotypic resistance to antituberculosis agents in persistent and dormant bacilli during chronic infection presents a major challenge for effective control of the disease.

Long-term antibiotic treatment lasting between 6 and 9 months have also led to patient non-compliance and contributed to the emergence of multi-drug resistant

tuberculosis[4]: Multi-drug resistant (MDR) and extensively-drug resistant (XDR) TB. MDR-TB is resistant to at least two first-line drugs, rifampicin and isoniazid, while XDR-TB is also resistant to second-line therapies, such as fluoroquinolones and injectable antibiotics[5]. Worldwide, approximately 20% of those infected have MDR-TB, and of these, 9.7% have XDR-TB[1]. Treatment of patients with XDR-TB is particularly difficult, and XDR-TB comprises a serious global health threat.[1]

On the other hand, latent tuberculosis is described as "the presence of any tuberculous lesion which fails to produce symptoms of its presence" and is estimated to affect about 23% of the world's population (1.7 billion people) [1]. About 5-10% of this group will develop active tuberculosis during their lifetime, among which the risk of reactivation is significantly higher in HIV-positive patients[6]. Effective treatment of latent tuberculosis is important to controlling TB. Preventive treatment of latent TB with isoniazid and fluoroquinolone was shown to result in substantial health benefits and reduced morbidity[7] and multidrug-resistance TB incidence[8]. However the challenges in addressing the latent infection include treatment cost and poor diagnosis.

Besides, latent TB typically requires at least 12 weeks of antibiotic treatment and the current recommended regime includes frontline anti-TB drugs such as isoniazid and rifampin[1], which raises more concerns over the development of drug resistance. The cessation of microbial kill and emergence of resistance during isoniazid therapy was observed[9]. Despite >98% adherence, extensive emergence of MDR-tuberculosis still occurs[10]. It was reported in a clinical simulation that approximately 1% of tuberculosis patients with perfect adherence would still develop MDR-tuberculosis due to pharmacokinetic variability[11]. In the same study, treatment failure was encountered at

extents of nonadherence ≥60% and a transient pyrazinamide-resistant subpopulation (3.55%) was observed in a hollow-fiber pharmacodynamics model[11].

Therefore, there is a need for new therapeutic agents with novel mechanisms of action that have the potential to target persistent tuberculosis and shorten the duration of treatment. Promising drug targets for the development of new anti-tuberculosis agents requires that these targets: (a) may be differentiated pharmacologically from their human counterparts, (b) are determined to be essential to *Mtb* infection via genetic and chemical inhibition studies, (c) is amenable to the development of antagonists or inhibitor. The identification of metabolic enzymes governing *Mtb* adaptation to host environment upon phagocytosis revealed potential novel targets for development of tuberculosis drugs[12]. The isocitrate lyases are among the first metabolic enzymes shown to be essential to *Mtb* persistence and virulence[13]. *Mtb* isocitrate lyases allow the bacteria persistent growth via glyoxylate shunt and the methyl-isocitrate lyase activity[14]. The enzymes also mediate response to antibiotics and other stress signals[15-17].

1.1. The significance of isocitrate lyases in *M. tuberculosis* pathogenicity and drug tolerance

Upregulation of *Mtb* isocitrate lyases (*icl1* and *aceA* or *icl2*) was observed in gene expression (mRNA) profiles and 2D-gel electrophoresis from extracts of *Mtb* in macrophages[12, 18, 19]. The enzymes are required for the persistent infection of *Mtb* in immune-competent mice[13]. Isocitrate lyase 1 has a dual role of metabolizing both isocitrate and methyl-isocitrate , which contributes to bacteria growth on fatty acid via glyoxylate shunt and methylcitrate cycle[14]. Essential roles of isocitrate lyases in *Mtb* are not limited to fatty acid-dependent growth. Succinate production from both isocitrate lyase and methyl-isocitrate lyase activity of ICLs

is important for maintaining membrane potential and possibly mediates reactive oxygen responses[15, 17, 20].

C_2 Dependent Growth via Glyoxylate Shunt and Methylcitrate Cycle

Mycobacterial survival during chronic stages of infection requires a metabolic shift to utilizing C_2 substrates generated by β-oxidation of fatty acids[13, 21]. The glyoxylate shunt is an important pathway for utilizing acetyl-CoA, a product of fatty acid catabolism[13, 22-25]. This shunt is initiated by the catalytic action of the isocitrate lyases (ICLs) which convert isocitrate into succinate and glyoxylate via a retro-aldol reaction[26]. Malate synthase (MS) then assimilates glyoxylate with acetyl-CoA to form malate[27, 28].

The glyoxylate shunt allows the net carbon assimilation from C_2 compounds via an abridgement of TCA cycle that bypasses the loss of carbon in the two carbon dioxide evolution steps (**Figure 1-1**). The net product of glyoxylate shunt is one malate/ succinate molecule from two acetyl-CoA molecules derived from acetate, and/or degradation of fatty acids or ethanol. On the other hand, products of the TCA cycle include "high-energy" compounds such as NADH, FADH$_2$, and GTP. The TCA cycle releases stored energy through oxidation of acetyl-CoA from fatty acid metabolism and glycolysis to generate ATP via electron transport chain[29]. In contrast to TCA cycle, the glyoxylate shunt comprises biosynthesis rather than energy production which is important for microorganisms during its stage of persistent growth[30]. In fact, ICL and MS were shown to be essential for *Mtb* infection[13, 25, 31].
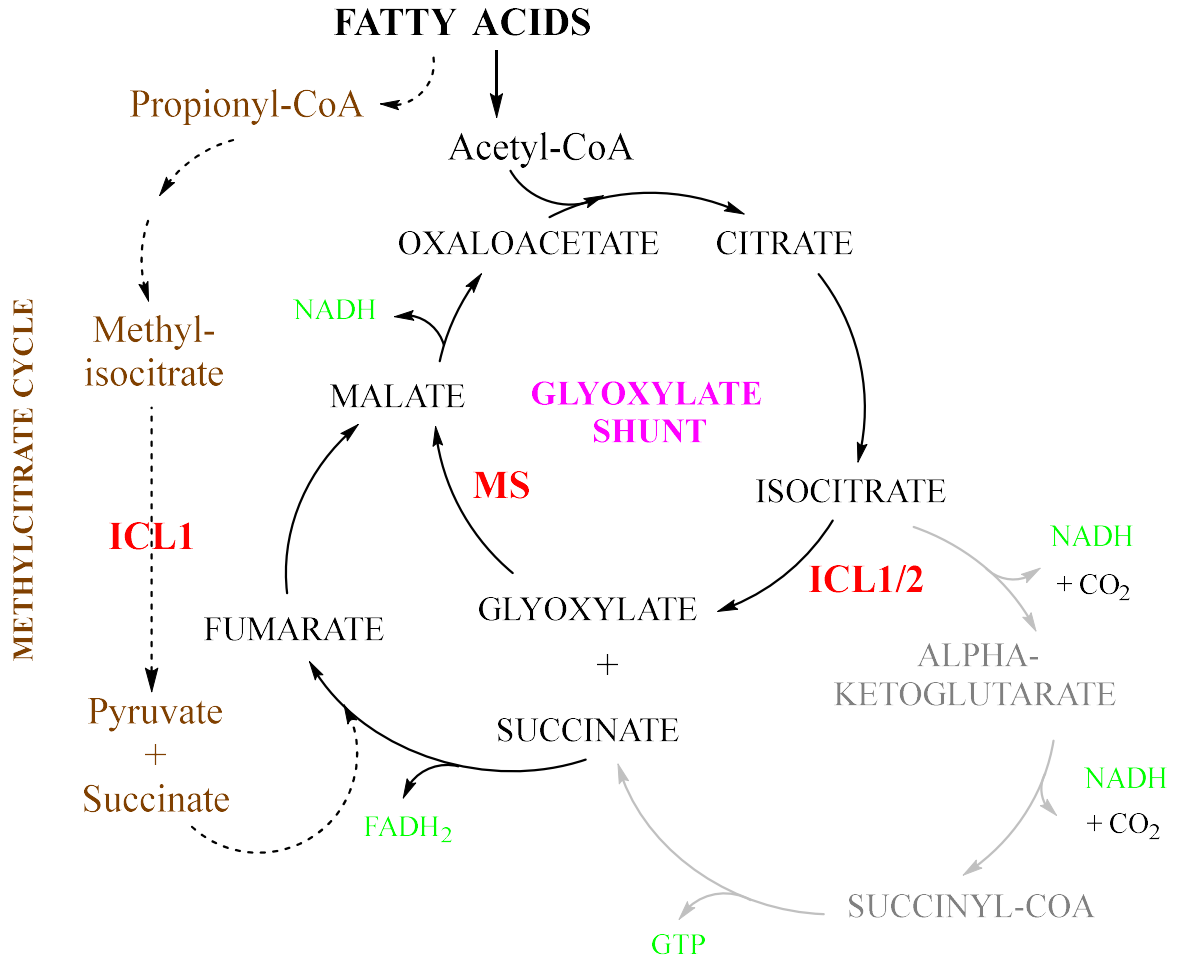
Figure 1-1 Isocitrate lyases 1 & 2 roles in *M. tuberculosis* utilization of fatty acids via glyoxylate shunt and methylcitrate cycle[24]

"Energy" compounds as products of TCA cycle are shown in green. The steps in TCA cycle bypassed by glyoxylate shunt are represented in grey. The mmethylcitrate cycle metabolites are labeled in brown.

Mycobacterial proteins with isocitrate lyase activity were first identified in a two-dimensional gel electrophoresis of cell extracts from *Mtb* and *M. avium* grown on murine bone marrow-derived macrophages[19]. N-terminal sequencing of one of the most prominent protein bands extracted from the SDS-gel exhibited similarity to isocitrate lyase of *Corynebacterium glutamicum* and *Rhodococcus fascians*, which led to the identification of

icl and *aceA* genes in *Mtb*. Protein products of these two genes were characterized with isocitrate lyase activity[19]. Nowadays *aceA* is also referred to as *icl2*.

ICL1 and ICL2 are members of isocitrate lyase/ phospho-enol-pyruvate (PEP) mutase family that include ICLs, methyl-isocitrate lyases, PEP mutase enzymes and decarboxylase[32-34]. Despite the overall homology between isocitrate lyase and methyl-isocitrate lyase (MCL), there was little overlap in function of these two enzymes in *E. coli* and other organisms[35, 36]. No isocitrate lyase activity was detected ($<10^{-3}$ s^{-1}) in MCLs from *E. coli*, *S. enterica* and *A. nidulans*[35, 37]. ICL enzymes contain the catalytic motif K[K/Q]CGH while MCL enzymes contain a slightly different motif KRCGH that comprises part of the active site. However, the arginine residue on the active-site loop of MCL does not confer substrate specificity in *S. enterica* MCL. Mutation of the corresponding arginine on the active-site loop of *S. enterica* MCL to lysine (R122K) did not result in any detectable isocitrate lyase activity[37].

It was not until the crystal structure of *E. coli* apo-MCL[38] and *Mtb* ICL1 in complex with ligands[39] became available that the dual function of *Mtb* ICL1 as isocitrate lyase and methyl-isocitrate lyase was studied[14]. ICL1 was shown to metabolize methyl-isocitrate into pyruvate and succinate, even though at a 15-fold lower catalytic efficiency than ICL1 catalysis of isocitrate (5-fold slower turnover rate and 3-fold higher K_m for methyl-isocitrate)[14, 19]. Co-crystallization of C191S ICL1 with methyl-isocitrate resulted in a crystal structure of C191S ICL1 in complex with pyruvate and succinate in 2 out of 4 subunits; the other two subunits existed in an open conformation with pyruvate bound to Mg^{2+} in the active site[14]. Therefore, *Mtb* ICL1 allows usage of products from both even and odd-chain

fatty acid metabolism via the glyoxylate shunt and methylcitrate cycle respectively (**Figure 1-1**).

The canonical roles of ICL activity in *Mtb* survival on fatty-acids carbon sources and during persistent infection are well supported. Gene expression (mRNA) of both glyoxylate shunt enzymes, isocitrate lyase 1 (ICL1) and malate synthase (MS), were found during infection of macrophages[18] and during periods in which the bacteria rely on substrates generated by the β-oxidation of fatty acids[19, 21]. Isocitrate lyase and methylcitrate cycle genes (*prpC* & *prpD*) were significantly upregulated during *Mtb* infection of macrophages[19]. *Mtb* malate synthase, on the other hand, was reported to be an extracellular enzyme, and acts as a laminin-binding adhesive protein, enhancing adherence of the bacteria to lung epithelial cells[30, 40].

The Joint Roles of ICL1 and ICL2 during Mtb Infection

M. tuberculosis relies on the action of the ICL enzymes, ICL1 and ICL2, for its survival on fatty acids, its *in vivo* growth, and virulence[19, 41, 42]. Both *icl1* and *icl2* genes were upregulated in *M. tuberculosis* isolated from mouse lungs as compared to bacteria grown *in vitro*[41]. The gene products of *icl1* and *icl2* only share about 27% homology overall. The KKCGH motif was conserved in both enzymes (**Figure 1-2**). Molecular modelling of ICL2 suggested that the active-site loop contains similar arrangement in both enzymes. The clinical importance of ICL2 remains a subject of debate. Only *icl1*, but not *icl2*, could restore ability to growth on C_2 substrate of *M. smegmatis* mutant[13]. Scission of isocitrate by catalysis of ICL2 was significantly less efficient than ICL1, and no appreciable methyl-isocitrate lyase activity was detected[14, 43]. In addition, the *icl2* gene contains a frame shift mutation, resulting in an inactive enzyme, in the clinical isolate *Mtb* Euro-American strain 630 and *Mtb* H37rv[44].

During *Mtb* infection of mice, a study showed that deletion of *icl1* alone significantly impairs

Mtb persistence in mice[13].

```
15    QEWDTNPRWKDVTRTYSAEDVVALQGSVVEEHTLARRGAEVLWEQLHDL----EWVNALG    70
      Q +  + R+  + R Y+A  VV  +G++  +H +AR  A    +E+L +L    + +   G
26    QRYFDSSRFAGIIRLYTARQVVEQRGTIPVDHIVAREAAGAFYERLRELFAARKSITTFG    85

71    ALTGNMAVQQVRAGLKAIYLSGWQVAGDANLSGHTYPDQSLYPANSVPQVVRRINNALQR    130
         +   AV   R G++AIYL GW  +   + +   PD + YP + VP     + AL
86    PYSPGQAVSMKRMGIEAIYLGGWATSAKGSSTEDPGPDLASYPLSQVPDDAAVLVRALLT    145

131   ADQ---------IAKIEGDTSVENWLAPIVADGEAGFGGALNVYELQKALIAAGVAGSHW    181
      AD+           +    T   ++   I+AD + G GG  +V  L +   + GV G H
146   ADRNQHYLRLQMSERQRAATPAYDFRPFIIADADTGHGGDPHVRNLIRRFVEVGVPGYHI    205

182   EDQLASEKKCGHLGGKVLIPTQQHIRTLTSARLAADVADVPTVVIARTDAEAATLITSDV    241
      EDQ    KKCGH GGKVL+P+ + I+ L +AR    D+  VP +++ARTDAEAA LI S
206   EDQRPGTKKCGHQGGKVLVPSDEQIKRLNAARFQLDIMRVPGIIVARTDAEAANLIDSRA    265

242   DERDQPFITG    251
      DERDQPF+ G
266   DERDQPFLLG    275
```

Figure 1-2 Comparison of amino acid sequence between *Mtb* ICL1 and ICL2

Protein-BLAST revealed that the highest identity region (based on E-value) includes the active-site loops of ICL1 (top) and ICL2 (bottom) and the homologous conserved motif (light orange)

Despite its poor isocitrate lyase activity, ICL2 alone can substitute for ICL1 and maintain *Mtb* growth and virulence. Deletion of *icl1* or *icl2* alone did not affect growth on these substrates except for on propionate. *Δicl1 Mtb* exhibited slower growth rate in propionate media in comparison with WT and *Δicl2 Mtb*[41] which could be accounted for by the fact that ICL2 could not metabolize methyl-isocitrate[14]. In contrast, the double mutation *Δicl1 Δicl2* impairs *Mtb* growth on fatty acid substrates such as acetate (C_2), propionate (C_3), polyoxyethylene sorbitan monolaurate (C_{12}) and pamilate (C_{16}). Consistently, deletion of both ICLs resulted in impairment of *Mtb* growth in resting bone marrow-derived macrophages and rapid clearance of the bacteria in activated bone marrow-derived

macrophages. The ability of *Mtb* to maintain growth in macrophages was rescued by complementation of the *Δicl1 Δicl2* strain with plasmids containing either *icl1* or *icl2*. A similar result was observed during *Mtb* infection of mice[41]. Therefore, *icl2* appears to have a functional role in *Mtb*, which is not mutually exclusive from *icl1*, that is, their catalysis achieves the same overall metabolic function.

A genome-wide transposon mutagenesis study, coupled with a next-generation sequencing (TnSeq) study of strain-specific genetic requirements, showed that there was a non-significant increase in transposon insertion count across *icl1* ($P < 0.05$) among eight clinical isolates in comparison with the reference strain H387rv. However, apparent counts of transposon insertions across *icl1* decreased 2-fold in *Mtb* Euro-American strain 630, that lacks the paralog, *icl2,* and increased in other isolates with intact *icl2*[44]. Even though the lower genetic requirement of *icl1* in isolates with intact *icl2* is not statistical significant at $P < 0.05$, this observed trend is consistent with the role of *icl2* as a "back-up" mechanism for *icl1*. However, it is intriguing that ICL2 possesses a significant slower catalysis and does not exert MCL activity. It is unclear if the redundancy of ICLs offers other metabolic advantages during persistent infection.

Roles of the ICLs in the Methylcitrate Cycle Are Not Essential to Mtb Infection of Mice
Despite the fact that methyl-isocitrate is a poorer substrate for ICL1 than isocitrate (5-fold slower turnover rate and 3-fold higher K_{m} for methyl-isocitrate), *icl* genes are required for *Mtb* growth on both even and odd-chain fatty acids[14, 42]. Analysis of *Mtb* genomic data revealed that even though the bacteria carry homologs of the genes *prp*D and *prp*C which provide for the biosynthesis of methyl-isocitrate from propionyl-CoA and oxaloacetate, *Mtb* lacks the third enzyme of the methylcitrate cycle, *prpB* gene, which metabolizes methyl-

isocitrate[45]. In *Mtb* ICL1 apparently plays a dual role for both the isocitrate lyase and methyl-isocitrate lyase enzymes[14]. Together with *icl1*, methylcitrate cycle genes, *prpD* and *prpC*, were upregulated upon internalization of the bacteria by macrophages, suggesting a functional role of ICL in methyl-isocitrate metabolism[12].

However, the essentiality of methylcitrate cycle is limited to *Mtb* growth on propionate media and in murine bone marrow-derived macrophages. Δ*prpDC Mtb* mutants lack the ability to synthesize methyl-isocitrate from propionyl-CoA, and could not afford growth on propionate media. Deletion of *prpD* and *prpC* impairs *Mtb* growth and survival in non-activated murine bone marrow-derived macrophages. The deletion did not lead to significant clearance of the bacteria from IFN-γ-activated murine bone marrow-derived macrophages[42]. On the contrary, the methylcitrate cycle appears to be dispensable to *Mtb* growth and persistence in mice infection[42]. Δ*prpDC Mtb* was able to maintain growth and infection in aerosol-infected C57BL/6 mice as well as wildtype *Mtb*. The mechanism, which differentiates the requirements of methylcitrate cycle during Mtb infection of mice and macrophages, were not addressed in the study.

Detoxification Role of Methyl-isocitrate Lyase Activity of ICL1 during Mtb Growth on Fatty Acids

A study of methylcitrate genes in *M. smegmatis* revealed that accumulation of methyl-isocitrate is toxic to the cells[46]. *M. smegmatis* contains an MCL homolog encoded by *prpB* gene located on the same operon with *prpDC*[45]. In contrast to *Mtb*, *prpDBC* is not essential for *M. smegmatis* growth on propionate[46]. In the same study, deletion of *prpDBC*, *icl1* and *icl2* led to a longer lag phase but still allowed *M. smegmatis* growth on 0.5% and 0.1% propionate. On the other hand, the Δ*prpB* Δ*icl1* Δ*icl2* mutant could not sustain growth on

propionate media or even on mixtures of propionate and glucose. Incomplete propionyl-CoA processing appears to cause cell toxicity[46].

Recently, both acetate and propionate were shown to be bactericidal to Δ*icl1* Δ*icl2 Mtb in vitro* growth[20]. Δ*icl1* Δ*icl2* mutant could not grow on a mixture of 0.2% dextrose with 0.2% acetate or 0.2% propionate. Since dextrose is a growth-permissive carbon source, impairment of Δ*icl1* Δ*icl2 Mtb* growth is likely due to incomplete metabolism of acetate and propionate. Δ*icl1* Δ*icl2 Mtb* growth was restored when 10 μg/mL vitamin B_{12} was included in media. Vitamin B_{12} is an activator of a separate pathway for utilizing propionyl-CoA via methylmalonyl-CoA mutase[47].

In the absence of ICLs and vitamin B_{12}, fatty acid metabolism leads to accumulation of methyl-isocitrate and deprivation of succinate. Methyl-isocitrate inactivates gluconeogenesis while reduction in succinate causes imbalanced membrane potential (**Figure 1-3**). The alternative vitamin B_{12}-dependent metabolism of propionyl-CoA provided a molecular basis for different responses of *Mtb* to deficiency in methylcitrate cycle during growth on non-activated macrophages vs. during growth on activated macrophages and mice infection.
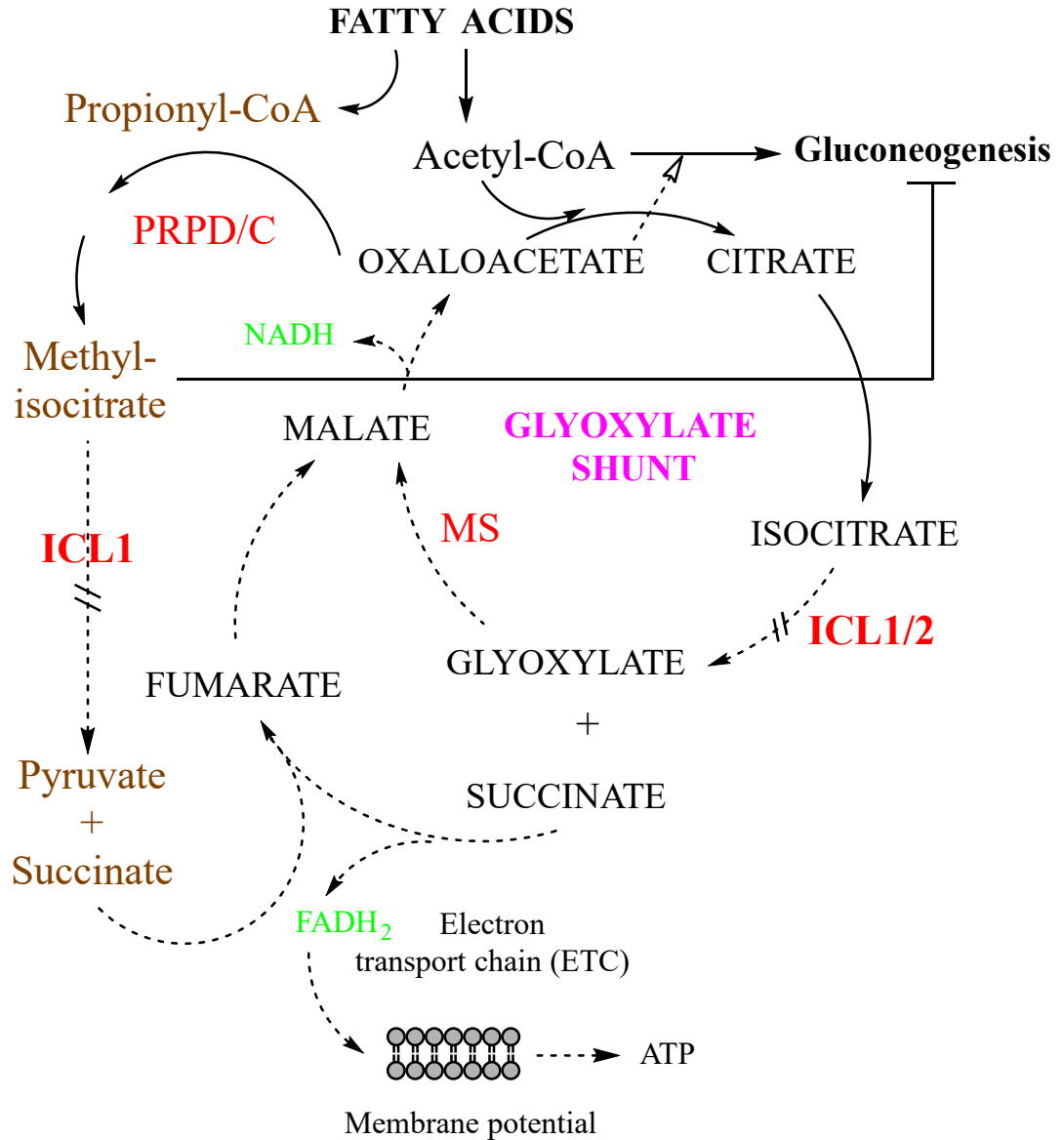
Figure 1-3 Consequences of ICL1 deficiency when metabolizing fatty acid carbon sources (adapted from Eoh and Rhee, 2018)[20]

ICLs Mediate Mtb Adaptation to Harsh Environments

The significance of ICL in *Mtb* pathogenicity extends beyond C_2 carbon sources-dependent

growth. ICL is also important for *Mtb* to switch into non-replicating states in response to

hypoxia and nutrient-starved environment within infected host[16, 48, 49]. The study of

adaptation of tuberculosis bacilli to microaerophilic conditions was one of the first *in vitro* model for *Mtb* persistent stage of infection.[49]. In this study, isocirate lyase activity increased four-fold in the microaerophilic adapted bacilli in the sediment of non-agitated liquid culture. These adapted bacilli appear to enter a non-replicating stage with a half-life of 116 hrs[49]. On the contrary, in another study of gene expression changes in *Mtb* response to hypoxia using the defined hypoxic model (a constant flow of low oxygen gas over the surface of a stirred, early log-phase culture is used to deplete the oxygen rapidly), *icl* was not among the 230 genes identified as the enduring hypoxic response[50]. Supporting the role of *icl* in non-replicating growth of *Mtb*, a more recent study reported the increase of isocitrate lyase protein level during hypoxia-induced dormancy[51]. Additionally, nutrient-starved Δ*icl1* mutant bacilli could not elicit changes in ATP levels nor sustain non-replicating growth. Upregulation of isocitrate lyase, but not malate synthase, was observed during long-term bacteriostasis[15, 52]. Coincidently, succinate, but not malate, increases drastically in hypoxia-induced quiescent *Mtb* whereas other tricarboxylic cycle (TCA) metabolites decrease[15]. These observations suggested that ICL activation is decoupled from TCA and glyoxylate shunt (**Figure 1-4**). Generation of succinate as an end product is utilized by succinate dehydrogenase to maintain membrane potential dynamics and ATP production via electron transport chain[15, 48].
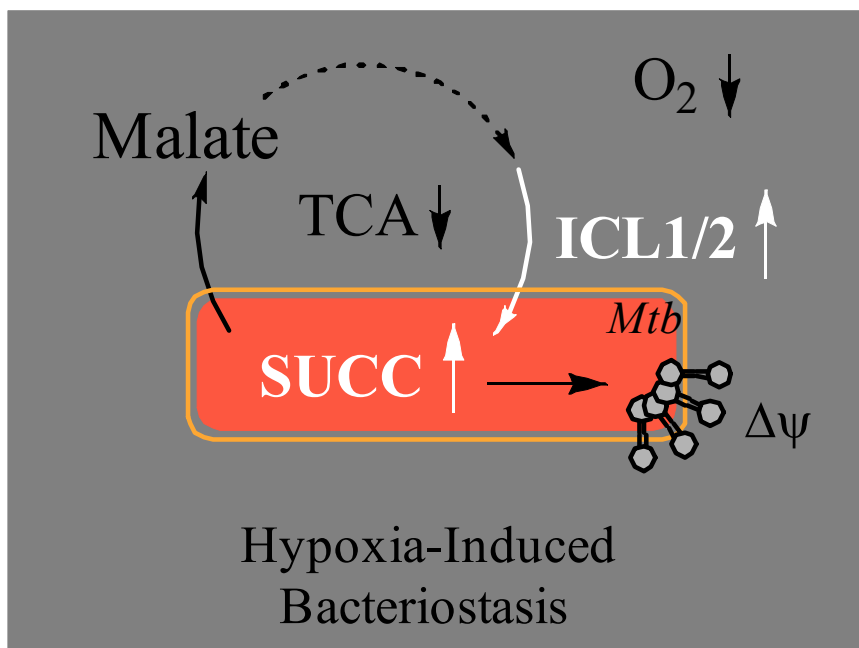
Figure 1-4 Decoupling of ICL activity and glyoxylate shunt/ TCA cycle during hypoxia-induced bacteriostasis[15]

Perhaps a more notable finding was that *M. tuberculosis* mutants that lack isocitrate lyase genes (*icl1* and *icl2*) were 100- to 1,000-fold more sensitive to antibiotic treatment[17]. Antibiotic tolerance is not merely a passive consequence of non-replicating *Mtb* and slow growth but an active adaptation of cellular processes to harsh environment[53]. It was reported that ICL mediates broad antibiotic tolerance via an adaptive respiratory response to reactive oxygen intermediates[17]. Antibiotic treatment led to a reduction in gene expression of TCA cycle enzymes such as succinate dehydrogenase, malic dehyrogenase and fumarase. On the other hand, gene expression of *icls* was induced[17]. There was an increase in some TCA cycle intermediates including pyruvate, succinate, and fumarate[17]. The remodeling of TCA cycle upon antibiotic exposure was attenuated in the Δ*icl1/2* mutant in contrast to the induction of reactive oxygen response genes. Elevated sensitivity of the *Mtb* mutants to rifampicin, streptomycin and isoniazid treatment was reversed by exogenous thiourea, an antioxidant

agent[17]. Therefore, the mechanism(s) by which ICLs may defend against antibiotics might be independent of glyoxylate shunt/ TCA cycle metabolism and remain to be elucidated.

1.2. Development of small-molecules to inhibit *Mtb* isocitrate lyases and glyoxylate shunt

Inhibitors of ICL hold great potential for the development of novel bactericidal compounds, which target non-replicating and persistent *M. tuberculosis*. Developing ICL inhibitors, however, has been a challenging endeavor to both academic and pharmaceutical entities. Currently, the major approach for discovering novel inhibitors is high-throughput screening of small molecule libraries. Despite multiple high-throughput screening campaigns encompassing approximately three-million small-molecule compounds[54], little progress has been made toward a competent ICL inhibitor.

The most potent ICL1 inhibitors to date are nitro-propionate[55] and bromo-pyruvate[56] whose cellular toxicity abolishes their therapeutic applications[57-61]. Both compounds were shown to form a covalent adduct with the active site cysteine of *Mtb* ICL1[39, 62]. 3-nitro-propionate is an inactivator of succinate dehydrogenase or mitochondria complex II[58, 59, 61, 63]. A crystal structure of mitochondria complex II, purified from chicken heart, showed that 3-nitro-propionate formed a cyclic adduct with the catalytic Arg297[58]. Bromo-pyruvate is an alkylating agent, which targets glyceraldehyde-3-phosphate dehydrogenase and reacts with other cysteine-containing proteins[56, 64].

Several studies have also taken a semi-rational approach to synthesize and screen focused libraries of potential ICL inhibitors[65-67]. Screening of a library of 22 nitro-propionamides resulted in four potent ICL inhibitors that inhibit *Mtb* growth at low micromolar concentrations. These compounds, however, showed no selective killing

between active and starved phase, thereby indication their cytotoxicity was not due to the inhibition of ICL[66]. All four compounds are fluoroquinolone derivatives whose bactericidal activity was shown to target bacterial DNA replication (i.e. DNA gyrase and DNA topoisomerase)[68-70].

In another study, conjugates of pyruvate and hydrazides including isoniazid and their corresponding copper complexes were reported to inhibit *Mtb* strain H37Rv[67]. No direct evidence supported the hypothesis that these conjugates inhibit ICLs[67]. None of these studies had fully integrated insights from catalytic mechanism and structure-guided studies into the design of their libraries. Nor has any study exploited a mechanism-based strategy to discover novel ICL inhibitors. Mechanism-based inhibitors often exhibit significant advantages in eluding non-specific (off-target) activities[71] that are problematic with current ICL inhibitors[29, 30].

However, development of ICL1 inhibitors is also challenging due to its small active site and the tri-anionic nature of its substrate. Di-anionic compounds were shown to have limited cellular uptake and permeability, which require additional medicinal chemistry to produce prodrug forms of lower or absent charge[72, 73]. The next enzyme in the glyoxylate shunt, malate synthase could provide an alternative target for inhibiting *Mtb* growth on fatty acids. Malate synthase was shown to be essential for both *Mtb* acute and chronic infection[31]. The enzyme utilizes acetyl-CoA as its substrate and therefore the active site is larger. Malate synthase activity plays an important role in glyoxylate detoxification during growth on fatty acid sources[25]. Potent inhibition of malate synthase by phenyl-diketo acids demonstrated efficacy in mouse model of tuberculosis [74].

On the other hand, a systemic evaluation of the metabolic changes of *Mtb* in the absence of malate synthase and isocitrate lyase activities showed that inhibition of isocitrate would cause more significant metabolic stress[75]. The recent discovery of CLYBL, a human homolog of malate synthase, suggested a role of this enzyme in the B_{12} synthesis pathway[76] whereas no ICL homolog is found in humans. Therefore, ICL remains the most significant enzyme target of the glyoxylate shunt, and possibly in latent TB.

1.3. Structure-guided rational approach to design novel inhibitors for *Mtb* ICLs

Although no therapies based on ICL inhibitors has yet been discovered, previous kinetic and biophysical studies provided substantial data, which enabled hypothesis-driven studies to elucidate new details on mechanisms of ICL catalysis and inhibition. Crystallographic analyses of *M. tuberculosis* isocitrate lyase 1 were first presented in the work of Sharma et. al. (2000)[39]. ICL1 contains a three-dimensional of dimer of dimer and has 222 symmetry that is expected for a member of the isocitrate lyase/phosphoenolpyruvate mutase (ICL/PEPM) family (**Figure 1-5**). C-terminal domain swapping between two non-crystallographically related subunits was observed at helix 12 and 13, which favors the formation of stable dimers[39]. In most cases, the structures showed the presence of Mg^{2+} in the active site of both the apo and ligand-bound enzymes.

Movement of the active-site loop characterized the conformation changes between apo-enzymes and ICL1 in complex with ligands. The position of the Mg^{2+} ion also shifted slightly in order to afford its coordination to oxygens on glyoxylate. The interaction for loop closure can be narrowed down to the binding pocket of succinate (and its analogs, bromo-pyruvate & nitro-propionate) which consists of H193, Q313, S315 and S317. The binding pocket of glyoxylate contains Mg2+ interacting with three water molecules and Asp153. In

the open conformation, the active-site loop of *M. tuberculosis* ICL1 does not exhibit interactions with the C-terminal region of the other subunit in the dimer. Upon ligand binding, this C-terminal region including 17 residues undergo a conformational change, which locks the active-site loop in a closed/ catalytically-active conformation that is solvent inaccessible. Electrostatic interactions between the Lys189 and Glu182 were proposed to act as a gatekeeper of ICL1 conformation changes as in other enzymes of ICL/PEP mutase enzymes[32, 33, 36, 77].
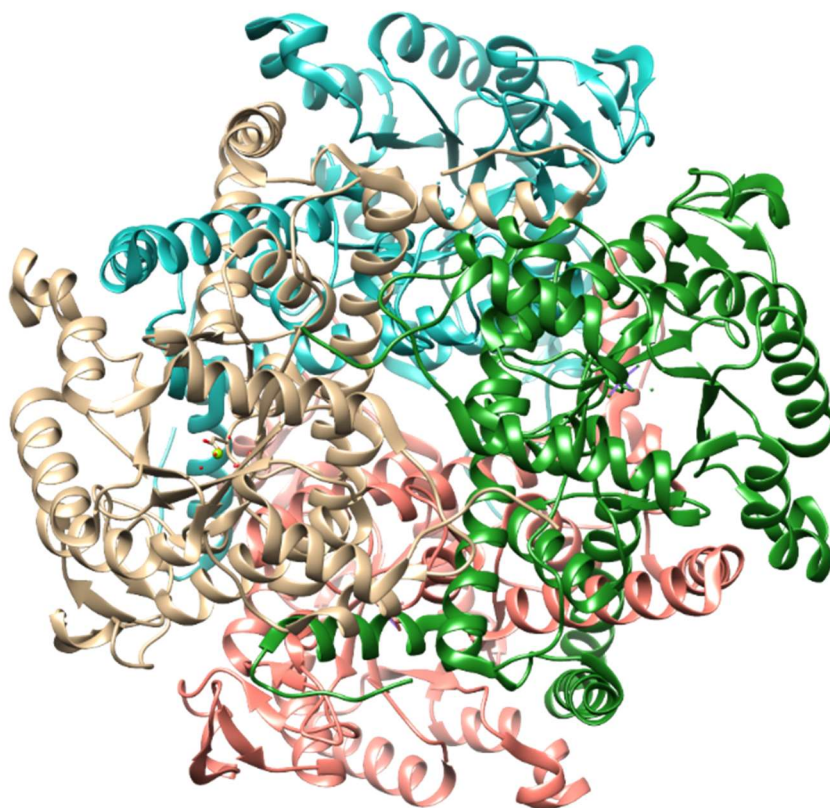
Figure 1-5 3-dimensional structure of *M. tuberculosis* ICL1 (PDB: 1F61)[39]
ICL1 contains the three-dimensional arrangement of dimer of dimer and has 222 symmetry

Retro-aldol catalysis of ICLs is initiated with the deprotonation of the hydroxyl group on (2R,3S)-isocitrate, which leads to C-C bond cleavage and the formation of glyoxylate and an *aci*-succinate intermediate (**Figure 1-6**). The conserved Cys191 is positioned to protonate *aci*-succinate, which yields succinate. ICLs also catalyze the aldol condensation of succinate and glyoxylate to isocitrate (K_{eq} = 107 ± 4 10^{-5} M)[78]. Consistently, in the work of Moynihan et. al., the active site Cys191 of *Mtb* ICL1 was shown to be the catalytic residue which deprotonates succinate in the reverse reaction[79].
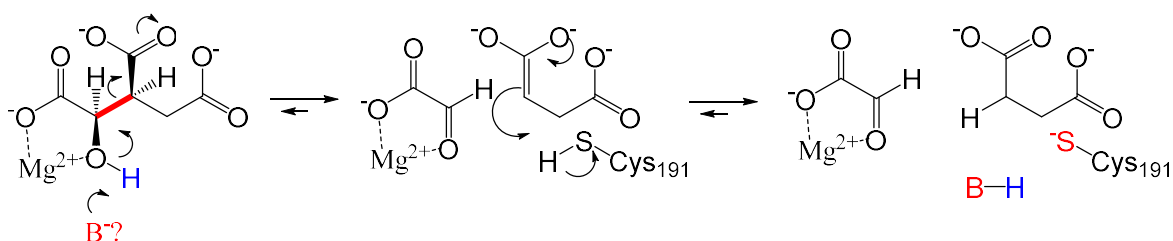
Figure 1-6 Reversible retro-aldol catalysis of *Mtb* isocitrate lyase 1

An unknown base (B⁻) catalyzes the deprotonation of isocitrate, leading to C-C bond cleavage and formation of glyoxylate together with an *aci*-succinate intermediate. Cys191 protonates an *aci*-succinate intermediate.

On the other hand, the discovery of ICL inactivators motivated future endeavors. Ko and McFadden (1980) showed that bromo-pyruvate is a potent covalent inactivator of *E. coli* ICL via formation of an adduct with the enzyme's active-site cysteine[56]. Co-crystallization of *M. tuberculosis* ICL1 with bromo-pyruvate also demonstrated that the covalent inactivation of ICL resulted from formation of a S-pyruvoyl adduct with the conserved Cys residue[39]. Exploitation of the nucleophilic activity of cysteines in biological systems provides a wide range of applications from selective labeling of the protein targets for bio imaging[80-83] to specific inhibition of enzymes for drug discovery[84-89].

These results inspired the application of a mechanism-based inactivation strategy that exploits the enzyme catalysis to inactivate ICL at the conserved cysteines. The advantage of mechanism-based inactivators is their selectivity for the enzyme target because specific enzyme catalysis is required to activate naïve inhibitors (**Figure 1-7**)[71, 90]. Aminoguanidine is an isoform-selective inhibitor of nitric oxide synthase[91]. Cycloserine, an approved treatment of active drug-resistance TB, is a mechanism-based inactivator of branched-chain aminotransferase[92]. Therefore, a major part of this research is devoted to the characterization of 2-vinyl-($2R,3S$)-isocitrate as a mechanism-based inactivator for ICLs.

$$E + I \rightleftharpoons \underset{\text{Binding}}{} EI \rightleftharpoons \underset{\text{Catalysis}}{} EX \xrightarrow{\text{Covalent inactivation}} E\text{-}X$$
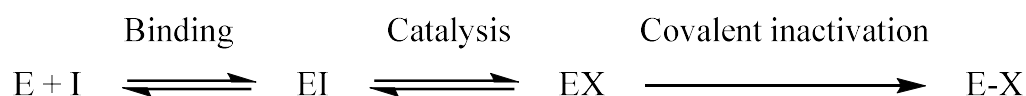
Figure 1-7 A schematic summary of suicide inactivation via enzyme catalysis

A broader definition of mechanism-based inactivators is not limited to suicide inhibitors that undergo enzyme catalysis to generate electrophilic species during enzyme inacivation. Mechanism-based inactivation discussed in this thesis includes transition-state analogs and quiescent inactivators that become more reactive upon interactions with active-site residues[93]. In all cases, a comprehensive knowledge of ICL1 catalysis and its inhibition/inactivation would then advise novel chemical motifs for inhibiting ICLs. In this thesis, kinetic studies via evaluation of pH-rate profiles and solvent kinetic isotope effects, together with a structural-guided analysis of ICL1 catalysis, revealed additional details on the ICL1 catalytic mechanism. The active-site chemical space was also characterized via inhibition and crystallographic studies of substrate analogs.

1.4. Justification

This thesis took part in the global endeavor to eradicate tuberculosis. Using a target-based approach, the thesis addressed both fundamental questions of enzyme catalysis and the discoveries of ICL inhibitors. Additionally, the research incorporated a wide range of chemical, biophysical, kinetic and *in silico* strategies to obtain a multi-pronged approach for "mechanism-based" inactivation of ICL.

1.5. Outline

The thesis includes a literature review centering on the role of isocitrate lyases in persistent tuberculosis treatment (section 1). This section also declares the research problems and its justifications (section 1).

Section 2-5 comprises a presentation of data collected during the course of the Thesis research. Section 2 displays data from pH profile and solvent kinetic studies of ICL1 and its mutants. Section 3 discusses the characterization of 2-vinyl isocitrate, a mechanism-based inhibitor of *Mtb* ICL. Section 4 describes a survey of substrate analogs, which led to the characterization of *cis*-EpS as a novel selective ICL inactivation in section 5.

Section 6 presents the conclusions and implications of this research as well as future directions.

1.6. Conclusions

Since ICL plays important roles in *M. tuberculosis* pathogenicity and drug resistance, it presents a valuable target to the development of novel tuberculosis treatment. Nevertheless, high-throughput screening campaign against ICL have not yielded any suitable lead compounds[4]. Current ICL inhibitors are non-specific and exhibits high cellular toxicity[64]. Recognizing the shortcomings of previous studies, this research focused on a rational

approach to discover novel ICL inhibitors. Mechanism-based inhibitors have shown promising clinical outcomes owning to their target specificity[91, 92].

Taking the first step toward rational development of effective ICL inhibitors, the thesis set out to uncover new details on the catalytic mechanism of ICL1. The characterization of 2-vinyl-(2*R*,3*S*)-isocitrate was a proof of concept for ICL mechanism-based inactivation, which instigated considerations for more suitable scaffolds of ICL1 inactivators. On the other hand, chemical and kinetic mechanisms of inhibition by substrate analogs and potential inactivators were evaluated in order to provide additional rationales to the enterprise.

2. ON THE CATALYTIC MECHANISM OF ISOCITRATE LYASES

2.1. Introduction

M. tuberculosis isocitrate lyases (ICL) belong to the ICL/PEPM (isocitrate lyases/ phosphonoenolpyruvate mutase) family. The family includes isocitrate lyases and methyl isocitrate lyases, which are products of two distinct genes in most organisms (e.g. *E. coli*)[35], and PEP mutase enzymes. Isocitrate lyases (ICLs) catalyze the retro-aldol cleavage of isocitrate into glyoxylate and succinate while methyl isocitrate lyases (MCLs) are responsible for the cleavage of methyl isocitrate into pyruvate and succinate. In *M. tuberculosis* (*Mtb*), isocitrate lyase 1 (ICL1) performs the dual function of both the isocitrate lyases and methyl isocitrate lyases[19]. Previous studies have provided ample data on the catalytic mechanism of isocitrate and methyl isocitrate lyases. Generally the retro-aldol cleavage occurs via a concerted, 2-step mechanism, for which the deprotonation of the hydroxyl group (OH) on either isocitrate or methyl isocitrate leads to carbon-carbon bond cleavage (C_2-C_3) and generates glyoxylate and an *aci*-succinate intermediate[55, 57]; *aci*-succinate accepts a proton to yield succinate (**Figure 2-1**).
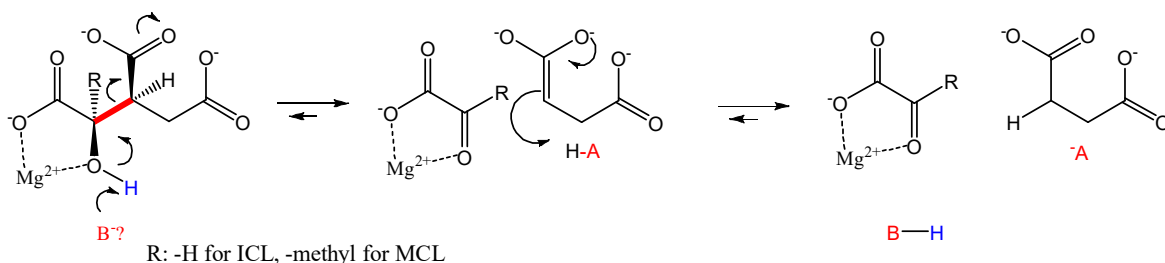
Figure 2-1 Previously proposed catalytic mechanism of ICL and MCL.

Mutagenesis studies of the ICL active site, together with structural analysis and genetic sequence analysis, have identified several key amino acid residues that are important

for ICL catalysis[79, 94-98]. Along with the emergence of ICL crystal structures, the convserved motif K_{189} KCGH$_{193}$ was reported to compose part of the ICL active-site[38]. *Mtb* ICLs contain homotetramers in the arrangement of dimer of dimers. Secondary structure elements of ICL1 form a unique topology, $(\beta\alpha)_2\alpha(\beta\alpha)_5\beta$. Mg^{2+} ion was found in the active site of both *apo*- and ligand-bound ICL1.

The active- site loops of ICL1 *apo*-enzymes are in an open conformation, which close upon ligand binding (glyoxylate (Glx) and 3-nitropropionate (3-NP)). Conformational changes during ICL1 catalysis and/or ligand binding are characterized by movement of the K_{189}KCGH$_{193}$ loop by about 15 Å (measured at the Cα of His193), to yield a closed, solvent-inaccessible active site (**Figure 2-2**). The position of the Mg^{2+} ion also shifts slightly in the active site upon ligand binding[39]. Molecular dynamics studies revealed that mutation of distal residues, such as Phe345 and His46, which are at least 10 Å away from the active site of *Mtb* ICL1, could result in significant loss in the activity due to increased conformational plasticity[99, 100].
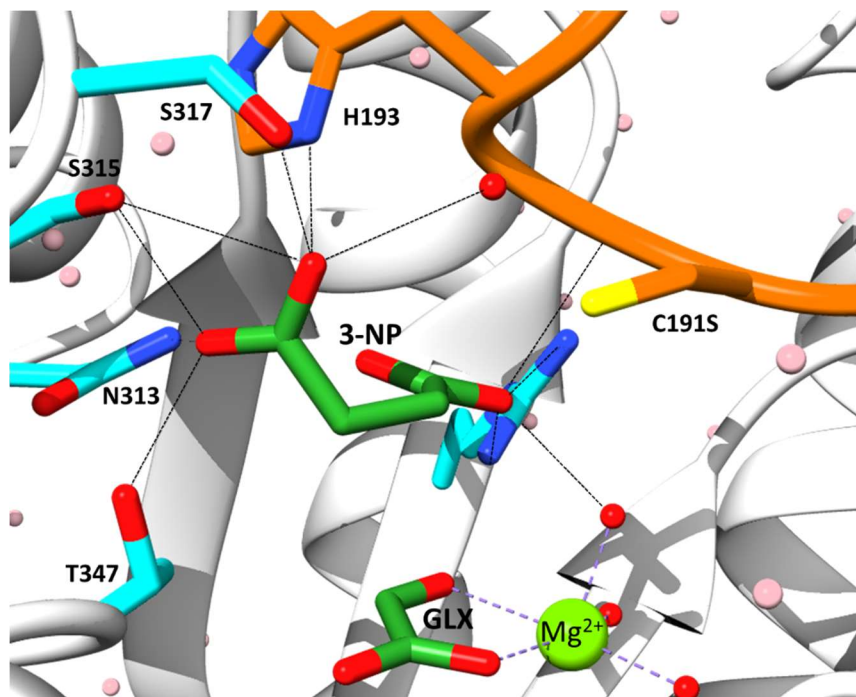
Figure 2-2 Structural features of ICL1-Glx-3NP active site

The crystal structure of C191S ICL1 (PDB: 1F8I) showed glyoxylate (Glx) and nitropropionate (3-NP) (green) bound in enzyme's active site. The ICL1 loop containing K189KCGH193 (orange) movement formed a closed catalytic pocket. Dashed-lines represent potential hydrogen bonds (black) and Mg^{2+} coordinations (purple) in which distance between hetero atoms are < 3Å

According to crystallographic analysis, the position of His_{193}, Cys_{191} and a water molecule adjacent to succinate suggested that these residues could be involved in the deprotonation/protonation step of succinate/*aci*-succinate formation (**Figure 2-2**). The conserved Cys191 seems to be well positioned for this catalytic step. In the work of Moynihan et. al., the active site Cys191 of *Mtb* ICL1 was shown to be involved in the protonation of *aci*-succinate (**Figure 2-3**). Additionally, glyoxylate is buried deeper in the active site, and succinate binding induced closing of the loop. In consensus, *M. tuberculosis* isocitrate lyase 1 comprises a uni-bi ordered kinetic mechanism in which succinate is the first product released and followed by glyoxylate (**Figure 2-3**).
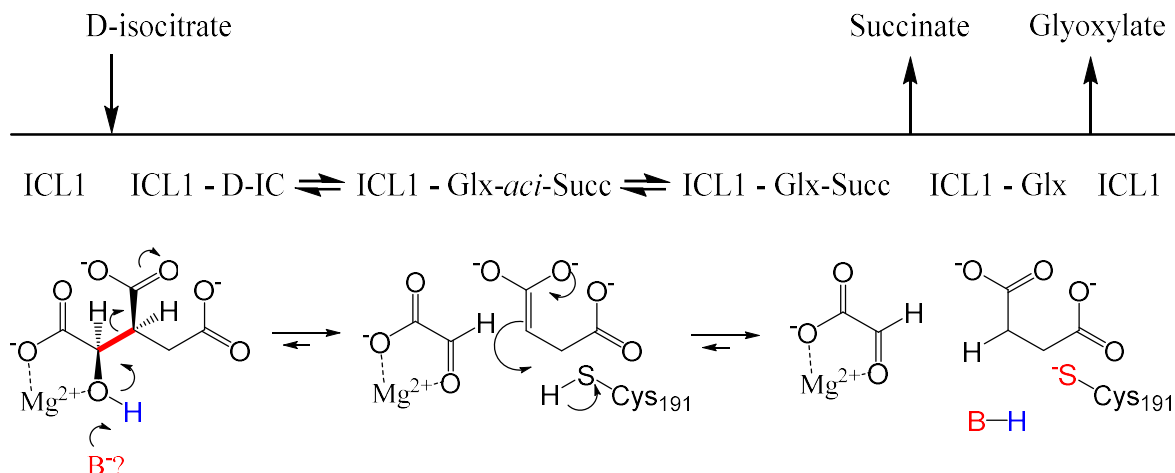
Figure 2-3 Proposed kinetic and chemical mechanism of *M. tuberculosis* isocitrate lyase 1

However, previous studies have yet to identify the catalytic residue(s) involved in the first deprotonation step of ICL retro-aldol cleavage reaction[39, 79]. Since this proton abstraction step was determined to be partially rate limiting in *Mtb* ICL1 catalysis[78, 79], its underlying molecular mechanism is essential to a full understanding of the ICL1 catalytic mechanism. Examining the crystal structures of ligand-bound *Mtb* ICL1, His180, Tyr189, and Mg^{2+}-water were in proximity (< 3 Å) to the hydroxyl group (-OH) of substrate (2*R*,3*S*)-isocitrate. Therefore, either His180, Tyr189, or Mg^{2+}-water could play a role in the first deprotonation step. On the other hand, many metalloenzymes exploit metal-activated hydroxide for catalysis, in which generation of a metal-activated hydroxide requires proton transfer to bulk solvent mediated by a proton shuttle residue[101, 102]. It is prudent to consider that *Mtb* ICL catalyzes the first deprotonation step of isocitrate in a similar fashion.

2.2. Methods

Materials

DL-Isocitrate (trisodium salt), D-threo-isocitrate (potassium salt), NaCl, glycolic acid, D-malic acid, dithiothreitol (DTT), and all other chemicals were obtained from Sigma-Aldrich unless otherwise specified.

Plasmids containing *Mtb icl1* was a gift from Dr. Andrew Murkin of Buffalo University, NY[79].

Protein Purification and Expression

Mtb ICL1 bearing an N-terminal, thrombin-cleavable His_6 epitope tag, was expressed in *E. coli* (BL21 (*DE3*)), and purified using affinity chromatography as previously described[79]. The plasmid was transformed into *E. coli* BL21 (*DE3*) by electroporation (E = 18.0 kV/cm). Transformed cells were cultured in Luria-Bertani broth containing 50 mg/L ampicillin at 37ºC. When the culture reached $OD_{600} = 0.6$, over-expression of ICL2 was induced by IPTG (0.1 mM) for 20 h at 18 ºC. Cells were then harvested and lysed (on ice) by sonication. Insoluble debris was separated from the lysate by centrifugation at 15,000g at 4ºC for 1 h. The supernatant was filtered through a 0.2-μM cellulose acetate membrane (VWR, Inc.), and loaded on to a HisPrep FF 16/10 column (GE Healthcare Life Science) at 0.5 mL/min. The column was washed with 10 column volumes of buffer containing 50 mM Tris-HCl (pH 7.5) and 25 mM imidazole, followed by elution of purified ICL1 with a gradient composed of 15 column volumes of a gradient of 15–40% elution buffer (50 mM Tris-HCl, pH 7.5, 500 mM imidazole). Eluted ICL1 was dialysed with 50 mM HEPES (pH 7.5) and stored in aliquots (>3.5 mg/mL) at –80 ºC.

Mutagenesis and Purification of ICL1 Mutants

Mutant ICL1s (C191S, K189R, K189Q, K190R and K190Q) were obtained via a protocol adopting the Quikchange method[103]. For each mutation, plasmids from 5-10 colonies were sent out for sequencing (Eton Bioscience) in order to confirm the mutagenesis result. Purification of mutant ICL1 enzymes were followed the same procedures for WT ICL1 as described above.

ICL Enzyme Assays

Unless otherwise specified, all assays were conducted in in a clear 96-well plate containing 250 µM reaction mixtures of 50 mM HEPES (pH 7.5), 5 mM $MgCl_2$, and 1 mM DTT at 37ºC. In the direction of isocitrate lysis, product glyoxylate was either converted to glycolate in a coupled-enzyme assay using *E. coli* lactate dehydrogenase (ε_{340} = 6220 $M^{-1}cm^{-1}$) or reacted with phenyl hydrazine-HCl to form a phenyl hydrazone product (ε_{324} = 17,000 $M^{-1}cm^{-1}$). All absorbance measurements were recorded with a Biotek® plate reader.

pH-rate Dependence of Catalysis

ICL1 catalysis was measured via recording of product (glyoxylate) formation over time using phenyl-hydrazine assay as described above. Serial dilution of (2*R*, 3*S*)-isocitrate was prepared at 10X of the final concentrations and transferred to the assay plate first. To the assay buffer containing HEPES, CHES, MOPS and MES (40 mM each, pH 5.8 – 8.4), 10 mM $MgCl_2$ and 1 mM DTT, ICL1 was added to the final concentration of 2 nM. Then enzyme mixture was transferred to the assay plate to start the reaction.

In order to determine pH-rate dependence of catalysis at different temperature, assay buffer was incubated at 28, 31, 34, 37, and 40 ºC prior to the addition of ICL1.

28

pH-rate Dependence of Inhibition by Maleate and Glycolate

ICL1 catalysis was measured via recording of product (glyoxylate) formation over time using phenyl-hydrazine assay as described above with varying inhibitor concentrations (glycolate: $0 - 500$ µM, and maleate: $0 - 2.5$ mM) at several fixed concentration of $(2R, 3S)$-isocitrate (12.5 µM 25 µM and 100 µM). Inhibitors (maleate or glycolate) was added first to the 96-well assay plate, and followed by the addition of $(2R, 3S)$-isocitrate. To the assay buffer containing HEPES, CHES, MOPS and MES (40 mM each, pH $5.8 - 8.4$), 10 mM $MgCl_2$ and 1 mM DTT, ICL1 was added to the final concentration of 2 nM. Then enzyme mixture was transferred to the assay plate (preincubated at 37ºC) to start the reaction. The K_i inhibition constant of glycolate, a competitive inhibitor, was analyzed in a 1/v vs. [I] while the K_{ii} inhibition constant of maleate, an uncompetitive inhibitor, was analyzed in a S/v vs. [I] plot as described before[104].

Solvent Kinetic Effects

Catalysis rate of ICL1(2 nM) was measured in D_2O and H_2O at varying pL with phenyl hydrazine as described above. (2R,3S) isocitrate, $MgCl_2$ and DTT were prepared in H_2O or D_2O appropriately. pD was adjusted by subtracting 0.4 from the pH meter reading.

Analysis of Mutant Enzymes

Catalysis rate was measured as described above. Higher concentrations of enzyme were added in the assay in order to compensate for the slow catalysis rate of K189R, K189Q and K190Q mutants (50 nM, 1 µM and 0.2 µM enzyme in final concentrations respectively). In analysis of pH-dependence of K189Q, $(2R,3S)$-isocitrate was adjusted to the appropriate pH of the assay mixture in order to minimize pH changes caused by addition of $(2R,3S)$-isocitrate.

Molecular Docking

Molecular models of ICL1 in binary complex with (2*R*,3*S*)-isocitrate were built by docking of a minimized model of (2*R*,3*S*)-isocitrate the crystal structure of the C191S mutant *Mtb* ICL1 (PDB: 1F81)[9] using Chimera/AutoDock Vina,[20] which performs fitting of small-molecule ligands with freely rotatable bonds separated by three consecutive covalent bonds or fewer. Glyoxylate and nitropropionate were removed from ICL1 crystal structure to provide space for isocitrate. Search volume was sampled from 5 -25 cubic Å in order to ensure both accuracy and non-bias posing of ligand in the active site. The second lowest energy pose of ICL1-isocitrate complex was selected for its orientation is more consistent with the position of glyoxylate fragment in the X-ray structure in comparison the the lowest energy model provided from Chimera/ Vinadock calculation.

Analysis of Kinetic Data

All data fitting was conducted by global fitting of nonlinear regression using Sigma Plot (Systat Inc) and GraphPad Prism.

Initial velocity data for the forward reactions of ICL were fitted to equations (1) and (2) for a hyperbolic curve and an allosteric model describing cooperativity, respectively.

$$\frac{v}{[E]_t} = \frac{k_{cat}[A]}{K_a + [A]} \tag{1}$$

for which

v is the initial velocity,

$[E]_t$ is the concentration of ICL monomers,

k_{cat} is the turnover number in units of s^{-1},

$[A]$ is the variable concentration of isocitrate

and K_a is Michaelis constant of isocitrate

h is the Hill slope

$$\frac{v}{[E]_t} = \frac{k_{cat}[A]^h}{(K_a)^h + [A]^h} \tag{2}$$

pH-rate profiles were fitted to equation 3-5 describing a bell-shape curve, half-bell with an acidic pK_a, and half-bell with a basic pK_b, respectively,

$$y = \frac{V_{max}^{lim}}{1 + 10^{(pKa - pH)} + 10^{(pH - pK_b)}} \tag{3}$$

$$y = \frac{V_{max}^{lim}}{1 + 10^{(pKa - pH)}} \tag{4}$$

$$y = \frac{V_{max}^{lim}}{1 + 10^{(pH - pK_b)}} \tag{5}$$

for which,

y is either a function of catalysis rate (V/K, V_{max}) or inhibition constant (pK_i)

V_{max}^{lim} is the pH-independent value of y,

and pK_a and pK_b are acid dissociation constants.

pH-rate profiles which approach a non-zero lower limit were fitted to equation (6) and (7).

$$y = \frac{V_{max}^{lim}\left(1 + \gamma 10^{(pK_a - pH)}\right)}{1 + 10^{(pK_a - pH)}} \tag{6}$$

$$y = \frac{V_{max}^{lim}\left(1 + \gamma 10^{(pH - pK_b)}\right)}{1 + 10^{(pH - pK_b)}} \tag{7}$$

for which,

y is either a function of catalysis rates (V/K, and V_{max}) or inhibition constants

(pK_i)

V_{max}^{lim} is the pH-independent value of y,

pK_a and pK_b are acid dissociation constants,

and γ is a fraction coefficient of the pH-independent value, which determines

the non-zero lower limit.

Inhibition constants (K_i or K_{ii}) were determined by global fitting of equation (8).

$$y = K_I([I] + Ycross \tag{8}$$

for which,

y is a function of catalysis rates (1/v, in competitive inhibition, or S/v, in uncompetitive inhibition) where S is a concentration of substrate and v is the initial velocity

[I] is concentration of inhibitor

K_I is either the competitive (K_{is}) or the uncompetitive (K_{ii}) inhibition constant

$Ycross$ is the

Thermodynamic constants of ΔH and ΔS from the temperature dependence of pK_1 and pK_b were determined by fitting data of pK vs. 1/T to equation (9).

$$pK_a^{app} = \frac{\Delta H}{2.303 \text{ x } RT \text{ x } 10^3} - \frac{\Delta S}{2.303 \text{ x } R} \tag{9}$$

for which,

pK_a^{app} is the observed pK_1 or pK_b value at a specific temperature

ΔH is the change in enthalpy upon ionization

ΔS is the change in entropy upon ionization

R is gas constant (R = 8.314 J/K.mol))

T is temperature in K

2.3. Results

Even though X-ray structures of *apo* and ligand-bound ICL1 provided valuable insights on the active site residues, including their identity, and 3-dimensional conformations, these images are static and often lack the information to portray enzyme catalysis, a highly dynamic process, fully. For capturing the key molecular changes in ICL1 catalytic mechanism, pH-dependence of ICL1 catalysis and inhibition together with solvent kinetic isotope effects were examined[105-107].

pH-dependence of ICL1 Stability

Extreme pHs (low and high) could affect enzyme stability by, among other things, disrupting quaternary structures. Unlike the rapid and reversible changes in the protonation states of active-site residues, pH effects on quaternary structure and protein folding level are often slower and could be either irreversible or reversible. In order to establish a suitable range of studying pH-dependence of ICL1 catalysis, a time-dependent stability test of the enzyme in extreme pH conditions (below pH 6.0 and above pH 9.0) was carried out. The normalized activity of ICL1 after incubation at extreme pH conditions for 0-40 min before the enzyme was diluted into the assay buffer at optimum pH 7.5 (**Figure 2-4**). ICL1 remained stable at high pH (up to pH 10) but lost its activity over time at lower pH (below pH 6). At pH 5, ICL1 lost 90% of its activity within 10 min of incubation (**Figure 2-4**).
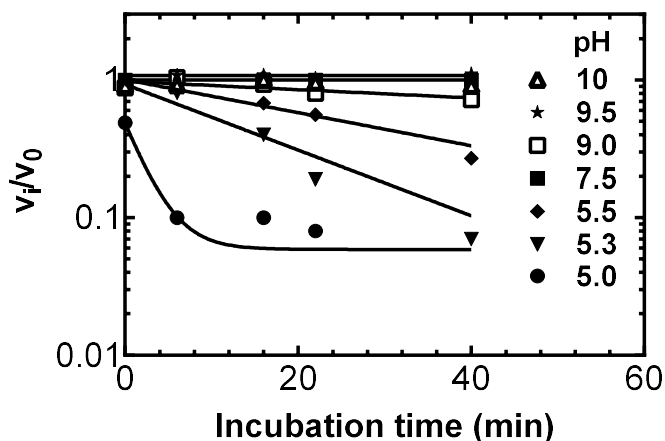
Figure 2-4 pH-dependence of ICL1 stability

ICL1 (1 μM) was incubated in a series of buffer solutions (pH 5.3, 5.5, 6, 7.5, 9.5, 10) for 0 – 40 min and diluted into assay buffer (pH 7.5) to measure remaining retro-aldol cleavage activity. The remaining activity was normalized to that of pH 7.5. Lines drawn through data points were from fitting into an exponential decay (v_i/v_0 = A exp(-kt) + B) where t is the incubation time (min) and k represents the rate of activity loss, A is the initial v_i/v_0 when t ~ 0 and B is the remaining activity when t ~ ∞.

This pH-stability test represented in **Figure 2-4** only detects irreversible changes in ICL1, pH changes could affect quaternary structure of enzymes in a reversible manner, i.e. changes in enzyme cooperativity[108]. Changes in ICL1 cooperativity at high pH (above pH 9) were shown in **Figure A-1**. At pH 9, ICL1 exhibited a non-ideal hyperbolic curve in the initial velocity plot in which the rate is not reaching a plateau at 10 mM of (2R,3S)-isocitrate. At pH 9.5 and 10 the curves are no longer hyperbolic, demonstrating a distinct change in the enzyme cooperativity. Preliminary studies of pH-rate dependence of ICL1 retro-aldol catalysis were conducted in a pH range of 5.0 – 9.0, in which the initial rate was corrected by a factor of 2 and 1.3 for pH 5.0 and pH 5.5 in order to account for activity loss due to enzyme instability at low pH as shown in **Figure 2-4**. A pH profile of k_{cat}/K_m displayed a bell-shaped curve which showed deviations from the fitted curve at pH < 5.8 and an apparently aberrant high value for k_{cat} at pH 9.0 (**Figure A-5**). Therefore, the following pH

rate studies of ICL1 catalysis and inhibition focused on pH range from 5.8 – 8.4 for measurements that are more reliable.

pH Profiles of ICL1 Catalysis and Inhibition

ICL1 retro-aldol catalysis consists of two chemical steps: first, the deprotonation of a hydroxyl group concerted with C-C bond cleavage and second, the protonation of the resulting *aci*-succinate. The pH-dependence of ICL1-catalyzed isocitrate cleavage was quantified by pH effects on V/*K* (or k_{cat}/K_m) and V_{max} (or k_{cat}). Effects on V/*K* over a range of pH reflects mainly the free enzyme form which is productive for binding of substrate and for forming the transition states (TS) along the reaction coordinate (**Figure 2-5**)[109]. On the other hand, effects on V_{max} captured the catalytic states that favor the TS formation and later steps in the presence of saturating substrates, which represents the E-substrate and subsequent complexes (**Figure 2-5**).
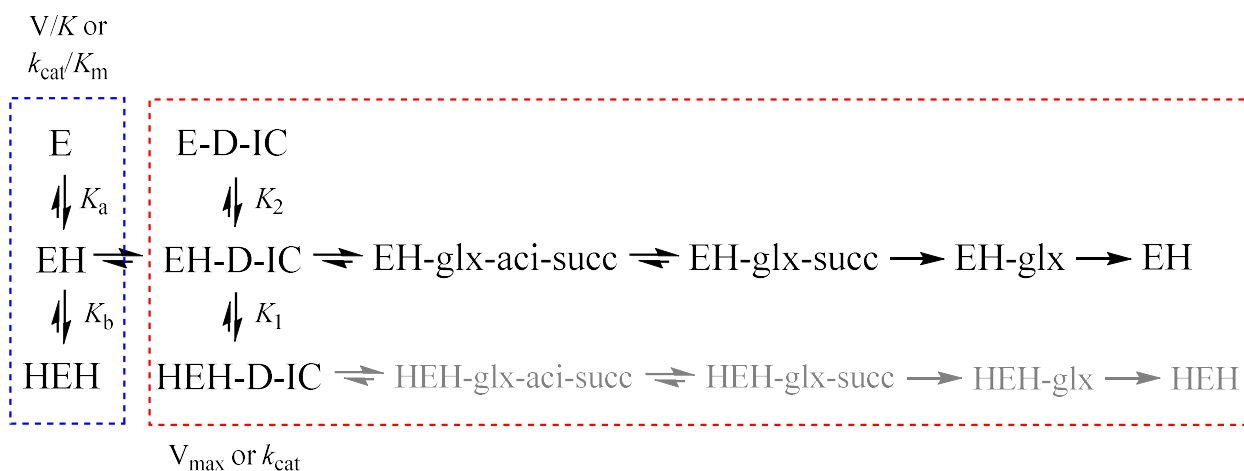

Figure 2-5 A simplistic model of possible pH effects on V/*K* and V_{max} of ICL1 retro-aldol catalysis

The profile of V/*K* or k_{cat}/K_m, from pH 5.8 – 8.4, exhibited a half bell-shaped curve in which increasing of pH led to a decrease in k_{cat}/K_m with an apparent slope of -1 and an

acid dissociation constant ($pK_b = 7.0 \pm 0.1$). Acid dissociation constants of substrate (isocitrate) are 3.2, 4.7, and 6.2, and so are 3, for which pK_b is unlikely to be associated with one of the carboxylate groups on isocitrate. Therefore, pK_b, derived from the pH-rate profile of k_{cat}/K_m, probably represented the acid dissociation constant of one acidic group on ICL1. In contrast, the profile of k_{cat} vs. pH adopted a wave-shaped curve indicating that there might be multiple rate limiting steps during ICL1 retro-aldol catalysis (**Figure 2-6**). As pH increased, k_{cat} increased, which is consistent with deprotonation of a general base catalytic residue ($pK_1 = 6.9 \pm 0.1$). The active-site residue reflected by pK_1 is likely involved with the first proton abstraction step in which deprotonation of the catalytic base (B^-) would increase the rate.

Yet complete protonation of this residue did not eliminate catalysis, and the remaining k_{cat} rate at pH 5.8 was about one-fourth of the turnover rate at pH 8.0. When K_1 is protonated, catalysis proceeds at a slower rate. One hypothesis is that both Mg^{2+}-bound water and Mg^{2+}-bound hydroxide might act as the catalytic base but the latter results in a faster catalysis. Enzymes which utilize metal-bound hydroxide as a specific base have been shown to exhibit inverse solvent kinetic isotope effects (sKIE < 1) due to the formation of metal-bound deuterium oxide ($M-OD^-$) is more favored than metal-bound hydroxide ($M-OH^-$)[102]. However, solvent kinetic isotope effects of ICL1 catalysis is normal for both V/K and V_{max} (**Figure A-6**, ^{kcat}sKIE = 1.3 ± 0.2 (low limit), ^{kcat}sKIE = 1.0 ± 0.2 (high limit) and $^{V/K}$sKIE = 1.7 ± 0.2) which suggested that deprotonation of another active side residue (described by pK_1) activates Mg^{2+}-bound water to accept a proton from the substrate, isocitrate. The proton shuttle from pK_1 residue to activate Mg^{2+}-bound water is similar to that in human carbonic

anhydrase[110] and arginase[111]. Nevertheless, the pK_1 value provided a tool to monitor the first deprotonation step during retrol-aldol catalysis of ICL1.
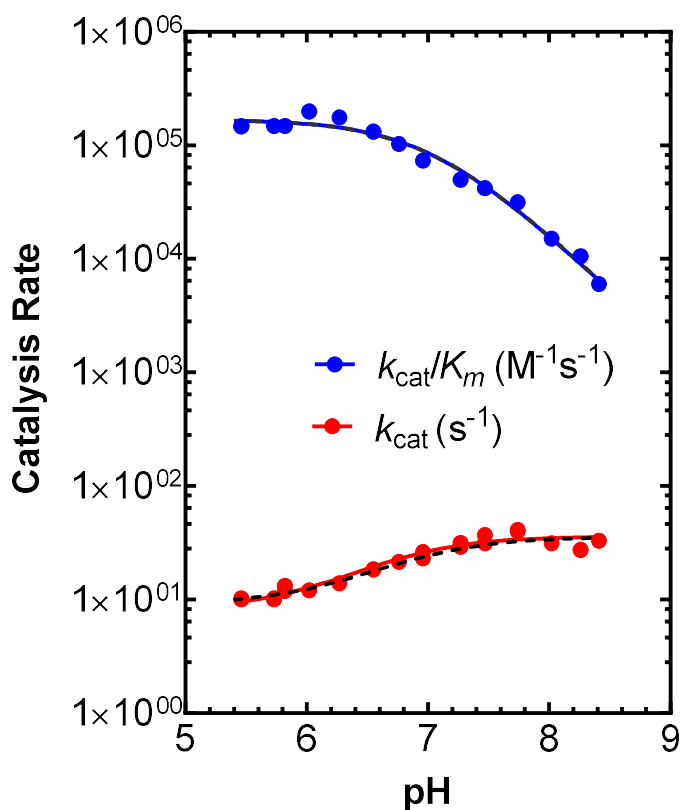
Figure 2-6 pH-rate profiles of ICL1-catalyzed isocitrate cleavage

Initial velocities of ICL1 catalysis at different concentration of (2R,3S)-isocitrate were fitted into equation (1) to obtain k_{cat}/K_m and k_{cat} data points. Continuous-lines were drawn from fitting k_{cat}/K_m and k_{cat} data points to equation (5) and (6), respectively. Dashed-lines were a result of global fitting of initial velocity data to equation (1), (5) and (6) simultaneously to yield pK_b and pK_1 values.

While pK values obtained from pH rate profiles of V/K (k_{cat}/K_m) or V_{max} (k_{cat}) are of substrates often inaccurate due to the "stickiness" of the substrate[112], the determination of provide pK values from that are perturbed from true values due to the stickiness of the variable subtrate. However, by measuring the pH dependence of competitive inhibitors, one

can elucidate more accurate pK values of the pKs of enzymatic groups. We evaluated the pH dependence of the inhibition constants (pK_i) of glycolate and maleate, which are, respectively competitive and uncompetitive inhibitors of ICL1 vs. isocitrate. As pH responses of V/K or k_{cat}/K_m For maleate, the plot of pK_i vs. pH was similar in form to that of V/$K_{isocitrate}$ vs. pH, and from fitting of the data to equation 5 we obtained a value of pK_b = 7.1 ± 0.1. (**Figure 2-7**). In contrast, the plot of pKi vs. pH for glycolate, a competitive inhibitor that mimics glyoxylate, was insensitive to pH changes from pH 6.2 – 8.0. Below pH 6.2, the value of pK_i decreases suggesting that binding of glycolate is favorable when an ionizable group on either ICL1 or glycolate is deprotonated. In contrast, the plot of pK_i vs. pH for glycolate suggests on its left-hand side the presence of a half bell-shaped curve bloew pH = 6.2, for which a value of pK_a was ~ 5.0 may be estimated, which is outside of the pH range of the experiment for a reliable measurement. Regardless, the protonation states of the active site residue described by pK_b played a key role in the binding interactions between ICL1 and the succinate-fragment rather than glyoxylate-fragment of isocitrate.
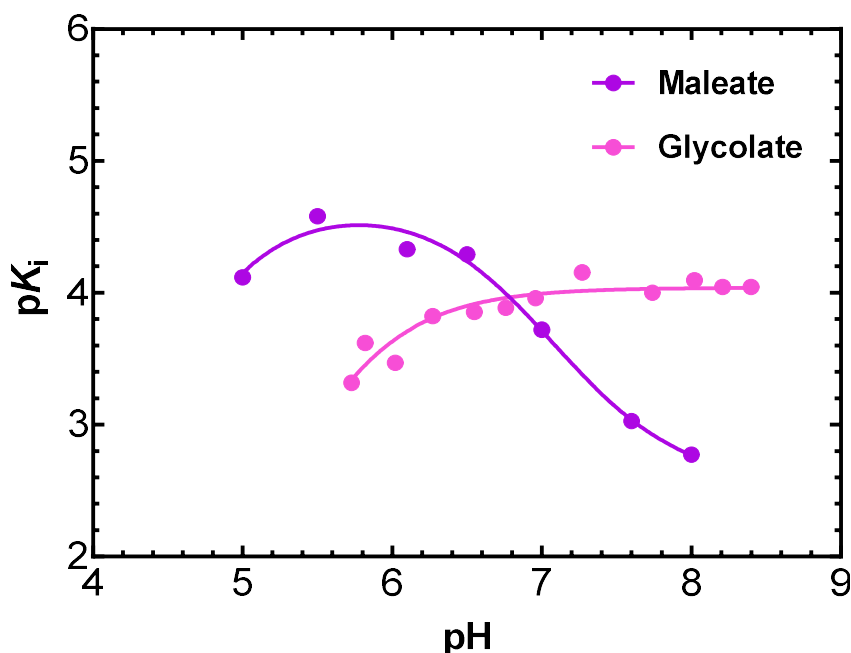
Figure 2-7 pH-dependence of inhibition constant, pK_i, of glycolate and maleate

K_i was determined using Cornish-Bowden's method[104] in duplicate. Initial velocity of catalysis was measured in varying concentrations of glycolate or maleate at several fixed concentration of (2R, 3S)-isocitrate. K_{is}, the competitive inhibition constant of glycolate, and K_{ii}, the uncompetitive inhibition constant of maleate, were determined by equation (8). Lines drawn from pK_i vs. pH experimental mean data points were from curve fitting into equation (4) & (7) for glycolate and maleate, respectively, which yielded $pK_a \sim 5$ for glycolate and $pK_b = 7.1 \pm 0.1$ for maleate.

Thermodynamic Constants of the Observed pK$_a$ Values

Thermodynamic properties of acid dissociation constants observed in pH-rate profiles could be used to identify the corresponding active site residues. pH-rate profiles of V/K and V_{max} were measured at increasing temperatures (25-41 °C) and the observed pK_a values were replotted against the reciprocal temperature, yielding the corresponding thermodynamic constants (ΔS and ΔH). For the pK_b obtained from the plot of V/K vs. pH, ΔH was 3.0 ± 3 kcal/mol and ΔS was -21 ± 1 cal/mol, consistent with the acid dissociation of carboxylate compounds[113, 114]. Even though, the pK_b value of 7.1 ± 0.1 is high for the ionization of

41

carboxylate residues (glutamate and aspartate), elevated ionization constants were observed in interior residues of hydrophobic enzyme pockets[115-117].
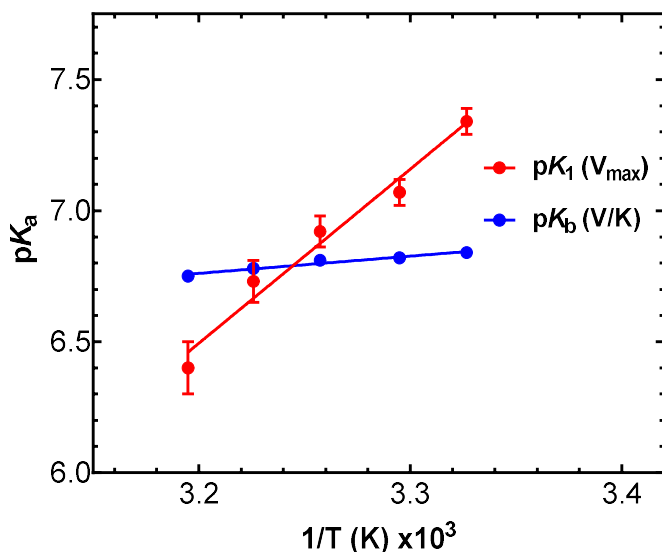
Figure 2-8 Temperature-dependence of pK_1 and pK_b

Initial velocities of ICL1 catalysis at different concentration of (2R,3S)-isocitrate were globally fitted into equation (1), (5) and (6) simultaneously to yield pK_b and pK_1 values at various temperatures (28-40°C). Lines drawn through pK_b and pK_1 were from linear regression analysis of pK_a vs. 1/T (K, x10^3). ΔH and ΔS values (shown in **Table A-1**) were calculated from equation (9).

For the pK_1 obtained from the plot of V_{max} vs. pH, both entropic and enthalpic values were considerably larger than typical values obtained from simple acid dissociations (ΔH = 30 ± 3 kcal/mol, ΔS = 60 ± 9 cal/mol), suggesting that these values were the results of conformational changes during catalysis[112] (**Figure 2-8**). Comparison of apo-ICL1 and ligand-bound ICL1 revealed that the active site loop undergoes a movement of at least 15 Å upon ligand binding (**Figure 2-9**). Therefore, the observed pK_1 in the plot of k_{cat} vs. pH likely described the side chain of an amino acid located on this flexible loop.
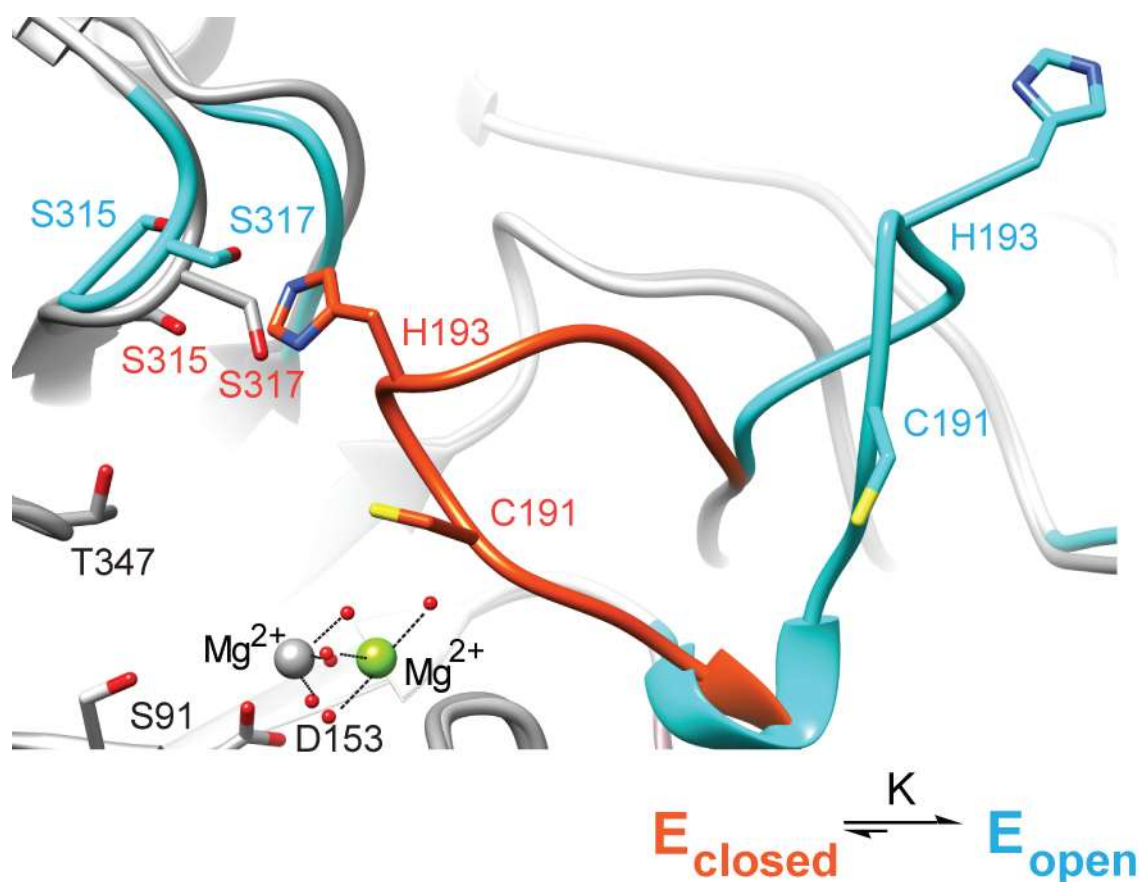
Figure 2-9 Movement of the active-site loop of *Mtb* ICL1 upon ligand binding

The figure showed an overlay of apo-ICL1 (E_{open}) structure (1F61, cyan) and ligand-bound-ICL1 (E_{closed}) structure (1F8I, orange) focusing on the active-site loop movement in which glyoxylate and nitro-propionate was removed for simplicity.

Structure-guided Identification of the Catalytic Base Residue

Data obtained from pH-rate profiles and solvent kinetic isotope effects, aided by crystal structures and molecular modelling (**Figure 2-10**, **Figure A-2**), indicated that Lys189 could be the catalytic residue underlying the initial deprotonation step of ICL1 retro-aldol catalysis. Tyr89 and His180 are in close proximity (< 3 Å) the hydroxyl group of isocitrate but they are unlikely to be deprotonated due to their buried location in ICL1 active site and their interactions with nearby carboxylic groups. Previous studies showed that Y89F and H180A

did not eliminate catalysis, which weaken the hypothesis of these residues as the direct proton donor/acceptor in ICL1 catalysis (Moynihan, unpublished work).
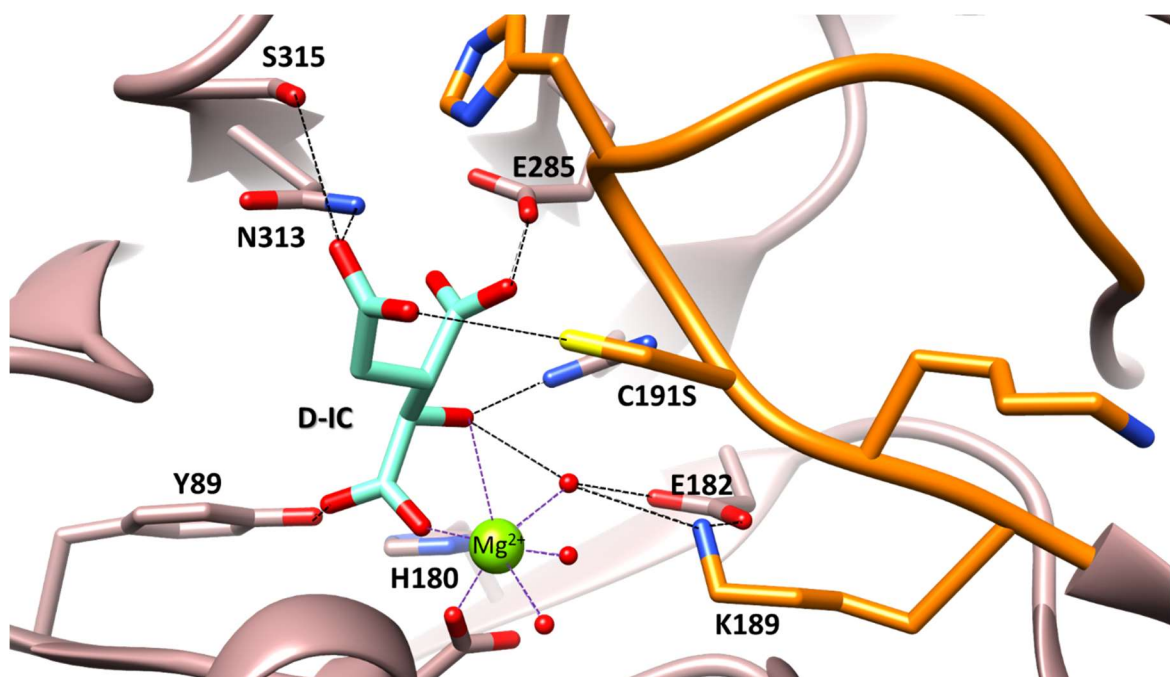
Figure 2-10 Molecular modeling of (2*R*,3*S*) isocitrate in ICL1 structure of closed conformation. Modelling of (2R,3S)-isocitrate (D-IC, cyan) in ICL1 active site was obtained with Chimera/VinaDock. Dash-lines display potential interactions (< 3Å) in D-IC-bound ICL1 active site.

A glutamate residue was also proposed as the catalytic base in ICL/PEPM family[33]. In ICL1, Glu182 is in favorable position to serve as the catalytic base to activate Mg^{2+}-bound water. However, the aberrantly large value of ΔH associated with K_1 suggested that the catalytic base residue likely involves a conformational change, such as movement of the active-site loop, whereas Glu182 is not located on this active loop. On the other hand, Glu182 does not interact with other carboxylic groups to facilitate the observed pK_1 value ($pK_1 = 6.9 \pm 0.1$) which is abnormally high for carboxylate residues. As for K189, even though, a pK_1 value of 7 is unusual low for a lysine, lysine residues buried in protein interior and/or interacting

with carboxylate groups reportedly comprise depressed dissociation constants as low as 5.3[118]. In fact, the amine group of Lys189 is within hydrogen bonding distance to the γ-carboxylate group of Glu182, supporting its depressed pK_1 value of ~7. In *Mtb* isocitrate dehydrogenase, an aspartate was proposed to deprotonate the catalytic base lysine[119]. O-succinylbenzoate synthase (OSBS) and acetoacetate decarboxylase are among examples of enzymes containing catalytic lysines that serve as a general base in catalysis[120, 121]. In these enzymes, the pK value of the catalytic lysine is approximately 7.0[121]. In addition, it was proposed that the presence of nearby positively charge residues (lysine and arginine) could direct the conformation of catalytic lysines and depress their pK_a[121, 122]. This maybe the feature of the dipeptide lysinyl-lysine in the active site of ICL enzymes. Even though, the distance between γ-N of Lys189 and Lys190 is approximately 10 Å in ICL1 crystal structures, amino acids with long side chains often have a broad conformation dynamics[122, 123]. Analysis of possible rotamers of K189 and K190 in solution suggested the electrostatic distance could be as short as 5.8 Å, which supports electrostatic interactions between the two residues[124].

Analysis of Lys189 and Lys190 Mutants

Therefore, ICL1 mutants in which the Lys189 and Lys190 residues were replaced by either glutamine or arginine were analyzed (**Table 2-1**). Among the lysine mutants studied, the K189Q ICL1 mutant exhibited the most significant decrease in the catalysis rate, followed by K190Q, K190R and K189R respectively (**Table 2-1**). The maximal rate of catalysis (k_{cat}) was 2.0 x 10^4-fold slower than wildtype ($^{K189Q}k_{cat} = 1.0$ x 10^{-3} s^{-1}; $^{WT}k_{cat} = 20$ s^{-1}) while the catalytic efficiency ($k_{cat}/K_{D\text{-}IC}$) decreased 3.0 x 10^6 fold ($^{K189Q}k_{cat}/K_{D\text{-}IC} = 0.3$ M^{-1}s^{-1}; $^{WT}k_{cat}/K_{D\text{-}IC} = 6.1$ x 10^5 M^{-1}s^{-1}).

Table 2-1 Summary of pH-rate profiles and kinetic parameters from mutant and WT ICL1s

	K190R	K189R	K190Q	K189Q	WT
k_{cat} (s^{-1})	10.8 ± 0.2	5.3 ± 0.4	0.5 ± 0.1	1.0 x 10^{-3}	19 ± 1
$K_{D\text{-}IC}$ (µM)	220 ± 10	580 ± 30	5.5 x 10^3	2.2 x 10^3	32 ± 6
$k_{cat}/K_{D\text{-}IC}$ (M^{-1}s^{-1})	5.4 x 10^4	8.8 x 10^3	1.0 x 10^2	0.3	6.1 x 10^5
pK_1	5.8 ± 0.1	6.4 ± 0.1	ND	NA	6.9 ± 0.1
pK_b	7.1 ± 0.1	6.8 ± 0.1	ND	*5.6 ± 0.2	7.0 ± 0.1
pK_2				7.3 ± 0.1	

* pK_b value is outside of the experimental range and might not represent a reliable estimate
Kinetic parameters of mutants and WT were measure in 50 mM HEPES (pH 7.5). ND – not determined.

Even though Lys190 points away from the active site, the K190Q mutation exerted significant effects on ICL1 catalysis. The maximal rate of catalysis (k_{cat}) was approximately 40-fold slower than wildtype ($^{K189Q}k_{cat} = 0.5$ s^{-1}; $^{WT}k_{cat} = 20$ s^{-1}). The catalytic efficiency

(k_{cat}/K_{D-IC}) decreased 6000-fold ($^{K189Q}k_{cat}/K_{D-IC} = 1.0 \times 10^2$ M^{-1}s^{-1}) in comparison with WT ($^{WT}k_{cat}/K_{D-IC} = 6.1 \times 10^5$ M^{-1}s^{-1}). On other hand, K190R showed the least disruption to catalysis of ICL1 ($k_{cat} = 10.2 \pm 0.2$) and the catalytic efficiency was reduced only by 10-fold ($^{K190R}k_{cat}/K_{D-IC} = 5.4 \times 10^4$ M^{-1}s^{-1}). It appears that the positive charge of Lys190 plays an important role in ICL1 catalysis. One potential role of Lys190 is the formation of salt-bridges and electrostatic interactions governing the active site loop conformation.

The pH-rate profile allows a more in-depth examination of effects on ICL1 catalysis caused by mutations of Lys189 and Lys190. In both the K189R and K190R mutants of ICL1, the observed pK_1 was lower than in WT ICL1 (**Table 2-1**). The more depressed pK_1 of Lys189 and Arg189 in the mutant enzymes, when compared to the pK_1 of Lys189 in WT ICL1, could be a result of stronger electrostatic effects between the Lys/Arg pair. Electrostatic force is reciprocally proportional to the distance between two charge groups which is reduced in the arginine mutants owning to a more disperse cationic sphere of Arg.

Proton transfers to residue 189 near pH 7.0 were important to ICL1 catalysis and could be the basis of the observed pK_1. In **Figure 2-11**, the pH-rate profile of the K189Q mutant was distinctly different from WT and other mutants. For the plot of k_{cat} vs. pH, replacing Lys189 with glutamine eliminated the pH-dependence of the pK_1 residue (**Table 2-1**). The proton transfer corresponding to pK_1 was abolished since glutamine is unable to accept or donate protons, supporting our proposal that the observed pK_1 as found in WT ICL1 pertains to Lys189.

The upward "wave-shaped" curve for WT ICL1, however is now instead, a downward "half-bell shaped" curve for K189Q mutant for which p$K_2 = 7.3$ (**Figure 2-11**). Perhaps, the pH effects from Lys189 in WT ICL1 obscured this pK_2. This pK_2, together with

the pK_1 from Lys189, accounted for the wave-shaped pH profile in which the favorable effects of Lys189 deprotonation were diminished by the deprotonation of the pK_2 residue (**Figure 2-12**).
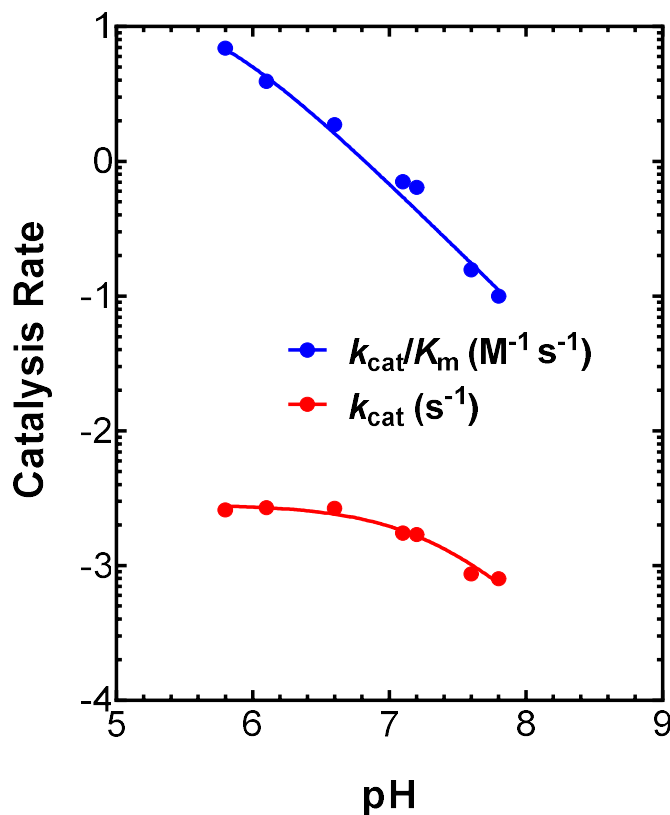
Figure 2-11 pH-rate profile of K189Q ICL1 mutant in the direction of isocitrate cleavage.

Initial velocities of ICL1 catalysis at different concentrations of (2R,3S)-isocitrate were fitted into equation (1), and global curve fitting to equation (1) and (5) simultaneously to obtain average k_{cat}/K_m and k_{cat} data points at variable pH shown above. Continuous-lines were drawn from fitting k_{cat}/K_m and k_{cat} data points to equation (5) to yield pK_b and pK_2 values.
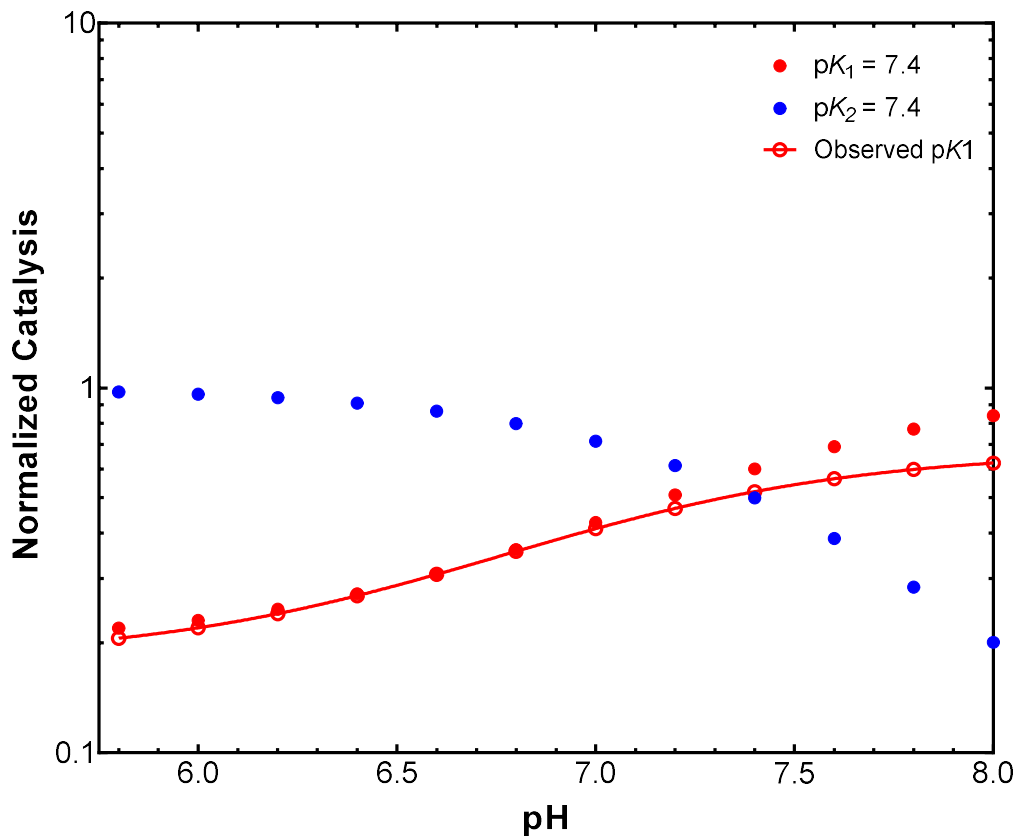
Figure 2-12 Simulation of opposing pH effects from pK_1 and pK_2 in ICL1 catalysis

Data were simulated for pH-rate dependence on two catalytic residues described by $pK_1 = 7.4$ in equation (6) and $pK_2 = 7.4$ in equation (5). The pH-dependence of observed catalytic rates (observed pK_1) were calculated by summation of individual rates ($1/k_{obs} = 1/k_1 + 1/k_2$), from which pK_b catalytic step is 10-fold faster than pK_1 (the maximal rates were normalized to 1). The line drawn through the observed pK_1 data points was from fitting into a wave equation, equation (6), whose estimated $pK_1 = 7.0$

For the plot of k_{cat}/K_m vs. pH, K189R and K190R ICL1 mutants behaved similarly to WT in which they both displayed a downward bell shape curve with a slope of -1. The values of pK_b were 6.9 and 7.0 for K189R and K190R ICL1 mutants respectively; these values are not significantly different from that of WT ICL1 (**Table 2-1**). In contrast, the plot k_{cat}/K_m vs. pH of K189Q mutant enzyme displayed a half-bell-shaped curve with a slope of approximately -2 (**Figure 2-11**). The slope of -2 in the plot of k_{cat}/K_m vs. pH suggested that catalysis is sensitive to the deprotonation of 2 different groups. The value of pK_b of 5.6 for

K189Q ICL1 was significantly lower than that of WT, which indicated a distinct protonation state of K189Q mutant required for substrate binding. Even though this value is below the experimental range and its value might not be estimated accurately, it showed that the K189Q ICL1 mutant had most likely adopted a different conformation for substrate binding and catalysis.

2.4. Conclusions

From the pH-rate profiles and the thermodynamic parameters (ΔH and ΔS) we have identified at least one crucial interaction for binding of succinate or isocitrate to ICL1 involving a putative carboxylate group whose $pK_a \sim 7$. Examining the crystal structure of ICL1 and its ligand narrowed the interactions to that of Glu285. This elevated pK_a of glutamate is expected for a buried residue within a highly anionic active site. In addition to facilitating succinate binding, the protonated Glu285 might play a role in stabilization of the oxyanion hole during ICL catalysis **(Figure 2-13)**.

It was also possible to pinpoint the origin of pK_1 to residues on the active-site loop, which indirectly catalyzed the first deprotonation step of isocitrate cleavage. According to ligand-bound ICL1 structures, Lys189 is the most probable candidate for activating Mg^{2+}-bound water that then initiates the deprotonation of isocitrate. Lys189 is located on the active-site loop, which adopts a conformation changes during catalysis. Together with crystal structures, pH rate profiles and mutagenesis studies supported that the residue interacts with a Mg^{2+}-bound water aligned favorably for proton abstraction (**Figure 2-13**). Some precedents of this concerted action between active site residue and metal-bound water are found with acetoacetate decarboxylase[121], human carbonic anhydrase[101], and menaquinone-specific isochorismate synthase (MenF)[125].
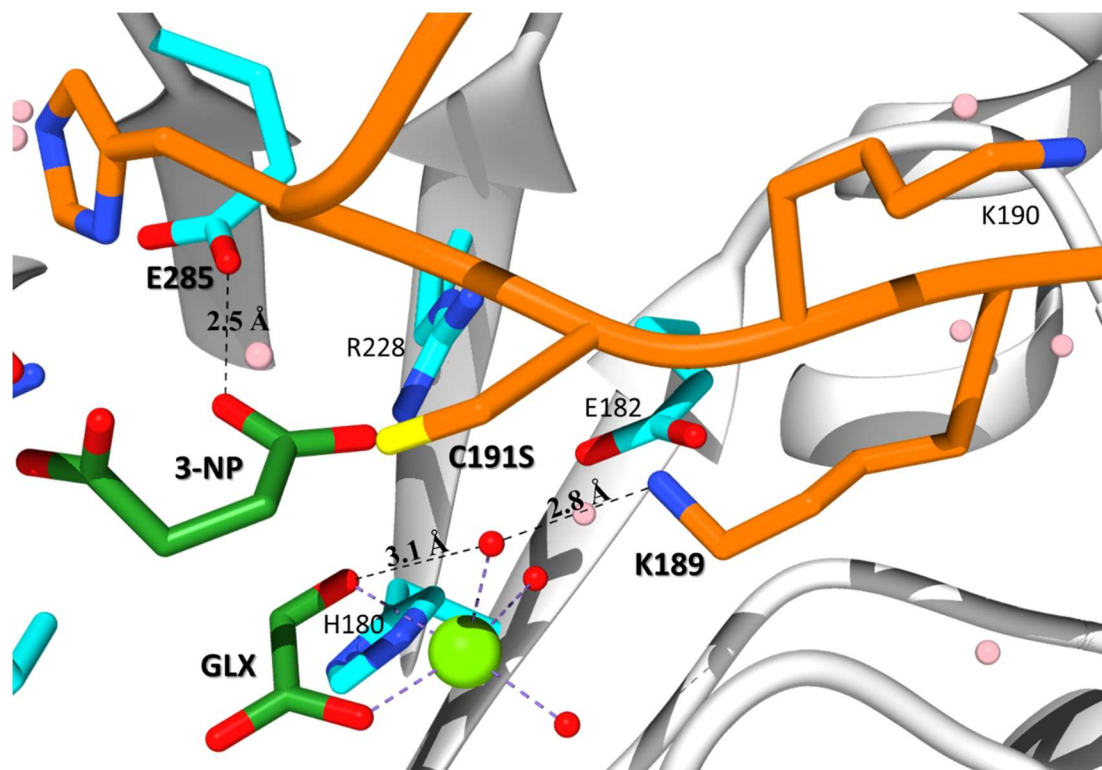
Figure 2-13 Lys189 and Glu285 positions in active site and the putative identity of pK_a values

The figure was prepared from the crystal structure of ICL1 in complex with glyoxylate and nitro-propionate[39].

On the other hand, the observed pH-rate profiles cannot completely rule out the possibility that K189Q mutant does not only affect the first deprotonation step but also plays other roles during catalysis. The K189Q mutation could hamper the protonation of *aci*-succinate, making this step more rate limiting. However, Lys189 is pointing toward the glyoxylate site rather than the succinate site. Perhaps, a more satisfying explanation is that the K189Q mutation, lacking the catalytic base to activate Mg^{2+}-bound water, adopts a catalytic pathway distinct from WT in which the first deprotonation step is coupled with the protonation of Cys191. It is expected for the K189Q mutant, which contains a deficient catalytic base residue, to accommodate catalysis via an alternative kinetic pathways and/or

conformation. These results further supported that Lys189 is important to ICL1 catalysis in which it acts as a base to facilitate the first deprotonation step of isocitrate cleavage via activation of Mg^{2+}-water (**Figure 2-14**).
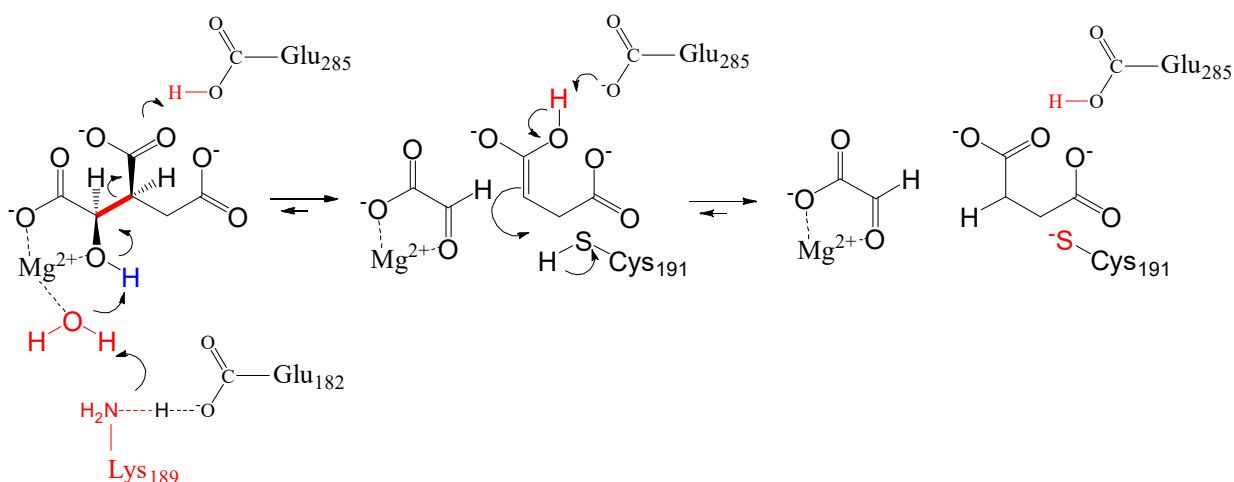
Figure 2-14 Putative assignments of Glu285 and Lys189 as the catalytic residues described by pK_b and pK_1

Notably, the role of a catalytic base lysine is conserved among enzymes in the enolase superfamily and other enzymes whose reactions exploit enolic intermediates[120, 126]. The *aci*-succinate intermediate in ICL catalysis is similar to that in mandelate racemase and other enolase superfamily enzymes[127, 128]. Structural similarities between isocitrate lyase and enolases suggest possible relationships in aspects of the mechanism. On the other hand, recent studies have suggested that acetylation and/or succinylation of Lys189 could underlie an *in vivo* negative feedback regulation of ICL activity, emphasizing both the nucleophilicity and the catalytic significance of the residue[129]. However, it is unclear if Lys189 acts alone or via a proton relay mediated by Glu182 and other residues. Further studies of ICL1 mutants (e.g. E182Q) are required to identify other components of this proton-shuttle network.

3. MECHANISM-BASED INACTIVATIONS OF *Mycobacterium tuberculosis* ISOCITRATE LYASES BY 2-VINYL ISOCITRATE[*]

3.1. Introduction

The catalytic mechanism of *Mtb* ICL[39, 79] is initiated when (2*R*,3*S*)-isocitrate (D-IC) coordinates an active-site magnesium ion, and undergoes a base-catalyzed, retro-aldol reaction to form glyoxylate and the *aci*-anion of succinate. We proposed that Lys189 activates an Mg^{2+}-bound water to catalyze the first proton abstraction (chapter 2). Movement of the active-site loop upon substrate binding brings Cys191 in position for protonation of *aci*-succinate to form succinate[39, 79] (**Figure 2-3**). It was reported that in the isocitrate synthesis direction, Cys191 act as a general base to catalyze the formation of *aci*-succinate from succinate[79]. The nucleophilic Cys191 also undergoes a substitution reaction (SN_2) with bromo-pyruvate, leading to the inactivation of ICL[56]. Even though, bromo-pyruvate is reactive[60] and presents a poor candidate for drug development, one could envision that mechanism based inactivation of ICL via targeting Cys191 nucleophilicity is promising. Not only have that mechanism-based inactivators had a history of proven success[71, 90, 92], ICL1 retro-aldol catalysis offers a unique opportunity to elaborate electrophilic substituents at C_2 of (2*R*,3*S*)-isocitrate analogs into active-site nascent inactivators (**Figure 3-1**). For instance, bromo-isocitrate (Br-IC) would undergo an ICL-catalyzed retro-aldol cleavage to yield bromo-pyruvate and succinate. As succinate is released, active-site generated bromo-pyruvate will react with Cys191 and inactivates the enzyme. Exclusive association with ICL active site would hinder bromo-pyruvate from reaction with off-target enzymes.

---

[*] Part of the data reported in this section is reprinted with permission from "Mechanism-based inactivator of isocitrate lyase 1 and 2 from *Mycobacterium tuberculosis*" by Pham V. T., Murkin A. S., Moynihan M. M., Harris L., Tyler C. P., Shetty N., Sacchettini J. C., Huang H., and Meek T. D. (2017) *PNAS 114*, 7617-7622, Copyright 2017 National Academy of Sciences
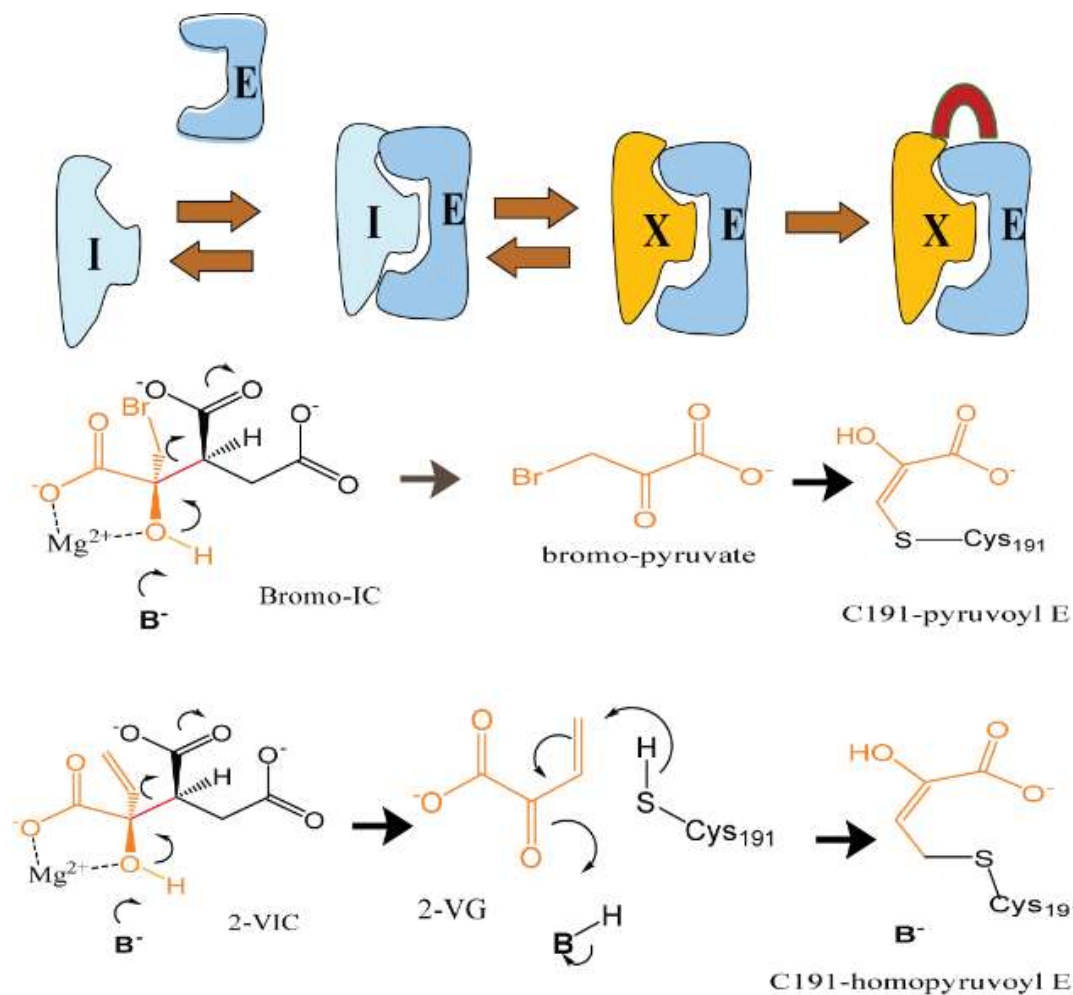
Figure 3-1 Hypothetic mechanism-based inactivation(s) of ICL1

ICL-catalyzed unmasking of nascent electrophilic substituents at C_2 of $(2R,3S)$-isocitrate analogs: 2-bromo-$(2R,3S)$-isocitrate (bromo-IC) and 2-viny-$(2R,3S)$-lisocitrate (2-VIC)

As *Mtb* ICL1 was able to catalyze the retro-aldol cleavage of both isocitrate and methylisocitrate, we proposed that 2-vinyl-$(2R,3S)$-isocitrate (2-VIC) would represent a suitable mechanism-based inactivator (**Figure 3-1**). ICL-catalyzed cleavage of the C_2–C_3 bond would produce succinate as well as an enzyme-bound Michael acceptor, 2-vinyl-glyoxylate (2VG), which is poised to react with the thiolate form of the proximal Cys191.

We described the kinetic and structural analysis of the mechanism-based inactivation of *Mtb* isocitrate lyases 1 and 2 by 2-VIC[43].

3.2. Methods

Materials

DL-Isocitrate (trisodium salt), D-threo-isocitrate (potassium salt), NaCl, dimethyl sulfoxide (DMSO), sodium glyoxylate (monohydrate), succinic acid, D-malic acid, glutathione (reduced form), dithiothreitol (DTT), Lactate dehydrogenase (LDH) and all other chemicals were obtained from Sigma-Aldrich unless otherwise specified.

Plasmids containing *Mtb icl1* was a gift from Dr. Andrew Murkin of Buffalo University, NY[79].

Icl2-pET26-b plasmid was provided by GlaxoSmithKline Pharmaceuticals, PA.

E. coli isocitrate dehydrogenase (ICDH) gene was obtained from Aska (-) clone containing *icd* gene on a pCA24N plasmid[79, 130].

Protein Purification and Expression

Mtb ICL1 bearing an N-terminal, thrombin-cleavable His$_6$ epitope tag, was expressed in *E. coli* (BL21 (*DE3*)), and purified using affinity chromatography as previously described[79]. The plasmid was transformed into *E. coli* BL21(*DE3*) by electroporation (E = 18.0 kV/cm). Transformed cells were cultured in Luria-Bertani broth containing 50 mg/L ampicillin at 37°C. When the culture reached OD$_{600}$ = 0.6, over-expression of ICL2 was induced by IPTG (0.1 mM) for 20 h at 18 °C. Cells were then harvested and lysed (on ice) by sonication. Insoluble debris was separated from the lysate by centrifugation at 15,000g at 4 °C for 1 h. The supernatant was filtered through a 0.2-μM cellulose acetate membrane (VWR, Inc.), and loaded on to a HisPrep FF 16/10 column (GE Healthcare Life Science) at 0.5 mL/min.

The column was washed with 10 column volumes of buffer containing 50 mM Tris-HCl (pH 7.5) and 25 mM imidazole, followed by elution of purified ICL1 with a gradient composed of 15 column volumes of a gradient of 15–40% elution buffer (50 mM Tris-HCl, pH 7.5, 500 mM imidazole). Eluted ICL1 was dialysed with 50 mM HEPES (pH 7.5) and stored in aliquots (>3.5 mg/mL) at –80 ºC.

Similarly, a truncated form of ICL2 (aa 1-605; GI: 489504700) with a C-terminal His$_6$ tag on PET-26b plasmid was expressed in *E. coli* BL21(*DE3*) and purified with affinity chromatography as described above.

ICL Enzyme Assays

Unless otherwise specified, all assays were conducted in in a clear 96-well plate containing 250 μM reaction mixtures of 50 mM HEPES (pH 7.5), 5 mM MgCl$_2$, and 1 mM DTT at 37ºC. In the direction of isocitrate cleavage, product glyoxylate was either converted to glycolate in a coupled-enzyme assay using *E. coli* lactate dehydrogenase (ε_{340} = 6220 M^{-1}cm^{-1}) or reacted with phenyl hydrazine-HCl to form a phenyl hydrazone product (ε_{324} = 17,000 M^{-1}cm^{-1}). In the direction of isocitrate synthesis, isocitrate product was converted to α-ketoglutarate in a coupled-enzyme assay using *E. coli* isocitrate dehydrogenase (ε_{340} = 6,220 M^{-1}cm^{-1}). All absorbance measurements were recorded with a Biotek® plate reader.

Inactivation Assays via Preincubation Method

The time-dependent inactivation of ICL1 by 2-VIC was assessed by pre-incubation studies, in which residual enzyme activity was measured as initial velocity of either the forward or reverse reactions after pre-incubation of enzyme with 2-VIC. For the reverse reaction of ICL, 0.6 mL-reaction mixtures containing 50 mM HEPES (pH 7.5), 5 mM MgSO$_4$, 0.8 μM ICL, and 0–40 μM inactivator were incubated in sealed Eppendorf tubes. Fifty-microliter

samples were withdrawn from the pre-incubation mixtures at 0–300 min for determination of residual ICL1 activity by spectrophotometric measurement (Cary 100 spectrophotometer; 340 nm) of the absorbance of NADPH formation using the isocitrate dehydrogenase assay.

For measurement of residual ICL activity during the forward reaction, 1 μM ICL1 or 15 μM ICL2 was incubated with varying inactivator concentrations (0-50 μM and 0-5 mM in inactivation of ICL1 and ICL2 respectively). The pre-incubation buffer contained 50 mM HEPES (pH 7.5), 5 mM $MgCl_2$, in the presence or absence of DTT. Samples were taken from pre-incubation mixtures, diluted 50-fold into assay buffer at various time interval to measure the residual activity over the period of preincubation time (0-60 min for ICL1 and 0-250 min for ICL1). Glyoxylate product from lysis of isocitrate was measured via the phenyl hydrazine assay as described above. Initial rates were normalized to that of an enzyme sample with no inactivator added.

Electrospray Ionization Mass Spectrometry

ICL1 (200 μM) was incubated for 20 h at 37 ºC with or without 0.5 mM 2-VIC in 50 mM HEPES (pH 7.5) and 5 mM $MgCl_2$. The protein samples were desalted on a Bio-Spin® 6 desalting column (BioRad, Hercules, CA, USA) to exchange the buffer with 10 mM ammonium acetate (pH 7.0), and samples were then diluted to 1 μM in a solution containing 50% (v/v) acetonitrile and 0.1% (v/v) formic acid. The diluted protein solutions were injected directly into an electrospray ionization time-of-flight mass spectrometer (MicroTOF-QII® mass spectrometer, Bruker Daltonics, Inc. Billerica, MA, USA), at a rate of 3 μL/min. Mass spectrometric data were collected in the positive mode over a period of 2 min in the mass/charge (m/z) range of 200 to 2000 with a nebulizer gas pressure of 0.4 bar and capillary voltage of 4500 V. The data were averaged and the multiply-charged ions were

then de-convoluted using a maximum entropy algorithm to yield the mass of the intact protein.

Quantification of Product Succinate in ICL Inactivation Studies

Succinic acid formed from ICL1-catalyzed cleavage of 2-VIC was detected using the succinate colorimetric assay kit and protocol of Biovision, Inc (Milpitas, CA, USA).

Molecular Docking

Molecular models of ICL1 binary and tertiary complexes were built by docking of 2-VIC, 2VG and (2R)-malate into the crystal structure of the C191S mutant *Mtb* ICL1 (PDB: 1F61 & 1F8I)[9] using Chimera/AutoDock Vina,[20] which performs fitting of small-molecule ligands with freely rotatable bonds separated by three consecutive covalent bonds or fewer. Search volume was sampled from 5 -20 cubic Å in order to ensure both accuracy and non-bias posing of ligand in the active site.

Protein Fluorescence

ICL1 (1 µM of monomers) in a buffer mixture of 50 mM HEPES (pH 7.5) and 10 mM $MgCl_2$ were incubated at room temperature for 50 min with 1 mM DL-isocitrate, 100 µM 2-VIC or 100 µM 3-bromo-pyruvate. The mixtures (200-µL final volumes) were excited at λ_{ex} = 290 nm, and the intrinsic fluorescence emission spectra (λ_{em} = 315–400 nm) were measured at room temperature in a Biotek Synergy plate reader using 96-well Greiner black, clear-bottom plates. The intrinsic fluorescence of ICL1 was also recorded in the presence of 10 mM glyoxylate, 10 mM succinate, and a combination of 10 mM glyoxylate and 10 mM succinate.

pH-rate Dependence of 2-VIC Inactivation

ICL1 catalysis was measured via recording of product (glyoxylate) formation over time using phenyl-hydrazine assay as described above. Serial dilution of 2-vinyl-(2R,3S)-isocitrate was prepared and added to the assay buffer containing HEPES, CHES, MOPS and MES (40 mM each, pH 5.8 – 8.4), 10 mM $MgCl_2$, and ICL1 (1μM). A sample of 2-VIC preincubated-enzyme mixture was transferred to the assay plate containing 1 mM of (2R, 3S)-isocitrate in reaction buffer at pH 7.5 (as described above) to start the reaction.

Solvent Kinetic Effects

Inactivation rate of ICL1 (2 nM) was measured in D_2O and H_2O at pL-independent range (pL 6.8 – 7.2) as described above. 2-vinyl-(2R, 3S)-isocitrate, (2R,3S) isocitrate, $MgCl_2$, DTT and all other buffer components were prepared in H_2O or D_2O appropriately.

X-ray Crystallography

2-homopyruvoyl-C191 ICL1 complexes were prepared by incubating no-tag ICL (~10 mg/mL, a gift from Sacchettini lab) in 50 mM Tris (pH 8.0), 10 mM $MgCl_2$, and 0.5 mM DTT with 3 mM 2-VIC overnight at 17 ºC. A concentration of 0.5 mM DTT did not impede covalent inactivation of ICL1-TF but was sufficient to prevent oxidation of the cysteine residues of ICL1. The hanging drop vapor diffusion method was used to produce crystals. A 1:1 volume ratio of the protein with a solution of 0.1 M Tris-HCl (pH 8.0), 0.2 M sodium acetate, and 20–30% (w/v) polyethyleneglycol 4000 (PEG 4,000) was used to crystalize the protein at 17 °C.

Analysis of Kinetic Data

Initial velocity data for the forward and reverse reactions of ICL were fitted to equations (1) (described in chapter 3) & and equation (10), respectively.

$$\frac{v}{[E]_t} = \frac{k_{cat}[A]}{K_a + [A]}$$

(1)

for which

v is the initial velocity,

$[E]_t$ is the concentration of ICL monomers,

k_{cat} is the turnover number in units of s^{-1},

$[A]$ is the variable concentration of isocitrate

and K_a is Michaelis constant of isocitrate

$$\frac{v}{[E]_t} = \frac{k_{cat}[A][B]}{K_{ia}K_b + K_b[A] + K_a[B] + [A][B]}$$

(10)

for which,

$[A]$ & $[B]$ is the variable concentration of glyoxylate and succinate, respectively

v is the initial velocity,

$[E]_t$ is the concentration of ICL monomers,

k_{cat} is the turnover number in units of s^{-1},

K_a is the Michaelis constant of glyoxylate

K_{ia} is the apparent dissociation constant of glyoxylate,

K_b is the apparent Michaelis constant of succinate.

Time-dependent inactivation of ICL was assessed by fitting of the pre-incubation data to equation (11).

$$\frac{v_i}{v_0} = \exp\left[-\left(\frac{k_{inact}[I]}{K_{inact} + [I]} + k_{bgd}\right)t\right]$$

(11)

for which,

v_i and v_0 are the initial rates at time t and 0, respectively.

t is the time of pre-incubation

[I] is the micromolar concentration of inactivator

k_{inact} is the maximal rate constant of inactivation

K_{inact} is the concentration of inactivator at which the observed rate constant of

inactivation is half that of k_{inact}.

k_{bgd} is the observed rate constant for background loss of ICL activity over the

experimental time courses, independent of the inactivator.

In addition, we fitted the time courses at each concentration of inactivator to equation (2), where resulting values of k_{obs} were then re-plotted using equation (9).

$$\frac{v_i}{v_0} = \exp\left[-k_{obs}t\right]$$

(12)

$$k_{obs} = \frac{k_{inact}[I]}{K_{inact} + [I]} + k_{bgd}$$

(13)

For the partitioning analysis of mechanism-based inactivation, data were fitted to equation (16)

$$\frac{v_i}{v_0} = 1 - \frac{[\text{2-VIC}]}{(1+p)[E_t]}$$

(14)

for which,

v_i and v_0 are, respectively, ICL1 activity measured after pre-incubation with

2-VIC or with no 2-VIC, [2-VIC]

61

[E_t] are the micromolar concentrations of inactivator and enzyme, respectively,

and p is the partitioning coefficient.

The fraction of enzyme activity protected from 2-VIC-induced inactivation is given by equation (6).

$$\left(1 - \frac{k_{obs}^{no\ DTT}}{k_{obs}^{DTT}}\right) = \alpha \frac{[L]^n}{K_D^n + [L]^n} \tag{15}$$

for which,

k_{obsDTT} is the rate of enzyme inactivation in the presence of DTT, glutathione or ($2R$)-malate,

k_{obs0} is the rate of inactivation in the absence of thiol,

α is a proportionally factor representing the maximal degree of protection,

[L] is the concentration of the thiol or ($2R$)-malate,

K_D is its dissociation constant,

n is the Hill coefficient.

3.3. Results

The Time-dependent Inactivation of Mtb ICL1 and ICL2 with 2-VIC

Pre-incubation of ICL1 (800 nM) with 0–40 μM 2-VIC over a time course of 0-70 min, resulted in a time-dependent loss of ICL1 activity conforming to first-order kinetics (**Figure 3-2A**). Measurement of residual activity of ICLs during the preincubation was via a 50-fold dilution into a solution containing high concentrations of glyoxylate and succinate. 2-VIC exhibited no appreciable inhibition of the coupling enzymes isocitrate dehydrogenase or

lactate dehydrogenase ($< 1 \times 10^{-6}$ min^{-1}). After a 65-min pre-incubation with 2-VIC at concentrations of ≥ 20 μM, more than 95% of ICL1 was inactivated. Data were fitted globally to equation (11) which describes a two-step irreversible inactivation. The results comprised a maximal rate constant of inactivation, $k_{inact} = 0.080 \pm 0.006$ min^{-1} and a concentration of 2-VIC leading to half-maximal inactivation, $K_{inact} = 22 \pm 3$ μM. Using the method of Kitz and Wilson[131], the apparent first-order rate constant of inactivation, k_{obs}, obtained from equation (12) demonstrated a hyperbolic dependence on the concentration of the inactivator upon fitting to equation (13) (**Figure 3-2**, inset), indicating saturation behavior of inactivation. Similarly, inactivation of ICL2 by 2-VIC is time-dependent and exhibits saturable kinetics ($k_{inact} = 0.019 \pm 0.001$ and $K_{inact} = 420 \pm 70$ μM).
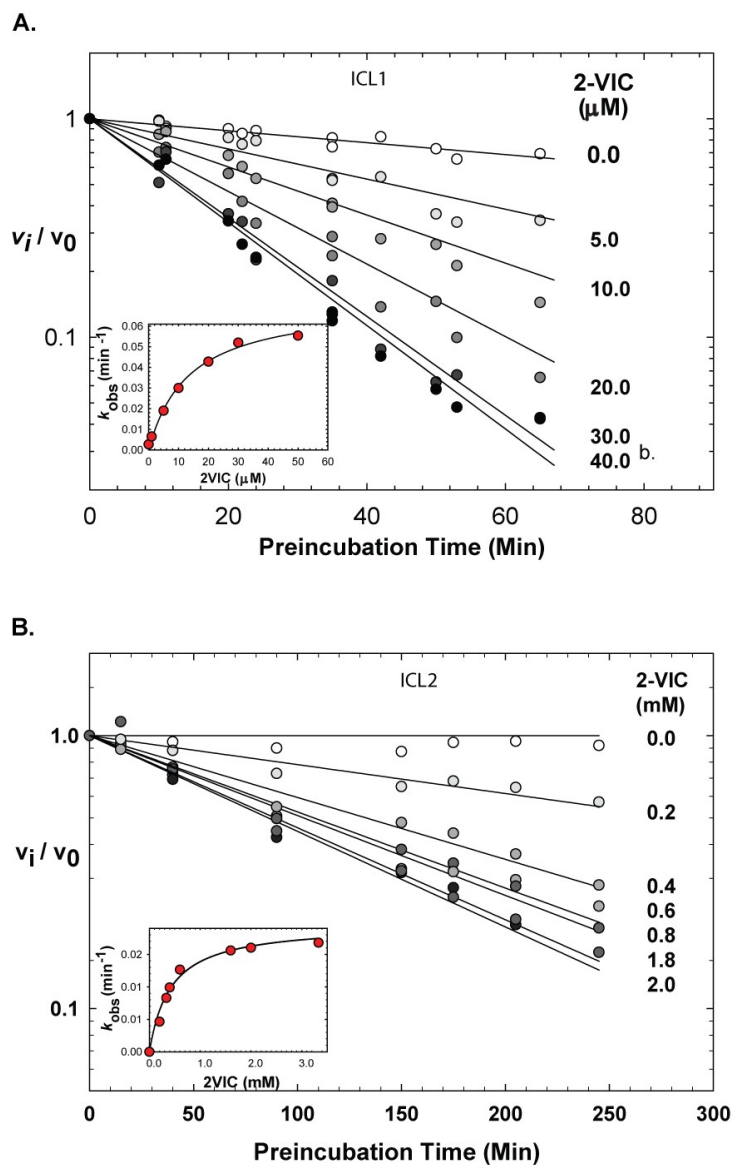
Figure 3-2 2-VIC-induced inactivation kinetic of ICL1 and ICL2

Residual ICL activity (v_i/v_0) of (A) ICL1 (800 nM) following pre-incubation with 0–40 µM 2-VIC; (B) ICL2 (2 µM) with 0–2 mM 2-VIC. Insets are replots of rates of inactivation (k_{obs}) vs. [2-VIC].[43]

Protection of ICL from 2-VIC Inactivation by (2R)-malate, Glyoxylate, Succinate, and

Added Thiols

(2R)-malate, a competitive inhibitor of isocitrate ($K_i = 310 \pm 30$ μM), served as an isocitrate

surrogate to demonstrate that the inactivation effected by 2-VIC occurs at the active site.

Pre-incubation of ICL1 with 50 μM 2-VIC in the presence of 0.1-3.0 mM (2R)-malate

exhibited a concentration-dependent ablation of ICL1 inactivation by 2-VIC (**Figure 3-3**).

The inactivation was mostly eliminated at 3 mM (2R)-malate, which is 10-fold higher than

its inhibition constant. The concentration dependence of protection from inactivation by

(2R)-malate was evaluated by fitting data to equation (15), resulting in an apparent

dissociation constant of $K_d = 360 \pm 60$ μM and a Hill coefficient $n = 0.56$ (**Figure 3-3**, inset).

Similarly, milimolar concentrations of succinate or glyoxylate afforded protection from
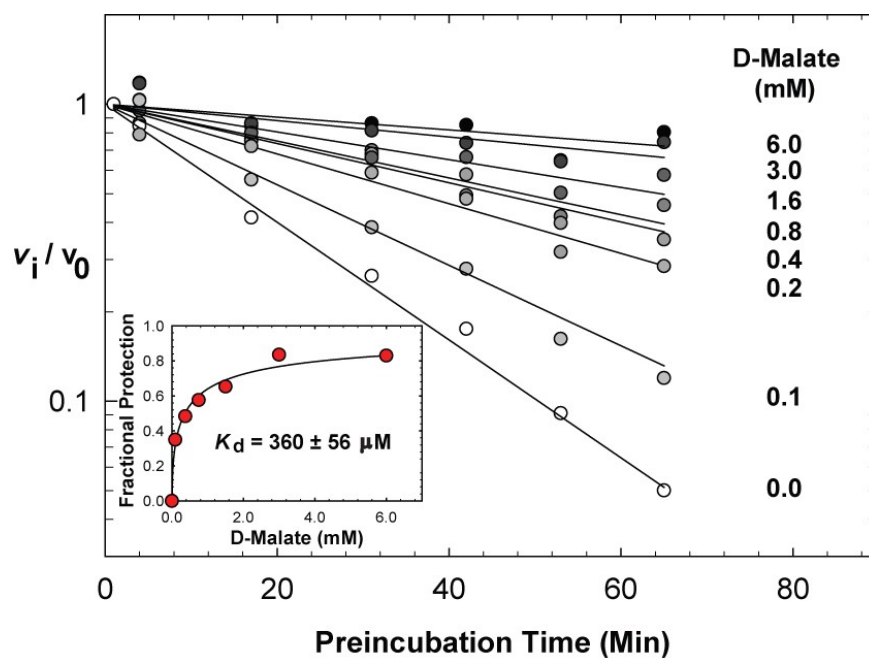
inactivation by 30 μM 2-VIC.

Figure 3-3 (2R)-malate protection of ICL1 from 2-VIC-induced inactivation[43]

Addition of either dithiothreitol (DTT) or glutathione to pre-incubation mixtures protected ICL1 from inactivation by 2-VIC. Addition of micromolar concentrations of either DTT or glutathione to pre-incubation mixtures of ICL1 and 2-VIC demonstrated concentration-dependent protection from 2-VIC inactivation of ICL1. As shown in **Figure 3-4**, increasing fixed concentrations of 10–1000 μM DTT in pre-incubation mixtures containing ICL1 and 2-VIC (30 μM) afforded increasing protection from inactivation and indicated apparent, saturable binding of DTT to ICL1. Fitting of the fractional protection vs. [DTT] (**Figure 3-4**, inset) to equation (15) provided an apparent binding constant of DTT of $K_d = 8.4 \pm 0.1$ μM. Similar results were found from protection studies using glutathione ($K_d = 3.8 \pm 0.2$ μM; **Figure 3-4**). The inactivation protection by exogenous thiols presumably occurs via the ability of thiols to react with an enzyme-generated electrophilic species.

DTT was shown to prevent the inactivation of *E. coli* ICL because of its reaction with 3BP during pre-incubation with the enzyme[56]. In order to determine if DTT reacts with intact 2-VIC in solution in the absence of enzyme, 1.0 mM 2-VIC was treated with 1 mM DTT for 60 min. These reaction mixtures were then diluted 10-fold into reaction mixtures containing ICL1, yielding final concentrations of 100 μM DTT and 100 μM 2-VIC. Both DTT-treated 2-VIC and fresh 2-VIC in the presence of 100 μM DTT resulted in the complete inactivation of ICL1 ($k_{obs} = 0.009$ min^{-1}). These results indicated that 2-VIC does not react with DTT during the inactivation studies. Accordingly, either the thiol compounds form covalent adducts with an electrophilic species outside the active site of ICL, thereby preventing its re-binding and reaction with ICL. The saturable protection by both thiol compounds suggested that they are associated with ICL1 complex and have access to an

enzyme-bound electrophile generated from 2-VIC, or its putative covalent enzyme-bound adduct.
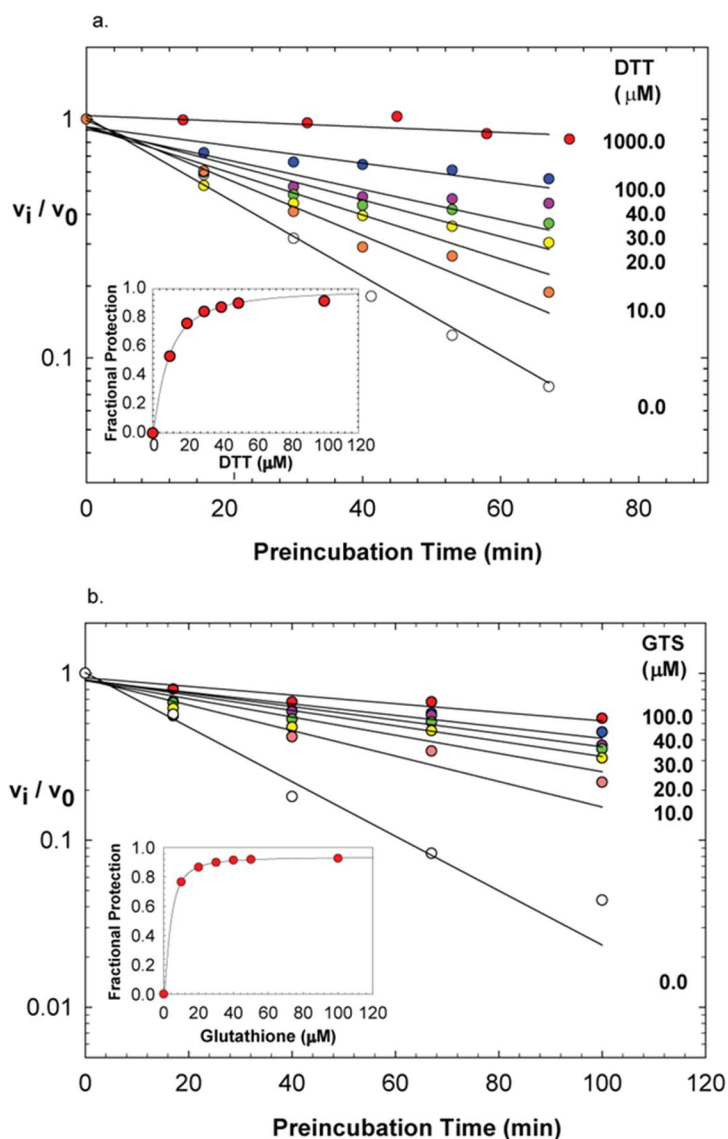

Figure 3-4 DTT and glutathione effects on 2-VIC-induced inactivation of ICL1

ICL1 (1 µM) was pre-incubated for the indicated time periods with 50 µM of 2-vinyl isocitrate (2-VIC) in the presence of 0–1,000 µM DTT or 0–100 µM glutathione (GSH). The lines drawn through the experimental data points of the plot were obtained by fitting of the data to equation 12. The inset shows the fractional protection from inactivation, by fitting of the observed rates of inactivation, k_{obs}, at each DTT or GSH concentration to equation (15)[43]

67

Partition Ratio

In order to determine the efficiency of 2-VIC inactivation, we measured its partitioning ratio. Partion ratio represents the fraction of bound 2-VIC that dissociates vs. the fraction which forms a covalent adduct with ICL1.[18] The residual catalytic activity of 2 μM ICL1 was determined after a 20-h pre-incubation with 0–3 μM 2-VIC (Fig. 2E). Fitting of the data (equation (14)) resulted in an x-intercept of 1.24 ± 0.04, from which we obtained a partitioning ratio (p) of 0.24 ± 0.04. This indicates that 1.24 mol of 2-VIC was required to inactivate 1 mol of ICL1.

As an independent determination of partition ratio, we measured the concentration of succinate produced from 2-VIC during the mechanism-based inactivation of ICL1. Here ICL1 was saturated with 2-VIC in order to prevent the rebinding of the released electrophilic species. The stoichiometric ratio of quantifiable succinate vs. inactivated ICL1 (**Figure 3-5**, inset) indicated that 1.24 molecules of succinate were released per inactivation event. Therefore, measurement of succinate production, an independent assessment of the partitioning ratio, again, shown to equal 0.24, indicating that 2-VIC is a highly efficient inactivator of ICL1. A similar analysis of ICL2 resulted in $k_9/k_{11} = 0.6 \pm 0.1$ (**Figure 3-5**).
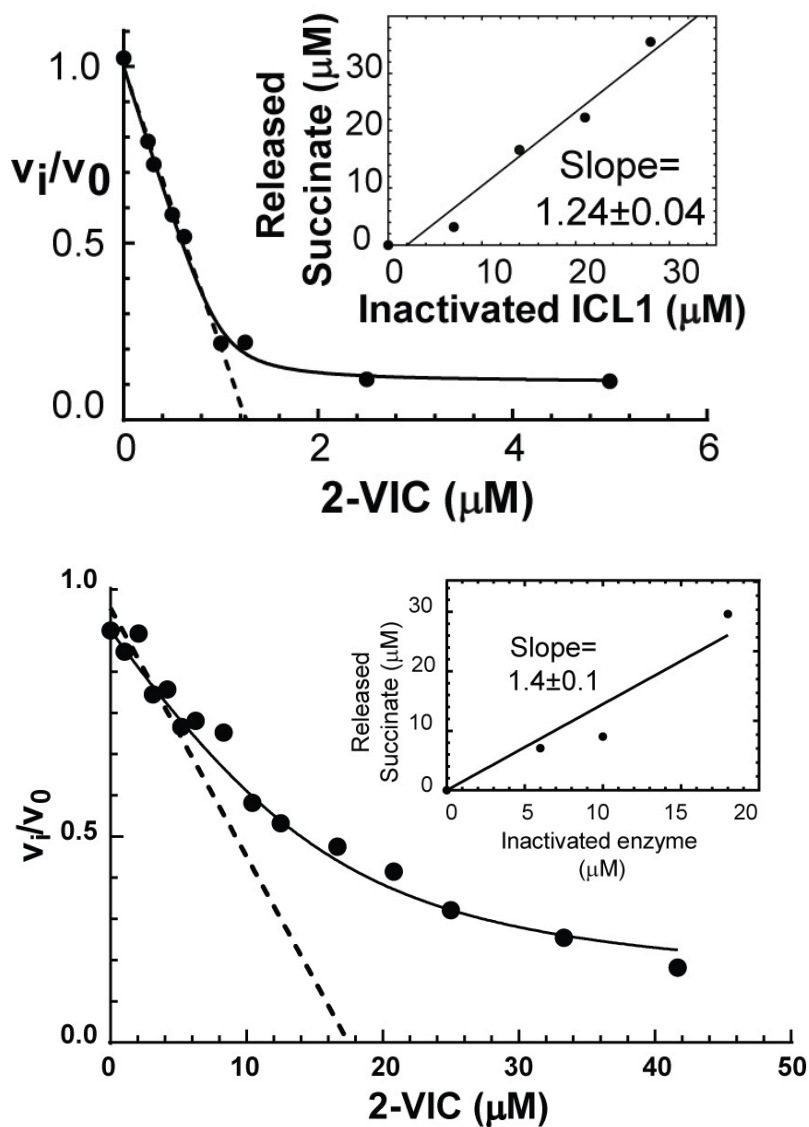
Figure 3-5 Inactivation titration and succinate production analysis of ICL1 and ICL2 partitioning ratio

Residual ICL1 activity (v_i/v_0) was measured after pre-incubation of ICL1 with equimolar concentrations of 2-VIC. The line drawn through the experimental data points results from fitting to equation (14) resulting in a value of p, the partitioning coefficient, of 0.24 ± 0.04. The dash-line was from linear regression analysis of data points in which 2-VIC is less than 10 μM.[43]

The titration curve showed a ∼ 10% residual activity left at 2-VIC concentrations that are two- to five-fold in excess of ICLs and exhibited deviation from linearity when [2-VIC] / [ICL] exceeded unity. This could arise from the product protection of succinate, which

prevents inactivation. However, further investigation of succinic effects at micromolar concentrations showed no appreciable protection from the inactivation. The second rationale was that formation of a reversible oxidized form of Cys191-SH depleted the "target" active-site cysteine during the extended period of pre-incubation in reaction mixtures, which are free of DTT. However, an experiment where fresh 2-VIC (50 µM) afford further inactivation of 20-hrs preincubated ICL1 sample invalidated this hypothesis. The third explanation is that slowly reversible dissociations of the covalent adducts led to the release of 2-VG and free enzymes. Indeed, dialysis of 2-VIC inactivated ICL1 for extended time (48 hours) allows fully regain of activity in comparison with untreated control samples in the presence of DTT. During the first 24 hrs of dialysis, dissociation rates of the covalent adduct appeared to be independent with DTT presence. Due the loss of enzyme activity via oxidation in both control and treated samples, reactivation beyond 24 hrs for samples dialyzed was not observed in the absence of DTT.

Mass Spectrometry of Mtb ICL1 Treated with 2-VIC

Electrospray ionization time-of-flight mass spectrometry (ESI-TOF MS) was performed to support the existence of an enzyme–inactivator covalent adduct. An untreated sample of ICL1 enzyme demonstrated a peak of an average mass of $48,788 \pm 1$ Da, consistent with the theoretical molecular weight of ICL1 monomers (48,787 Da) (**Figure 3-6**). A 2-VIC-treated ICL1 sample displayed a major peak at $48,887 \pm 1$ Da (**Figure 3-6B**). The apparent increased mass of the enzyme by 99 ± 1 Da is consistent with the addition of $C_4H_3O_3$ to an ICL1 monomer resulting from formation of a covalent adduct between ICL1 and 2-vinyl-glyoxylate (2VG).
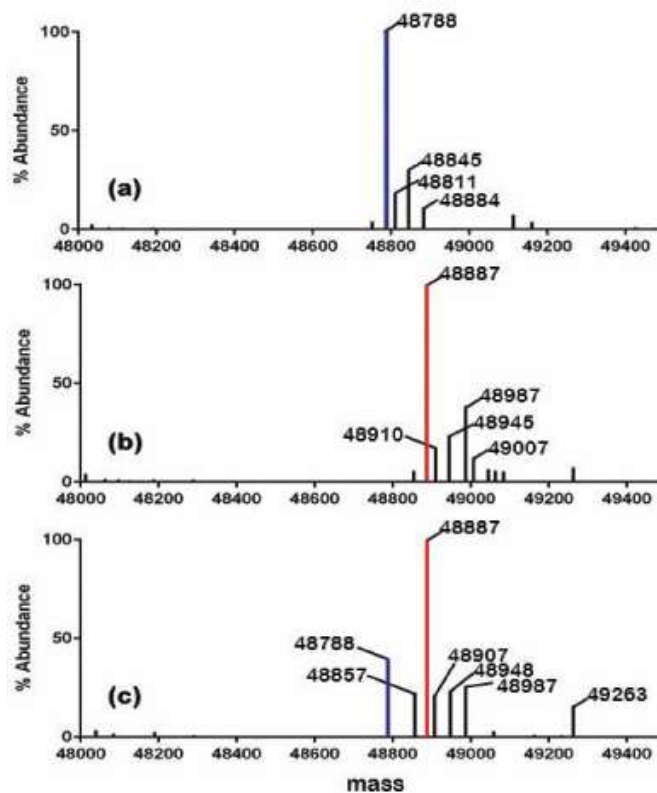
Figure 3-6 ESI-mass spectrometric analysis of 2-VIC-treated Mtb ICL1

(a) Untreated *Mtb* ICL1 as characterized by a de-convoluted protein peak of 48,788 Da. (b) 2-VIC-treated ICL1 for which the peak of 48,788 Da is absent and replaced by a major peak of 48,887 Da. (c) Mass spectrum collected after 2-VIC-treated ICL1 was subjected to treatment with 10 mM DTT, as characterized by a major peak at 48,887 Da and a minor one at 48,788 Da at an apparent ratio of 61:39.

Kinetic analysis revealed the reactivation of 2-VIC-treated ICL1 (~35%) after incubation of the treated sample with 1 mM DTT for 3-4 hours. Resdiual activity of ICL1 was normalized to an untreated sample as a control. Consistently, treatment of the 2-VIC-inactivated ICL1 with 10 mM DTT for 90 min demonstrated an approximate 60:40 ratio of the 48,887-Da and 48,788-Da (2-VIC–ICL1 and ICL1) species, indicating that treatment with DTT had removed nearly 40% of the covalent adduct from the inactivated enzyme (**Figure 3-6C**).

Crystallographic Analysis of 2-VIC-Treated Isocitrate Lyase

As kinetic and mass spectrometric characterization of the inactivation of ICL1 by 2-VIC is consistent with covalent alkylation of the enzyme, we sought a crystallographic assessment of the mechanism of inactivation. Crystal structure of 2-VIC-treated ICL1 at 1.8 Å resolution displayed the electron density of a covalent, thioether-linked, homopyruvoyl (HP) moiety attached to the active-site Cys191 in all four subunits of the asymmetric unit (**Figure 3-7A**). Occupancy of the covalent adduct was different in the four monomers. Chain A exhibited the highest occupancy for the electron density of all atoms, and all of the interactions described below refer to those of Chain A. Although the α-hydroxy-carboxylate substituent of 2-VIC would be expected to bind initially to the Mg^{2+} ion in order to undergo retro-aldol cleavage to form 2VG, the observed homopyruvoyl adduct is not coordinated to this Mg^{2+} ion.
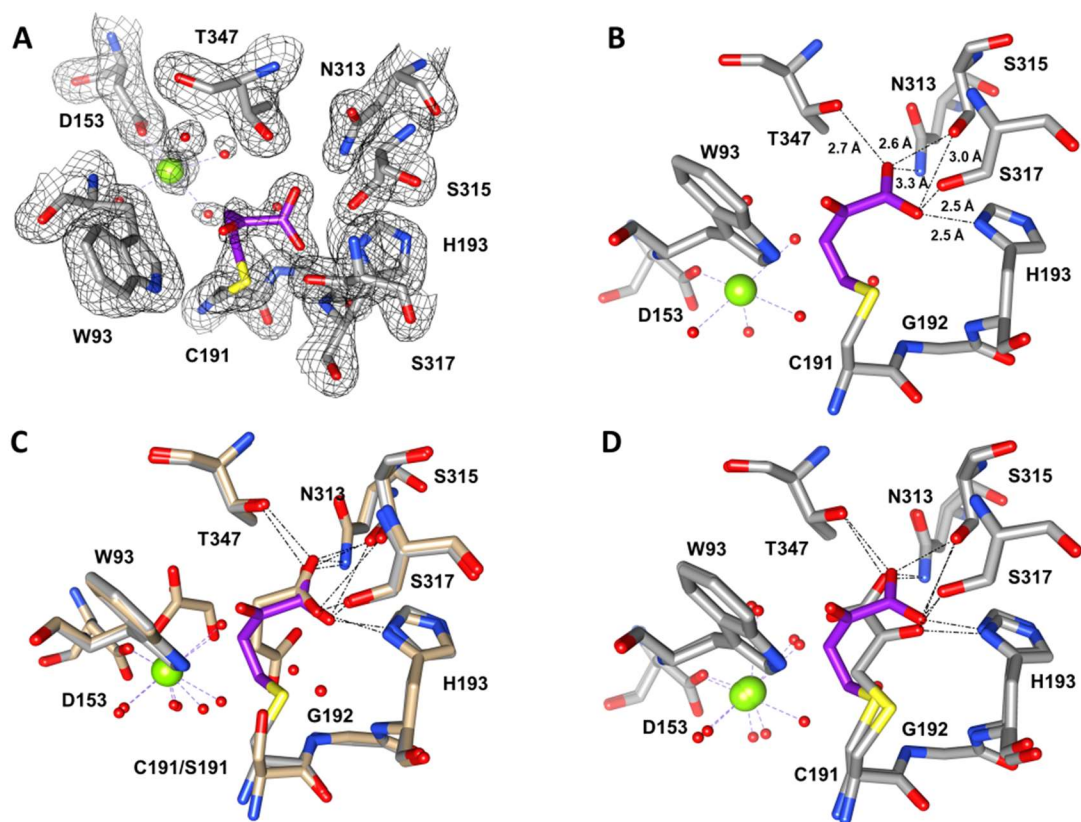
Figure 3-7 X-ray structural characterization of 2-VIC-treated ICL1

(**A**) Density map structure of ICL1 displaying the S-homopyruvolyated Cys191 residue following treatment with 2-VIC. (**B**) Cys191 modified with 2-VIC (purple). Potential hydrogen bonds (dashed lines) and interatomic distances are shown. (**C**) Superposition of crystal structures of ICL1 bound to glyoxylate and 3-NP (gold) or after treatment with 2-VIC (purple); (**D**) Superposition of active-site structures of ICL1 including Cys191 (yellow) treated with 3-bromo-pyruvate (S-pyruvoylated enzyme, gray)[9] and 2-VIC (S-homopyruvoylated, purple). The labeling scheme is: nitrogen, blue; oxygen, red; sulfur, yellow; water, red spheres; Mg^{2+} ion, green sphere; and hydrogen bonds, dashed lines.[43]

Instead, the covalently-tethered keto-acid (electron density was modeled as an α-keto acid) has turned away from the Mg^{2+} ion toward the succinate binding site, as in the case of 3BP.[9] One of its carboxylate oxygens forms apparent hydrogen bonds with His$_{193}$ and Ser$_{315}$ (both at distances of 2.5 Å). The other carboxylate oxygen is within hydrogen-bonding distance to Asn313, Ser317, and Thr347 (3.3 Å, 2.6 Å, and 2.8 Å distances, respectively; **Figure 3-7B**). The α-keto oxygen forms no apparent hydrogen bonds with the protein, and

it is oriented toward the indole ring of Trp93; Trp93 possibly prevents the re-coordination of the cysteine-tethered keto-acid to the Mg^{2+} ion.

In the crystal structure of the C191S ICL1 mutant complexed with glyoxylate and 3NP[9], the bound 3NP is structurally indistinguishable from succinate, and this structure provides a model for ICL1-glyoxylate-succinate complex. When the 3NP-bound structure is overlaid with the HP-ICL structure, the HP moiety appears to bind preferentially in the succinate-binding pocket (**Figure 3-7**). According to previous structures of *Mtb* ICL1, 3NP effects hydrogen-bonding distances with Asn313, Ser315, Ser317, and Thr347, as well as His$_{193}$ of the active site loop, as does the Cys191-attached HP substituent. In order for the homopyruvoyl group to adopt these interactions, the succinate formed from 2-VIC would need to dissociate from enzyme. The closed active site provides adequate sequestration of the reactive 2VG for its eventual migration to and reaction with Cys191. Additionally, the homopyruvoyl group attached to Cys191 in ICL1 assumes a binding mode which is very similar to that of the *S*-pyruvoylated form of 3BP-treated ICL1.[9] **Figure 3-7** shows the overlay of the structures of 3BR-treated ICL1 (gray, PDB ID: 1F8M) and 2-VIC-treated ICL1 (purple). All of the residues in the active site are nearly superimposable. In both covalently-modified structures, the binding site in which glyoxylate is chelated to the Mg^{2+} ion is vacant, as both *S*-pyruvoyl and *S*-homopyruvoyl groups bind in the succinate binding pocket, and interact with the same five residues via apparent hydrogen bonds. Unlike the *S*-homopyruvoyl structure, only one of the carboxylate oxygens from the *S*-pyruvoyl group is in adequate proximity to Thr347, Ser315, and Asn313 for hydrogen bonding. The α-keto group of the S-pyruvoyl complex is within hydrogen-bonding distance to Ser317 and His193.

Effects of Ligand Binding *and Reaction* ***with Cys****191* *on the Intrinsic Protein Fluorescence*

of ICL1

The intrinsic protein fluorescence of *Mtb* ICL1 (λ_{ex} = 290 nm, λ_{em} = 320 nm) is diminished

by ligand binding, and by covalent reaction with 3BP and 2-VIC (Fig. 4A). Tyrosine and

tryptophan residues proximal to the active site of ICL1 (e.g., Tyr89 and Trp93 (**Figure 3-7**)

likely contribute to the observed changes in fluorescence upon ligand binding in the active

site. In comparison with the unliganded enzyme, 3BP-inactivated ICL1 exhibits the highest

diminution in protein fluorescence (–60%) followed by [ICL1 + Glx] (–50%), [ICL1 +

isocitrate] (–55%), and 2-VIC-inactivated enzyme (–40%). Since isocitrate and the products

of enzymatic turnover (glyoxylate and succinic acid) exists in equilibrium, the nearly

identical fluorescence emission spectra of [ICL1 + isocitrate] and [ICL1 + Glx] suggests that

the binary ICL1–Glx complex, and not ICL1-isocitrate, would be the predominant species

in [ICL1 + isocitrate] sample. The decrease in intrinsic protein fluorescence accompanies a

significant change in ICL1 conformation, as reported in crystallographic analysis of ICL1,

arising in part from the large (15Å) movement of the aforementioned active-site loop
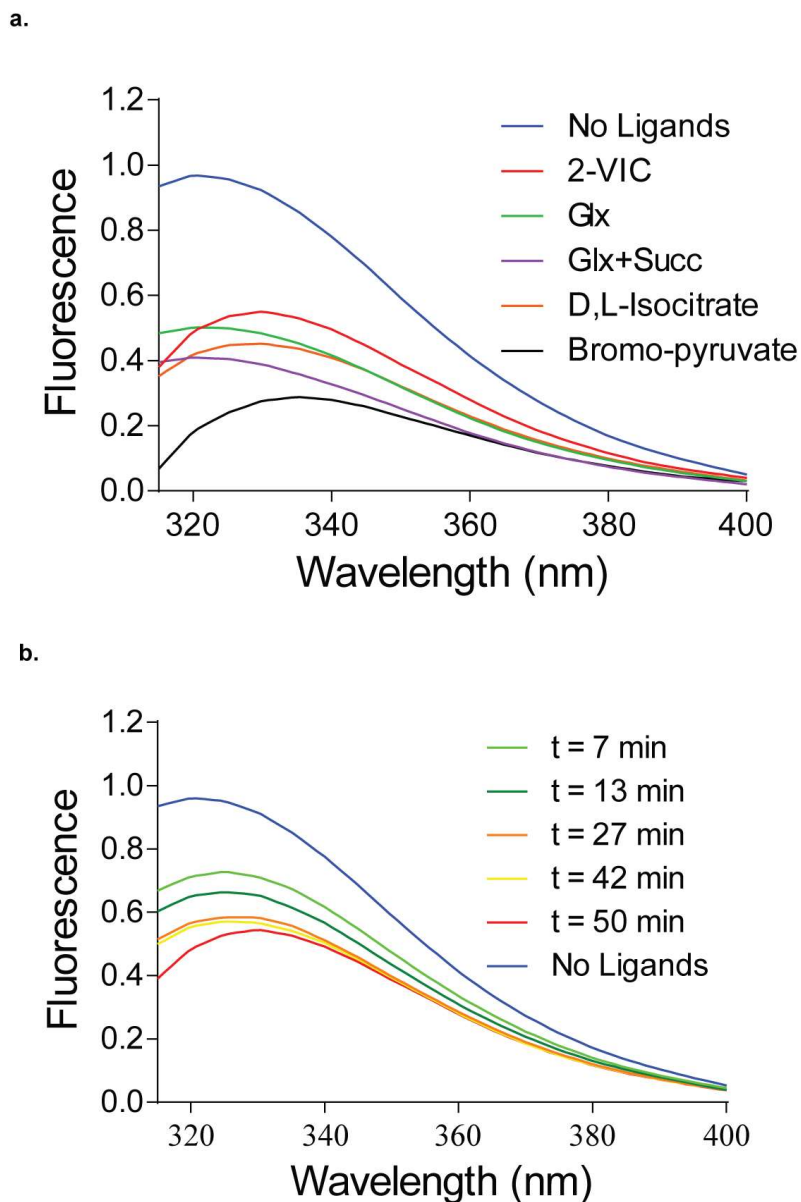
(containing Cys191) upon ligand binding.[56]

Figure 3-8 Ligand-induced fluorescence changes of ICL1[43]

Notably, the apparent covalent inactivation arising from added 0.1 mM 2-VIC (red) or 0.1 mM 3BP (black) led to a diminution of ICL1 fluorescence, which is consistent with the closed conformation of the active site for the covalently-modified-ICL1 structure. We also observed a time-dependent shift and decrease of the relative fluorescence of ICL1, from 1.0 to an invariant value of 0.6, during a 20-minute incubation of ICL1 with 100 μM 2-VIC

(**Figure 3-8B**). An apparent, first-order rate constant of change in fluorescence ($k_{obs} = 0.01$ min^{-1}) was comparable to k_{inact} obtained from kinetic studies.

Rate Limiting Step(s) of 2-VIC Inactivation

In order to determine whether catalysis of 2-VIC or the Michael addition of 2-VG to Cys191 is the rate limiting of ICL1 inactivation, the rate of succinate formation from 2-VIC in the presence of DTT was determined in an end-point assay. DTT blocks the Michael addition step but allows the retro-aldol cleavage of 2-VIC to yield 2-VG and succinate. In parallel, the apparent inactivation rate in the absence of DTT was also evaluated. The rate of 2-VIC catalysis was 0.06 ± 0.01 min^{-1} whereas inactivation rate was 0.04 ± 0.01 min^{-1}. Therefore, the Michael addition step is at least 2-fold faster than the catalysis step (**Figure 3-9**).
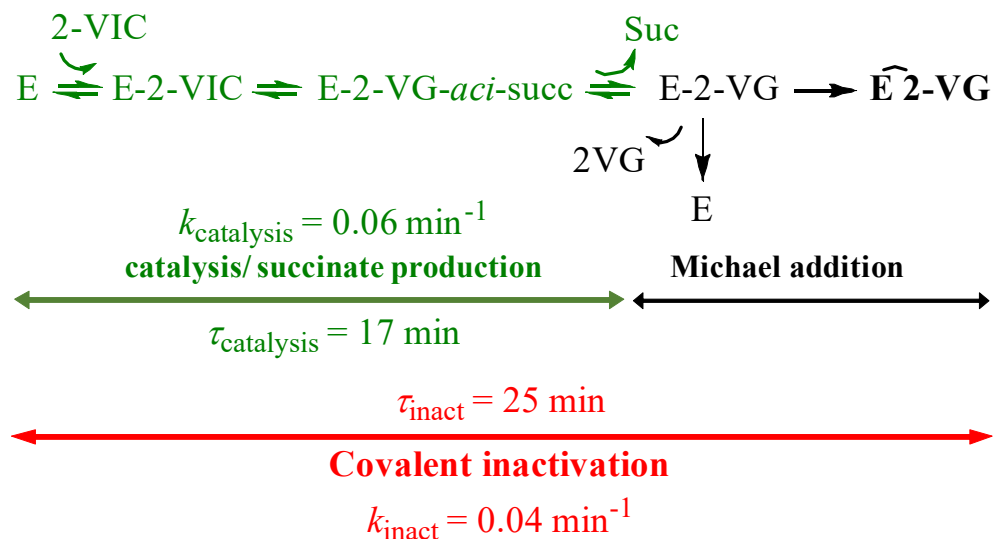

Figure 3-9 Comparisons of overall inactivation rate and catalysis/ succinate production rate to reveal the rate limiting(s) step of 2-VIC mechanism-based inactivation
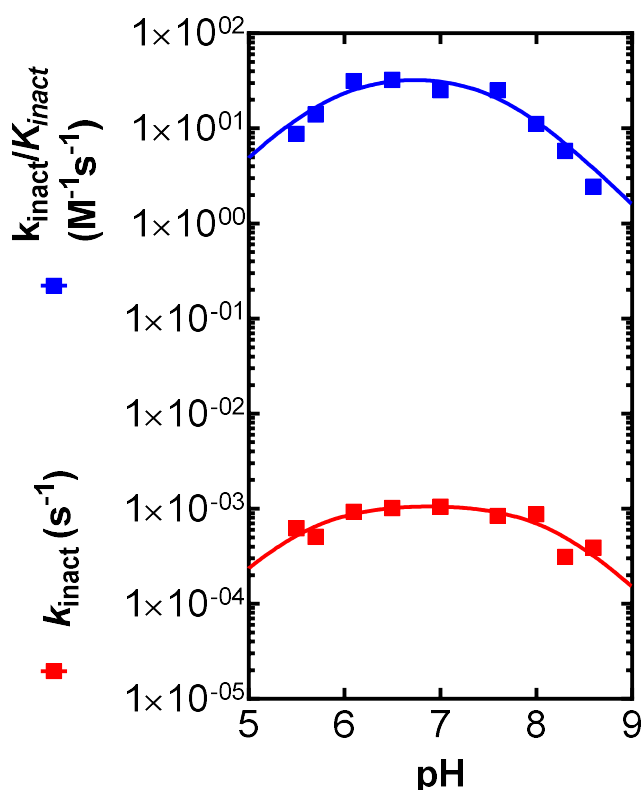
Figure 3-10 pH-rate profiles of 2-VIC inactivation

Residual ICL activity (v_i/v_0) of ICL1 (800 nM) following pre-incubation with 0–40 μM 2-VIC was fitted into equation (8) to obtain k_{inact} and k_{inact}/K_{inact} values shown in red and blue, respectively. The lines drawn through data points were from fitting k_{inact} and k_{inact}/K_{inact} values to equation (3).

pH-rate profiles of 2-VIC inactivation exhibited bell-shaped curves whose pK_b values were similar to that obtained from the plot of k_{cat}/K_m vs. pH. Therefore, these pK_b is likely to represent the same residue (Glu285). The plot of k_{inact} vs. pH exhibited a wider pH independent region, or a more flatten "bell-shaped" curve, which suggests effects from multiple rate limiting steps[112]. The lack of a pK_a describing the nucleophilic thiolate in pH-rate profiles implied that the Michael addition is not the sole rate-limiting step. On the other hand, solvent kinetic isotope effects revealed an inverse effect for the maximal rate of inactivation (k_{inact}) and a small normal effect for k_{inact}/K_{inact} ($^{sKIE}k_{inact} = 0.5 \pm 0.1$ & ^{sKIE}

$k_{inact}/K_{inact} = 1.8 \pm 0.2$). This result is consistent with the Michael addition step as being partially rate limiting since Cys191 thiolate formation is more favorable in D_2O.

3.4. Conclusions

In order to evaluate the structural changes occurring during 2-VIC inactivation, 2-VIC and its reaction products 2VG and succinate were docked into the closed conformation of ICL1 crystal structures using AutoDock Vina[132] based on these previous crystallographic structures. A proposed chemical mechanism, accompanied with docked structures of the enzyme species and ligands formed during ICL1 inactivation by 2-VIC, is depicted in Fig. 5. The unliganded form of ICL1 preferentially maintains the open conformation (Fig. 5, E_{open}), in which the active-site loop (residues 189–193) is distal to the bound Mg^{2+} ion. Molecular docking of 2-VIC into the active site of C191S ICL1, for which the 1-carboxylate and 2-hydroxyl groups are coordinated to Mg^{2+} (E–2-VIC), suggests that 2-VIC binds to ICL1 (step k_1) in the same manner as isocitrate (E_{closed}–2VIC). Ligand binding (E_{closed}) results in movement of the active-site loop and the Mg^{2+} ion. This brings Cys191 into position for catalysis. Base-catalyzed cleavage of the C_2–C_3 bond (k_3) produces Mg^{2+}-bound 2VG (green) and the *aci*-anionic form of succinate (E–2VG–*aci*-Succ). Protonation of *aci*-succinate by Cys191 (k_5) then produces succinate and the thiolate form of Cys191 (E–2VG–Succ). Modeling of ICL1–2VG–succinate complex is consistent with the coordination of 2VG to the Mg^{2+} ion, and its interaction with active-site residues is similar to that of unsubstituted glyoxylate. It is noteworthy that succinate blocks access of Mg^{2+}-bound 2VG to the thiolate ion of Cys191, which is accounted for by the protection from 2-VIC inactivation afforded by added succinate (k_8). We propose that the expulsion of succinate from the partially or fully opened active site of E–2VG–Succ (k_7) allows 2VG to rotate and

migrate to the succinate binding site, forming the covalent complex ICL-HP via Michael addition of the Cys191 thiolate to 2VG (k_{11}). Desorption of succinate in a partially-opened active site allows 2VG (a) to react with the thiolate ion of Cys191 to form the covalent binary complex ICL-HP, (b) or to escape from the active site (k_9), or (c) to access added thiols for pre-emptive reaction with enzyme-bound 2VG (k_8).

The release of 2VG from the ICL1–2VG complex occurs at a rate which is 20% that of its reaction with Cys191 to form E-HP, as indicated by the partitioning analysis from which $k_9/k_{11} = 0.24$. We propose that the E–2VG complex (vacant succinate subsite) is the complex at which covalent reaction with enzyme is interdicted by added thiols (k_8). We also observed that extended incubation of DTT with ICL1-HP resulted in reactivation of about 35% of the labeled enzyme, which was not observed with ICL1-3BP. This suggests that the apparent restoration of free Cys191 from S-homopyruvoylated ICL1 mediated by DTT, as observed both kinetically and by mass spectrometric analysis, likely occurs by a DTT-catalyzed retro-Michael reaction.

Kinetic, mass spectrometric, protein fluorescence, molecular modelling, and X-ray crystallographic data are all consistent with the proposed chemical mechanism of inactivation of ICL by 2-VIC shown in **Figure 3-11**. Our results demonstrate that 2-VIC comprises a true mechanism-based inactivator of both ICL1 and ICL2, effectively providing the chemical equivalent of the affinity label 3BP, namely, 2-vinyl-glyoxylate, almost exclusively confined to the active site of *Mtb* ICL, and which forms a covalent bond with its conserved active-site cysteine.
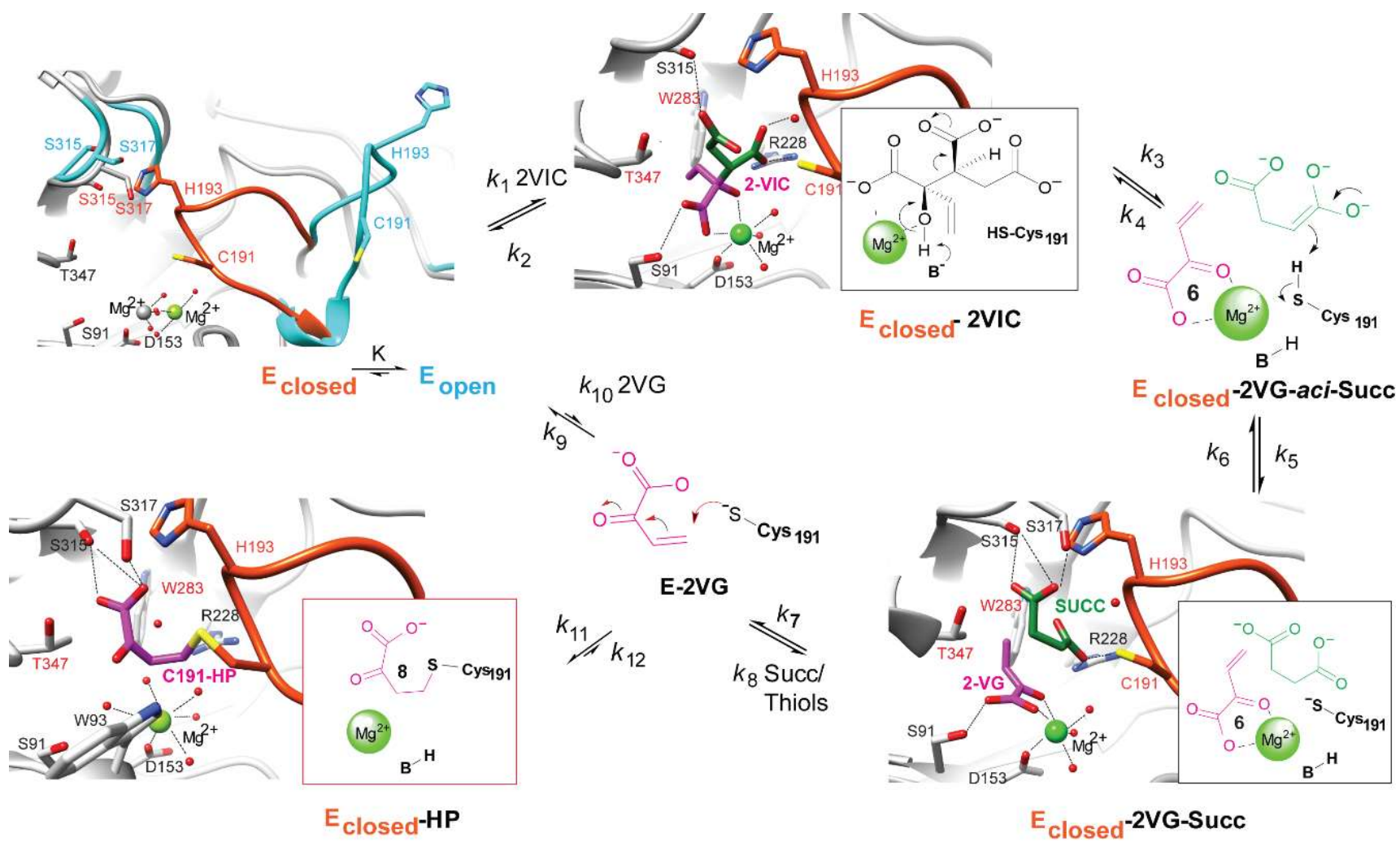
Figure 3-11 Proposed inactivation mechanism of ICL1 by 2-vinyl isocitrate

As a drug discovery strategy for tuberculosis, mechanism-based enzyme inactivation of isocitrate lyase in *Mycobacteria* offers significant advantages over existing inhibitors, which include: a specific covalent reaction confined to active-site Cys191 residues; irreversible, or slowly reversible, covalent inactivation comprises long residence time on the enzyme targets[85]; and the conserved active-site catalytic groups, such as Cys191, will be less likely to develop resistance via mutation of the targeted residue. Recently, benzothiazinones was reported to be potent anti-mycobacterial agents, and are mechanism-based inactivators of DprE1, an enzyme located in the cell wall of *Mtb*[133]. Reduction of a nitro substituent in the benzothiazinones resulted in a nitroso group which subsequently reacts with a cysteine residue in the active-site of DprE1[133]. The inactivation kinetic parameters of these compounds are comparable to those of 2-VIC. Our results encouraged the development of new analogues of 2-VIC that will provide mechanism-based inactivation as well as anti-mycobacterial activity in cell culture and in *in vivo* models of tuberculosis infection.

4. INHIBITION OF *Mycobacterium tuberculosis* ISOCITRATE

LYASE 1 BY SUBSTRATE ANALOGS

4.1. Introduction

Despite the availability of ICL1 crystal structures and exposure of the enzyme to high-throughput screening campaigns, no ICL1 inhibitors have emerged with drug-like properties including 2-vinyl-(2*R*,3*S*)-isocitrate (2-VIC), the previously discussed mechanism-based inactivator of *Mtb* ICL[4, 24, 43]. Apart from the favorable partitioning ratio (~ 0.24), 2-VIC inactivation occurs at a much slower rate than ICL1 catalysis (k_{cat}/k_{inact} = 1.5 x 10^4). The major rate limiting step during 2-VIC inactivation is the catalysis of 2-vinyl-(2*R*,3*S*)-isocitrate (2-VIC) to form 2-vinyl-glyoxylate (2-VG). As the active site of ICL1 is solvent-accessible during succinate release, 2-vinyl-glyoxylate is apparently intercepted by free thiols prior to the Michael reaction with Cys191, halting the inactivation[43]. Conversely, unmasking succinate-analog electrophiles would obviate the succinate dissociation step and circumvent thiol effects. Replacement of succinate with a better leaving group, which encompasses a more stable carbanion intermediate, would also enhance inactivation rate. Therefore, novel scaffolds of ICL1 alternative substrates are desirable for enhancing the efficiency of mechanism-based inhibitors against *Mtb* ICL.

Discovering of suitable succinate-substitution and alternative substrates requires further characterization of substrate analogs as ICL1 inhibitors. The structure of ICL1 with glyoxylate and nitropropionate bound in the active site highlighted important electrostatic interactions between the enzyme and carboxylate groups of the ligands. The enzyme also undergoes a significant conformation change, which facilitates retro-aldol cleavage of D-IC into glyoxylate and succinate. It was reported that ICL1 active-site loop assumes an open

and closed conformations in apo-ICL1 and ligand-bound ICL1 respectively whereas the loop becomes disordered in ICL1-glyoxylate complex[39]. Therefore, understanding the inhibition mode of ICL1 substrate-analogs are essential to direct inhibition specificity towards a desired enzyme conformation.

However, to date there have been very few structural-activity-relationship (SAR) studies of *Mtb* ICL1 substrate analogs[4]. In this thesis, a series of mono-, di- and tri-carboxylate compounds were evaluated as ICL1 inhibitors (**Table A-6**). The selection of ICL1 substrate analogs was guided by crystal structures of ICL1 co-crystalized with its known inhibitors[39]. Mode of inhibition and the corresponding inhibition constants were employed to explore binding synergy among ligands whereas selected potent inhibitors were co-crystallized with ICL1 in order to provide more structural insights into ICL1-ligand contacts.

4.2. Methods

Materials

DL-Isocitrate (trisodium salt), D-threo-isocitrate (potassium salt), NaCl, dimethyl sulfoxide (DMSO), sodium glyoxylate (monohydrate), succinic acid, D-malic acid, glutathione (reduced form), dithiothreitol (DTT), Lactate dehydrogenase (LDH) and all other chemicals were obtained from Sigma-Aldrich unless otherwise specified.

Plasmids containing *Mtb icl1* was a gift from Dr. Andrew Murkin of Buffalo University, NY[79].

E. coli isocitrate dehydrogenase (ICDH) gene was obtained from Aska (-) clone containing *icd* gene on a pCA24N plasmid[79, 130].

Protein Purification and Expression

Mtb ICL1 bearing an N-terminal, thrombin-cleavable His$_6$ epitope tag, was expressed in *E. coli* (BL21 (*DE3*)), and purified using affinity chromatography as previously described[79]. Eluted ICL1 was dialysed with 50 mM HEPES (pH 7.5) and stored in aliquots (>3.5 mg/mL) at –80 ºC.

ICL Enzyme Assays

Unless otherwise specified, all assays were conducted in in a clear 96-well plate containing 250 μM reaction mixtures of 50 mM HEPES (pH 7.5), 5 mM MgCl$_2$, and 1 mM DTT at 37ºC. In the direction of isocitrate cleavage, product glyoxylate was either converted to glycolate in a coupled-enzyme assay using *E. coli* lactate dehydrogenase (ε_{340} = 6220 M^{-1}cm^{-1}) or reacted with phenyl hydrazine-HCl to form a phenyl hydrazone product (ε_{324} = 17,000 M^{-1}cm^{-1}). In the direction of isocitrate synthesis, isocitrate product was converted to α-ketoglutarate in a coupled-enzyme assay using *E. coli* isocitrate dehydrogenase (ε_{340} = 6,220 M^{-1}cm^{-1}). All absorbance measurements were recorded with a Biotek® plate reader.

Inhibition Assays

For the forward reaction of ICL, residual activity ICL1 (2 nM) was measured in the presence of varying inhibitors concentrations (0 – 10 mM) at fixed concentrations of (2R,3S)-isocitrate (25 – 100 μM). For the reverse reaction, competitive inhibition vs. succinate was measured by following the initial velocity of isocitrate synthesis catalyzed by ICL1 (10 nM) in the presence of varying inhibitors (0 – 10 mM) at a fixed concentration of glyoxylate (100 μM) and succinate (250-1000 μM) using the isocitrate dehydrogenase coupling assay as described above. Similarly, competitive inhibition vs glyoxylate was determined by observing the initial velocity of aldol condensation reaction catalyzed by ICL1 (10 nM) in

the presence of varying inhibitors (0 – 10 mM) at fixed concentrations of glyoxylate (100-500 µM) and succinate (250 µM). Inhibition effects for each inhibitors were determined at two or more fixed concentration of substrates.

Graphical analysis of inhibition patterns in Bowden plots[104] was used to characterize inhibition mode and to estimate inhibition constants (K_{is}, the competitive inhibition constant and K_{ii}, the uncompetitive inhibition constant vs. the substrate). A global analysis of inhibition constants (v_0 vs. I plot at 6 – 8 concentrations of (2R,3S)-isocitrate) was also evaluated when IC$_{50}$ values were less than 1.0 mM in the presence of 25 µM (2R,3S)-isocitrate for competitive inhibition and in the presence of 100 µM (2R,3S)-isocitrate for uncompetitive inhibition. Glyoxylate product from isocitrate cleavage was measured via the phenyl hydrazine assay whereas isocitrate formation was measured in a coupled-enzyme assay as described above.

Yonetani-Theorell Analysis

Analysis of enzyme interaction with multiple inhibitors was carried out at varying concentration of the first inhibitor at fixed levels of the second inhibitors as described before[134, 135]. Inhibition of ICL1 (2 nM) was measured as the change in initial velocity of ICL1 catalysis of 50 µM (2R,3S)-isocitrate. Data was plotted as 1/v vs. the competitive inhibitor concentration and the synergistic value α was calculated by equation α = "x-axis intercept" x K_m/S, where K_m is the Michaelis-Menten constant and S is concentration of isocitrate.

X-ray Crystallography

Hydroxycitrate-bound ICL1 structure was obtained from co-crystallization of *Mtb* tag-free ICL1 (10 mg/ml) and 10 mM hydroxycitrate (> 1000-fold K_i) in buffer containing 0.1 M HEPES (pH 7.6), 0.2 M NaCl, and 25-30% PEG 4,000. The same mother liquor was used as the cryo-protectant, and crystals were flash-frozen in liquid nitrogen, and maintained chilled under a stream of liquid nitrogen (100 K) throughout data collection. High-resolution diffraction data for crystals were collected on an ADSC Quantum 315 detector at a wavelength of 0.9793 Å from beamline 19ID of the Structural Biology Center (SBC, Advanced Photon Source, Argonne National Laboratory). Detailed data transformation and structure refinement is obtained by Dr. Inna Krieger of the Sacchettini lab, Texas A&M.

Analysis of Kinetic Data

Inhibition constant (K_i or K_{ii}) was determined by global fitting of equation (8).

$$y = K([I] + Ycross \qquad (8)$$

for which,

y is a function of catalysis rates (1/v, in competitive inhibition, or S/v, in uncompetitive inhibition) where S is a concentration of substrate and v is the initial velocity

[I] is concentration of inhibitor

K is either the competitive (K_i) or the uncompetitive (K_{ii}) inhibition constant

Ycross represents the y-value at which point intersecting lines of different substrate concentrations meets.

Binding energy differences were determined by equation (16)

$$\Delta\Delta G = RT(\ln\frac{K_I^1}{K_I^2}) \qquad (16)$$

for which,

K is either the competitive (K_i) or the uncompetitive (K_{ii}) inhibition constant;

[1] and [2] desginate the ligands in the comparison,

R is the gas constant

T is temperature (K).

Dose response curve of inhibition was fitted to equation (17) in order to estimate IC_{50} and Hill coefficient values.

$$y = \frac{100}{1 + (\frac{[I]}{IC_{50}})^h} \tag{17}$$

for which,

y is the percentage of normalized response (v_i/v_0),

I is the concentration of inhibitors,

IC_{50} is the concentration of inhibitor to exert 50% inhibition

h is the Hill coefficient

4.3. Results

Steric Effects Hinder ICL1 Inhibition by α-hydroxyl mono-carboxylate Compounds

Of the evaluated α-hydroxyl mono-carboxylate compounds, many were ICL1 competitive inhibitors vs. isocitrate except for 2(R)-hydroxylbutanoate that exhibited mixed/noncompetitive inhibition. Here competitive inhibition vs. (2R,3S)-isocitrate is described by K_{is} and uncompetitive inhibition (inhibition of E-glx binary complex) is described by K_{ii}. Glycolate, a reduced form of glyoxylate, was the most potent competitive inhibitor of isocitrate ($K_{is} = 70 \pm 10$ µM) among all mono-carboxylate compounds tested. Carbon chain extension to glycolate resulted in steric hindrance and drastic decreases of active-site affinity (**Figure 4-1**). D-lactate, which is glycolate with an additional methyl group, increased the inhibition constant by 20-fold ($K_{is} = 2.3 \pm 0.3$ mM).

glyoxylic acid

$K_d = 20 \pm 3\ \mu M$ $K_{is} = 70 \pm 7\ \mu M$ $K_{is} = 2.3 \pm 0.3\ mM$ $K_{is} = 10 - 15\ mM$ $R = benzyl, phenyl$
$K_{ii} = 10 - 20\ mM$ $K_{is} > 10\ mM$
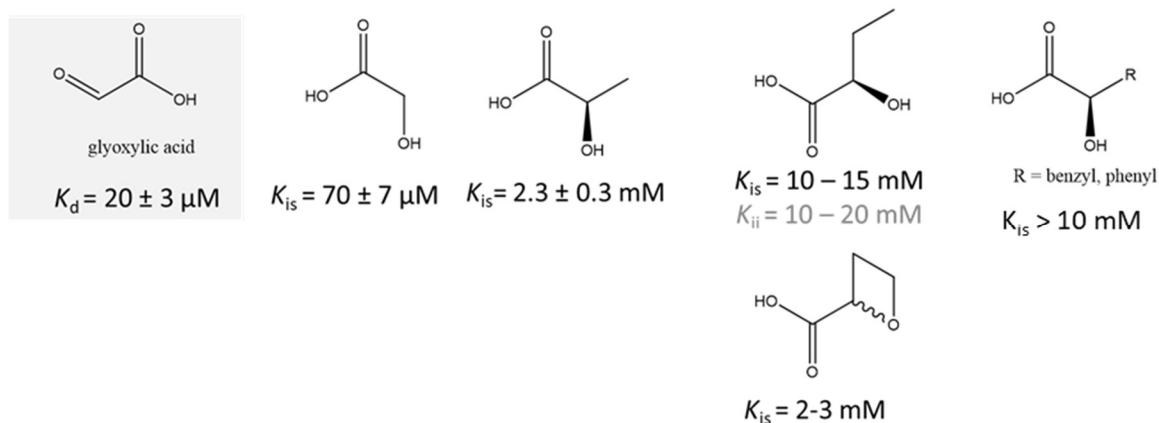
$K_{is} = 2\text{-}3\ mM$

Figure 4-1 Reduced inhibition effects of α-hydroxyl mono-carboxylate compounds due to presumably steric hindrance

As the substituents on carbon 2 became larger, inhibition was diminished. Addition of an ethyl group reduced active site affinity by another 7-fold (2(R)-hydroxylbutanoate: K_{is} ~ 10-15 mM). Owing to a more compact geometry of the oxetane ring compared to 2(R)-hydroxylbutanoate, 2-oxetane-carboxylate displayed a significant improved inhibition (K_{is} ~ 2-3 mM). Incorporation of a benzyl group led to a competitive inhibitor whose $K_{is} = 5 \pm 1$ mM. On the other hand, no inhibition of ICL1 was observed with phenyl lactate derivatives ($K_{is} \gg 10$ mM). Steric penalty energies were estimated from the differences in inhibition constants between 2-subsituted-glycolate and glycolate (equation 16). **Figure 4-2** showed the correlation between penalty energies and R group size representing by A-values[136].
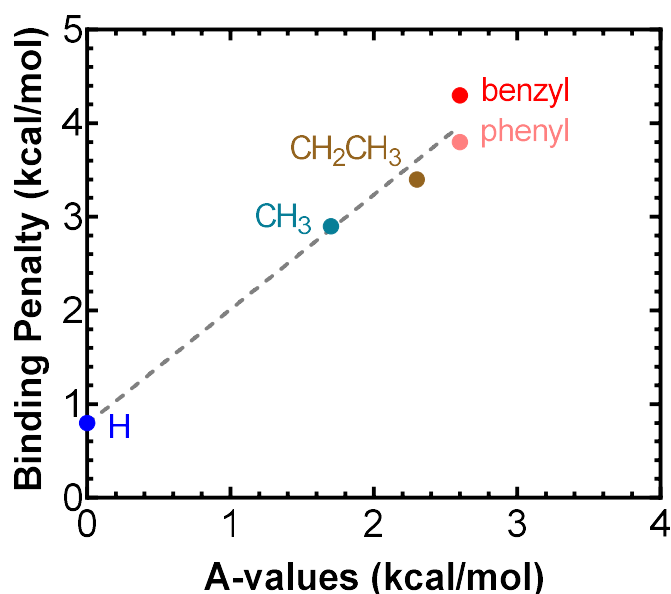
Figure 4-2 Linear correlation between steric hindrance (A-values) and differences in binding energy ($\Delta\Delta G$, kcal/mol) of R-substituted α-(R)-hydroxyl-monocarboxylate

Mono-carboxylates as Succinate Analogs

The ability of mono-carboxylates compounds to replace succinate in the active site of ICL1 was limited to compounds with a less bulky, electron-withdrawing group. Succinate analogs act as uncompetitive inhibitors vs. isocitrate whose inhibition constant is described by K_{ii} in contrast with competitive inhibitors vs. isocitrate whose inhibition constant is described as K_{is}. Nitropropionate ($K_{ii} \sim 100$ µM) was the best inhibitor in this group, followed by cyanopropionate ($K_{ii} = 3.4 \pm 0.7$ mM) and succinylsemialdehyde ($K_{ii} = 10 \pm 0.7$ mM). Both nitropropionate and succinylsemialdehyde were shown to be substrates for ICL1[62]. Interestingly, γ-hydroxylbutanoate and 3-(aminosulfonyl)propanoate did not did not exert any observable inhibition effects on ICL1 ($K_{ii} \gg 10$ mM) which could be accounted for by their inability to stabilize the carbanion intermediate. Other mono-carboxylate compounds with bulky ring substituents also exhibited no inhibition of ICL1 ($K_{ii} \gg 10$ mM).
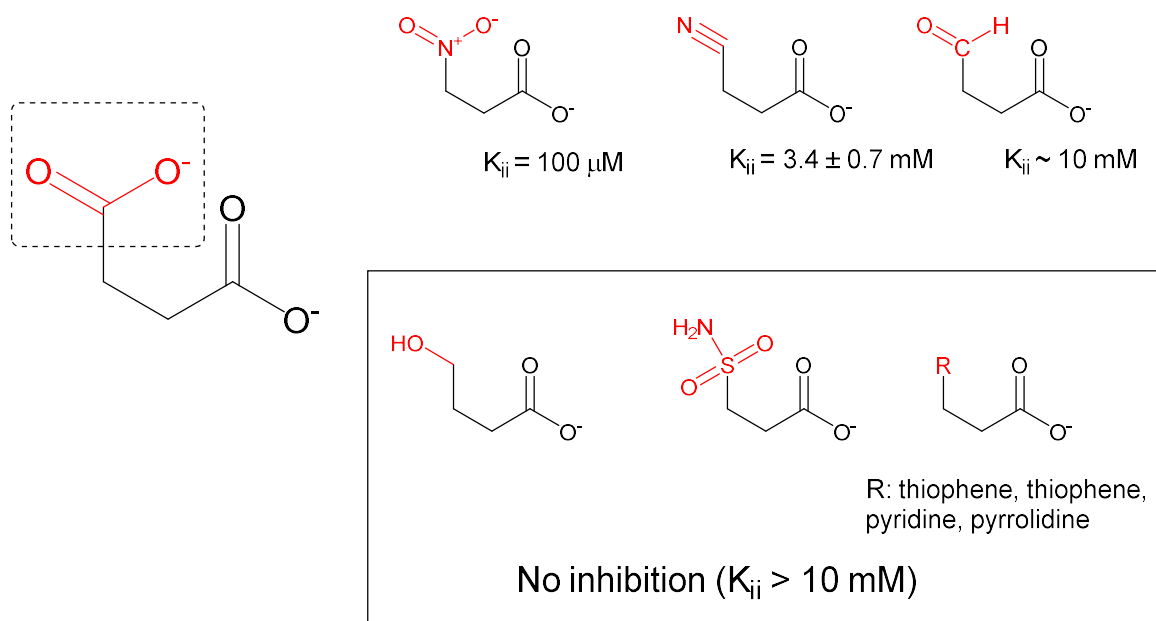
91

$K_{ii} = 100 \ \mu M$ $K_{ii} = 3.4 \pm 0.7$ mM $K_{ii} \sim 10$ mM

R: thiophene, thiophene, pyridine, pyrrolidine

No inhibition ($K_{ii} > 10$ mM)

Figure 4-3 Mono-carboxylates as succinate analogs

Cis-di-carboxylates are Better Succinate Analogs than Their Trans-isomers

Addition of a carboxylic acid group to D-lactate yielded (2R)-malate whose $K_{is?}$ is 350 ± 30 µM, a 7-fold improvement compared to D-lactate ($\Delta\Delta G \sim 1.2$ kcal/mol). Similarly, α-hydroxylglutarate achieved competitive inhibition vs. isocitrate ($K_{is} = 700 \pm 50$ µM), which is approximately 15-fold better than its mono-carboxylate counterpart, α-hydroxylbutanoate ($\Delta\Delta G \sim 1.6$ kcal/mol).This increase in binding affinity suggested that the second carboxylic acid group, the equivalent of 3-carboxy group on isocitrate, allows favorable interactions with ICL1 active site. Notably, maleic acid, a structurally-frozen mimic of the *cis-*configuration of succinate binds to the same site as succinate with which it has 2-fold improvement in affinity (Maleate: $K_{ii} = 300 \pm 20$ µM; succinate: $K_{ii} = 650 \pm 50$ µM). On the other hand, the *trans-* isomer fumarate is a poor competitive inhibitor vs. (2R,3S)-isocitrate

($K_{is} = 1.9 \pm 0.4$ mM). Therefore, from the example of this study, a *cis*-conformation of but-2-en-1,4-dioic acid inhibitors is preferred for binding to the ICL-Glx complex. *Cis* and *trans*-aconitate are tri-carboxylate compounds, which exerted competitive inhibition vs. isocitrate. Inhibition by *cis*-aconitate was 9-fold better than trans-aconitate (*cis*-aconitate: $K_{is} = 550 \pm 80$ μM and *trans*-aconitate: $K_{is} = 5 \pm 1$ mM).

Substitutions at C_3 and C_4 of Isocitrate

Strikingly, replacement of 2,2-hydrogens in succinate with fluorine resulted in 10-fold decrease in binding affinity (2,2-difluorosuccinate: $K_{ii} = 6.6 \pm 0.8$ mM). In contrast, chloro-succinate demonstrated a moderate inhibition of the enzyme by binding to the ICL1-glx complex ($K_{ii} = 2.5 \pm 0.2$ mM). Both compounds are poor inhibitors of apo-ICL1 (2,2-di-fluoro-succinate: $K_{is} = 1.7 \pm 0.2$ mM and chloro-succinate: $K_{is} = 2.2 \pm 0.5$ mM) when compared to (2*R*)-malate, which supported the significance of the 2-(*R*)-hydroxyl group in glyoxylate/ isocitrate analogs (ΔΔG ~1.1 kcal/mol).

Oxaloacetate exhibited a mixed inhibition pattern from which $K_{ii} = 260 \pm 20$ μM and $K_{is} = 140 \pm 40$ μM. In comparison with (2*R*)-malate, oxaloacetate displayed moderate improvement in competitive inhibition vs. isocitrate (ΔΔG ~ 0.6 kcal/mol). In contrast, as an uncompetitive inhibitor, binding of oxaloacetate to the ICL1-glx complex showed a 20-fold increase from (2*S*)-malate (ΔΔG = 1.8 kcal/mol), which underlines a preference for sp^2 character in the C – O bond. It appears that greater electron-withdrawing inductive effects of R-substituents are correlated with improved binding affinity in mono-substituted succinate (=O > -Cl > -OH).
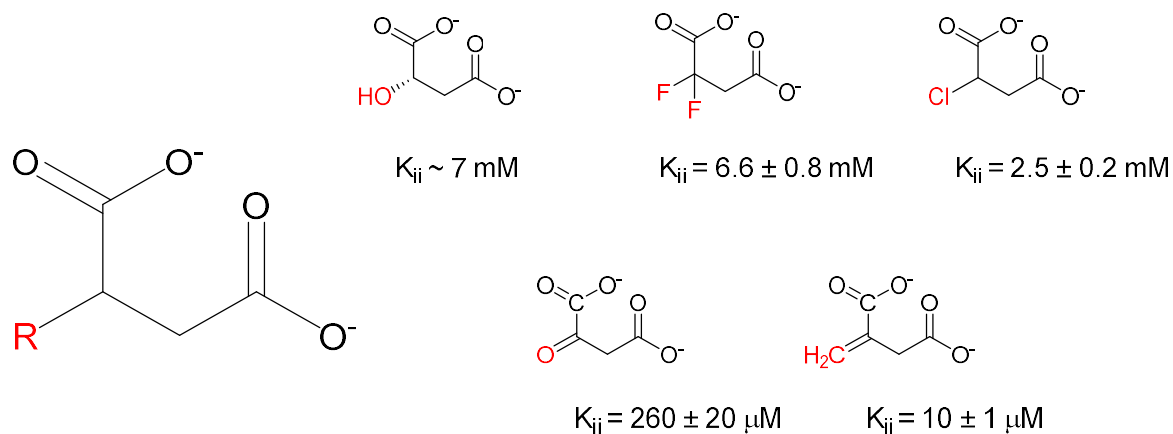
Figure 4-4 Comparisons of 2-mono-substituted succinate compounds

Among di-carboxylate compounds, itaconate, a methylene-succinate, displayed the most potent uncompetitive inhibition ($K_{ii} = 10 \pm 1$ μM). Inhibition due to itaconate is 500-fold better than that of citraconate *($\Delta\Delta$G ~ 3.8 kcal/mol)* and 26-fold better than that of oxaloacetate ($\Delta\Delta$G ~ 2.0 kcal/mol), which could not be accounted for by steric hindrance, hybridization states of carbon-2 and/or inductive effects. It has been suggested that itaconate acts as a transition state analog, which forms a more stable carbanion due to effects of resonance and charge delocalization. These results encouraged installation of small, sp^2-like electron-withdrawing group on succinate fragment.

In addition, hydroxycitrate was a potent competitive inhibitor vs isocitrate ($K_{is} = 8.0 \pm 0.7$ μM), which indicates that substitution of a hydroxyl group on carbon-3 of isocitrate does not deter binding of this analogue, albeit, this substituent prevents catalysis. On the other hand, introduction of a keto group on carbon-4 of isocitrate yielded α-hydroxy-β-oxalosuccinate, which only afforded a moderate competitive inhibitor vs. glyoxylate ($K_{is} = 90 \pm 30$ μM). Therefore, from this study, the additional moiety is more favorable at C-3 than the C-4 position of isocitrate.

4.4. Conclusions

The survey of ICL1 substrate analogs emphasized the binding stringency of the ICL1 active site. In particular, the "binding penalty" contributed by substitution at carbon-2 is directly correlated to steric hindrance (A-values), which helps to predict inhibition effects of other R-group installments at this position. The preference of ICL1 for binding of *cis*- rather than *trans*-but-2-ene-dionic acid suggested that the energetically less favored *syn*-conformation of dicarboxylic acids is preferred for inhibition by saturated succinate-analogs. Cyano, aldehyde and nitro groups may substitute for one of the carboxylate group for succinate analogs. Succinate analogs with substituents at the C-2 position are allowed, and their inhibition is correlated with electron-withdrawing effects of the substituents (=O > -Cl > -OH > -H). The exception is itaconate, which might effect a transition state analog. A linear correlation analysis of inhibition constants has led to the semi-quantitative structural-activity relationship (q-SAR) portrayed in **Figure 4-5**.
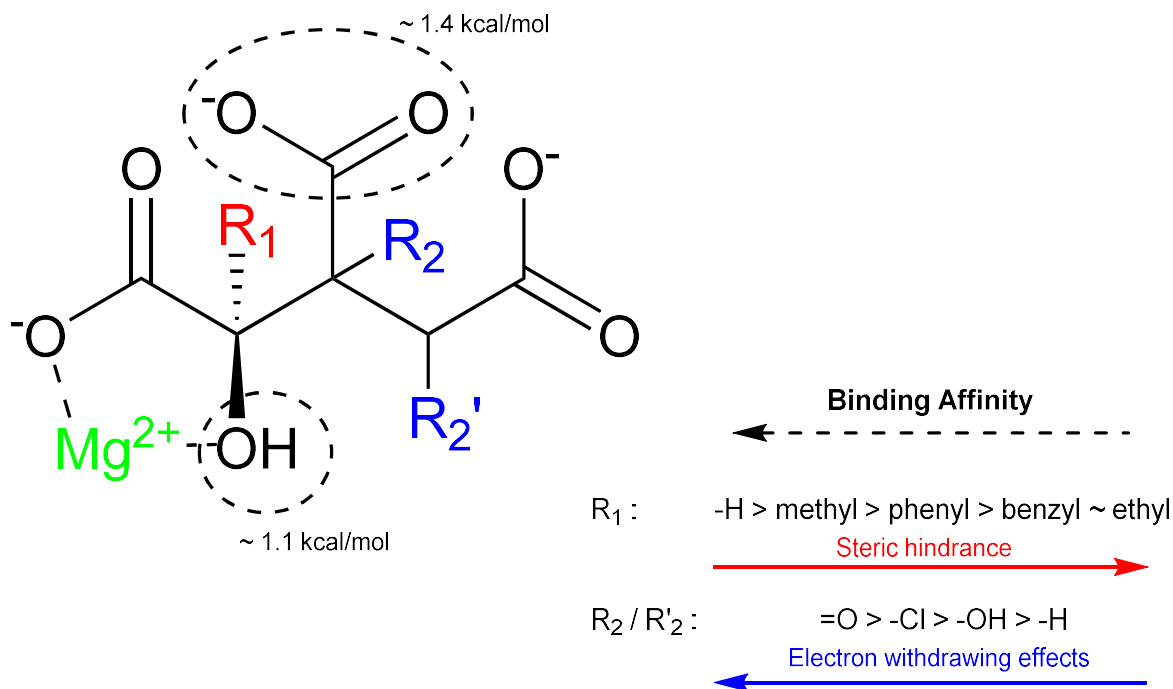
Figure 4-5 Semi-quantitative structural-activity relationship analysis of isocitrate analogs

The results of our survey suggests that the identification of new inhibitors of ICL1 which are structural analogues of its three substrates (isocitrate, glyoxylate and succinate) will be challenging due to the apparent stringency evident from even conservative substitution of these ligands. A noteworthy finding, however, is that the substitution of a 3-hydroxyl group on isocitrate (2-hydroxy-citrate) is tolerated by ICL1, to afford an isocitrate-analogue inhibitor that binds with a potency similar to that of the substrate. 2-Hydroxy-citrate, or (2*R*,3*R*)-hydroxy-citrate as shown in the crystal structure of ICL1 co-crystalized with hydroxy-citrate, is in effect a conjugate of the two ICL1 inhibitors, glycolate and (*R*)-malate. Interestingly, substitution of a hydroxyl group on carbon-3 of isocitrate prevented its scission by ICL1 catalysis. This suggests that substitution of oxygen-bearing groups on carbon-3 may afford suitable inhibitors of ICL1 or perhaps, isocitrate analogues that form covalent adducts with the enzyme or induce time-dependent inhibition. Additionally, we

observed synergistic binding between glyoxylate and succinate analogs such as that of maleate and glycolate/(R)-lactate. Therefore, the conjugation of glyoxylate and succinate analogs could provide improved ICL1 inhibitors.

5. *Cis*-2,3-EPOXY-SUCCINATE, A SELECTIVE INACTIVATOR

OF *Mycobacterium tuberculosis* ISOCITRATE LYASES

5.1. Introduction

Current *Mtb* ICL inactivators either caused catastrophic cellular effects or were interdicted by thiols, and hence have limited therapeutic potentials[4, 24]. Nitropropionate is a covalent inactivator of ICL but also a suicide inactivator of succinate dehydrogenase[58, 61]. 3-bromo-pyruvate is a potent inactivator of ICL but also reacts with thiols[56] and other active-site cysteines in enzymes such as glyceraldehyde-3-phosphate dehydrogenase[60]. More suitable inhibitors for *Mtb* ICLs should have improved specificity.

As detailed in Chapter 3, 2-vinyl-(2*R*,3*S*)-isocitrate (2-VIC) is a mechanism-based inactivator of *Mtb* ICLs, for which ICL catalysis unmasks a Michael acceptor, 2-vinyl-glyoxylate, to efficiently form a covalent adduct with Cys191[43]. The active-site generated 2-vinyl-glyoxylate (2-VG), a glyoxylate analog, migrates to the succinate binding pocket and reacts with Cys191 following succinate dissociation[43]. As the active site of ICL1 is exposed during the dissociation of succinate[14], 2-vinyl-glyoxylate is apparently intercepted by free thiols in lieu of its the reaction with Cys191. Therefore, by incorporation (masking) of electrophiles into succinate analogs could bypass the succinate dissociation step and thiol protection.

ICLs undergo a significant conformation changes upon ligand binding, which differentiates the apo-ICL1 form from the ligand-bound ICL1 complex. Succinate-analogs are uncompetitive inhibitors vs. isocitrate, which bind solely to ICL1-Glx complex, not to apo-ICL1. Conversely, D-isocitrate can only bind to apo-ICL1. We hypothesized that succinate-analogs would potentially have specificity for ICL against other enzymes utilizing

(2R,3S)-isocitrate, such as isocitrate dehydrogenase. In fact, maleic acid, a competent uncompetitive ICL1 inhibitor, exhibited no inhibition effects on isocitrate dehydrogenase[24, 137]. The survey of substrate analogs revealed that *cis*-olefinic-di-carboxylic acids comprise significantly improved uncompetitive inhibitors compared to their *trans*-di-carboxylic acid analogs (which, where analyzed, are isocitrate-competitive inhibitors) and succinate analogs allow substitution at C-2 ($K_{ii} < 5$ mM). As mentioned above, the micromolar inhibition arising from 2-hydroxycitrate and maleic acid suggests that *cis*-epoxy succinate (EpS) would bind to the succinate sub-site of ICL1 as a succinate analog, which position the epoxide group proximal to Cys191 and lead to the formation of a covalent adduct, a malylated-ICL1, upon opening of the epoxide ring.

5.2. Methods

Materials

D-threo-isocitrate (potassium salt), NaCl, dimethyl sulfoxide (DMSO), sodium glyoxylate (monohydrate), succinic acid, (R)-malic acid, glutathione (reduced form), dithiothreitol (DTT), Lactate dehydrogenase (LDH) and all other chemicals were obtained from Sigma-Aldrich unless otherwise specified.

Plasmids containing *Mtb icl1* was a gift from Dr. Andrew Murkin of Buffalo University, NY[79].

Icl2-pET26-b plasmid was provided by GlaxoSmithKline Pharmaceuticals, PA.

E. coli isocitrate dehydrogenase (ICDH) gene was obtained from Aska (-) clone containing *icd* gene on a pCA24N plasmid[79, 130].

ICL Enzyme Assays

Unless otherwise specified, all assays were conducted in in a clear 96-well plate containing 250 μM reaction mixtures of 50 mM HEPES (pH 7.5), 5 mM $MgCl_2$, and 1 mM DTT at 37°C. In the direction of isocitrate cleavage, product glyoxylate was either converted to glycolate in a coupled-enzyme assay using *E. coli* lactate dehydrogenase (ε_{340} = 6220 $M^{-1}cm^{-1}$) or reacted with phenyl hydrazine-HCl to form a phenyl hydrazone product (ε_{324} = 17,000 $M^{-1}cm^{-1}$). In the direction of isocitrate synthesis, isocitrate product was converted to α-ketoglutarate in a coupled-enzyme assay using *E. coli* isocitrate dehydrogenase (ε_{340} = 6,220 $M^{-1}cm^{-1}$). All absorbance measurements were recorded with a Biotek® plate reader.

Inhibition Assays

For the forward reaction of ICL, residual activity ICL1 (2 nM) was measured in the presence of 0–5 mM *trans*-EpS and two concentrations of (2*R*,3*S*)-isocitrate (50 μM and 100 μM). Graphical analysis of inhibition patterns in Cornish-Bowden plots[104] was used to characterize the apparent mode of inhibition and to estimate inhibition constants (K_{is} and K_{ii}). Glyoxylate product from lysis of isocitrate was measured via the phenyl hydrazine as described above.

Inhibition of TCA Cycle and Other Enzymes

A list of enzymes tested for analysis of the selectivity of inactivators is included in **Table A-7**. Inhibition of enzymes of the TCA cycle and ATP-citrate synthase was carried at a fixed concentration of substrates, approximately $2K_M$, and in the presence of 1 mM *cis*-epoxy-succinate. Remaining enzyme activity of succinyl-CoA synthetase was detected via a pyruvate kinase/lactate dehydrogenase-coupling assay. Malate dehydrogenase and citrate synthase activity was measured by following the formation of oxaloacetate via reaction with

phenyl-hydrazine (A_{324}). Similarly, phenyl-hydrazine was used to determine activity of oxoglutarate dehydrogenase by detection of oxoglutarate product formation at A_{324}. For fumarase, formation of malate was coupled with malate dehydrogenase and phenyl-hydrazine assay in which oxaloacetate and NADH formation was measured concurrently (A_{324} and A_{340} respectively). Formation of isocitrate from citrate by citrate synthase and ATP-citrate synthase was measured by isocitrate dehydrogenase-coupling assay in which NADPH formation was observed with A_{340}.

Inactivation Assays via Preincubation Method

For measurement of residual ICL activity during the forward reaction, 1 μM ICL1 or 15 μM ICL2 was incubated with varying inactivator concentrations in pre-incubation buffer containing 50 mM HEPES (pH 7.5), 5 mM $MgCl_2$, in the presence or absence of DTT. Samples were withdrawn from pre-incubation mixtures, diluted 50-fold, and glyoxylate product from lysis of isocitrate was measured via the phenyl hydrazine assay as described above. Initial rates were normalized to the control sample in which no inactivator was added.

Inactivation Assay via Continuous Progress Curve Method

Apparent rates of ICL inactivation (k_{obs}) were measured as time-dependent changes of initial rates (v_0) to slower final rates ($v_s = 0$) were obtained from time courses of glyoxylate formation via reaction with phenyl-hydrazine (as above). To 0.25-mL reaction mixtures containing 2 nM ICL1, (2R,3S)-isocitrate was added to final concentrations of 25-200 μM, followed by rapid addition of *cis*-EpS (final concentrations of 0-2.5 μM). Time course of glyoxylate time courses were recorded at $OD_{324 \, nm}$ for 0-10 min. Final concentrations of 0 – 200 μM *cis* – EpS was added to observe the time-dependent inactivation of ICL2 (20 nM).

Thrombin Cleavage of H$_6$-ICL1

Incubation of thrombin (200 units, GE27-0846-01) and H$_6$-ICL1 (20 mg) for 20 hrs in buffer containing 50 mM HEPES, 10 mM (2R,3S)-isocitrate, 10 mM MgCl$_2$ and 1 mM DTT yielded 80% tag-free enzyme (16 mg) after quick removal of uncut H$_6$-ICL via binding to a 5 mL Histrap™ HP column (GE). Tag-free ICL1 was collected in 20 mL elution with binding buffer containing 50 mM Tris-HCL (pH 7.5), 150 mM NaCl and 20 mM Imidazole. Eluted tag-free ICL1 was concentrated and buffer exchanged into a buffer consisting of 50 mM HEPES (pH 7.5) , and 10 mM MgCl$_2$.

X-Ray Crystallography

(S)-malynyl-C191 ICL1 complexes were obtained from crystallization of thrombin-cleaved tag-free ICL1 (10 mg/ml), treated with 2 mM *cis*-epoxy-succinate for 1 hour prior to the hanging-drop set up to produce crystals. The hanging-drop composed a 1:1 volume ratio of the protein and a mother liquor solutions containing 0.1 M Tris-HCl (pH 8.0), 0.2 M sodium acetate, and 20-30% PEG 4,000. Collection of X-ray diffraction and analysis of the crystal structure were conducted in a collaboration with Dr. James Sacchettini.

Inhibition of Mtb Growth on Acetate and Glucose

Inhibition of *Mtb Mc^2 7000* growth was done in a collaboration with Dr. Sachettini group as described before[74].

Synergistic Inhibition of Substrate Analogs

Yonetani-Theorell plots, in which the effects of two inhibitors on an enzymatic reaction are determined simultaneously[134, 135], allow evaluation of synergistic binding between substrate analogs (**Table A-5**). Inhibition of ICL1 in the presence of multiple inhibitors was examined at an isocitrate concentration equal to $2K_M$ (50 µM). Agonistic synergy was observed between maleic acid and either glycolate or (*R*)-lactate ($\alpha < 1$) (**Figure A-8** & **Figure A-9**). Since maleate binds to the ICL1-binary complex, formation of ICL1-glycolate or ICL1-D-lactate was expected to promote the association of maleate. Synergy between glyoxylate analogs and succinate analogs is also demonstrated in the potent inhibition of hydroxycitrate, a conjugation of glycolate and (2*R,S*)-malate ($K_{is} = 8 \pm 1$ µM). On the other hand, binding of (2*R*)-malate, a competitive inhibitor vs. isocitrate, and maleate, an uncompetitive vs. isocitrate, is neither agonistic nor antagonistic since they binds to two different enzyme forms (**Figure A-10**). Similarly, no significant synergistic interaction was observed between (2*R*)-malate and succinate even though their binding is not mutually exclusive. A more extensive comparison of substrate analog interactions is required in order to understand the synergistic inhibition of ICL1.

Differential Gel Electrophoresis (DIGE)[138]

E. coli B21 (*DE3*) was transformed with PUC19 (control) or *Mtb* ICL1-containing plasmids and allow to recover in 0.5 mL of LB with vigorous shaking at 37ºC for 45 min. Fifty µL of cell culture was evenly spread on a LB-agar plate containing 100 µM carbenicillin and incubated overnight at 37ºC. A single colony was picked for 10 mL overnight culture at 37ºC. *E. coli* cell pellets were harvested by centrifugation at 6,000 g, 4ºC. Cell lysate was obtained via physical disruption of cell pellets with a sonicator in a lysis buffer containing

50 mM HEPES (pH 7.5) and 10 mM MgCl$_2$. After sonication, lysate was clarified with centrifugation at 17,000 g, 4ºC for 10 min and supernatant was treated with or without *cis*-EPS (1 mM). For commercial preparations of enzymes of the TCA cycle and other enzymes, reaction mixtures containing 2.5 μg of each enzyme was prepared in a buffer containing 50 mM HEPES, 10 mM MgCl$_2$ and 1 mM DTT.

Protein samples were sent out for DIGE at the protein lab of biochemistry department. Samples were then precipitated in chloroform/ methanol and dissolved in labeling buffer ((7M urea, 2M thiourea, 4% CHAPS, 10 mM Tris, pH 8.3). Treated and untreated samples were then labeled with Cy5 and Cy2 (CyDye, GE; 28-9345-30), respectively, on ice and in dark for 60 min. Lysine (10 mM) was added and incubated for 15 min to quench excessive dye. Untreated and treated samples were mixed and diluted into rehydration solution containing Destreak solution (GE; 17-6003-19), bromophenol blue, LB and Pharmalytes (Sigma-Aldrich; P1522) to a volume of 250-μL. The mixture was used to rehydrate a 13 cm, pH 3-10NL DryStrips. pI focusing performed on a GE Ettan IPGPhor (v2); total 25,000 volt hours. Strips were then incubated with DTT (10 mg/ml) and Iodoacetamide (25 mg/ml) for 10 min each before loaded onto a 12% polyacrylamide slab gel. Gels were imaged on a FLA9500 Typhoon imager (GE) in which blue and green channel images were recorded separately. Further processing of gel images were carried out with ImageJ to analyze/ calculate the differential shift between the blue and green channel image[139]. Common protein spots in both images were obtain by applying the "MIN" operator. Protein spots found exclusively in one untreated or treated sample were obtained from "substract" operator. The images showing common protein spots, exclusively treated and exclusively untreated protein spots result were then merged into a single image.

Analysis of Kinetic Data

Irreversible, time-dependent inactivation of ICL was also assessed by fitting of the product

formation curve to a modified form of the product vs. time equation reported by Morrison

and Walsh [140].

$$[\text{Product}] = \frac{v_i \exp^{k_{obs} t}}{k_{obs}} + C \tag{18}$$

$$k_{obs} = \frac{k_{inact} [I]}{K_I^{app} + [I]} \tag{19}$$

for which,

[Product] is concentration of glyoxylate formation measured by changes in

mOD_{324}

v_i are the initial rates at time 0 (mOD/s)

t is the time of reaction (s)

[I] is the concentration of inactivator

k_{obs} is the apparent rate of [EA] depletion or [EI*] formation

k_{inact} is the maximal rate constant of inactivation

K_I^{app} is the apparent concentration of inactivator at which the observed rate

constant of inactivation is half that of k_{inact},

and C is a constant representing experimental background noise.

During analysis of the mode of inhibition or inactivation, re-plots of the apparent

inactivation rates, k_{obs}, vs. substrate concentration were fitted to equation (19) and (20) for

competitive and uncompetitive inactivators, respectively.

$$k_{obs} = \frac{k_{max}}{1 + \frac{[A]}{K_A}} + k_{bgd} \tag{20}$$

$$k_{obs} = \frac{k_{max}}{1 + \frac{K_A}{[A]})} + k_{bgd} \tag{21}$$

for which,

k_{obs} is observed inactivation rate,

k_{max} is the maximal observed inactivation rate at a single concentration of

inactivator (s^{-1})

[A] is the concentration of the variable substrate ((2R,3S)-isocitrate,

glyoxylate or succinate, μM)

K_a is its Michaelis constant,

and k_{bgd} is the minimum observed inactivation rate, if different than 0.

The plot of apparent K_{inact}, representing concentration of inactivator to achieve half of maximal inactivation rate vs. substrate concentration was evaluated by equation (21) for an uncompetitive inactivation.

$$K_{\text{inact}}^{\text{app}} = K_{\text{inact}}\left(1 + \frac{K_A}{[A]}\right) \tag{22}$$

for which,

K_I^{app} is the apparent concentration of inactivator at which the observed rate constant of inactivation is half that of k_{inact},

[A] is the concentration of the variable substrate ((2R,3S)-isocitrate, glyoxylate or succinate (µM),

and K_a is its Michaelis constant

5.3. Results

Cis Conformation was Essential for the Time-Dependent Inactivation of ICL1 by epoxy-succinate

ICL1 retro-aldol catalysis of isocitrate cleavage was rapidly reduced in the presence of *cis*-EpS. Time courses of glyoxylate formation from ICL1-catalyzed cleavage of 200-µM isocitrate (~8K_M) in the presence of *cis*-EpS (0 – 0.83 µM) is shown in **Figure 5-1A**. The data demonstrated a profound time-dependent inhibition or inactivation of ICL1 in the presence of an isocitrate concentration that is ~8K_M.
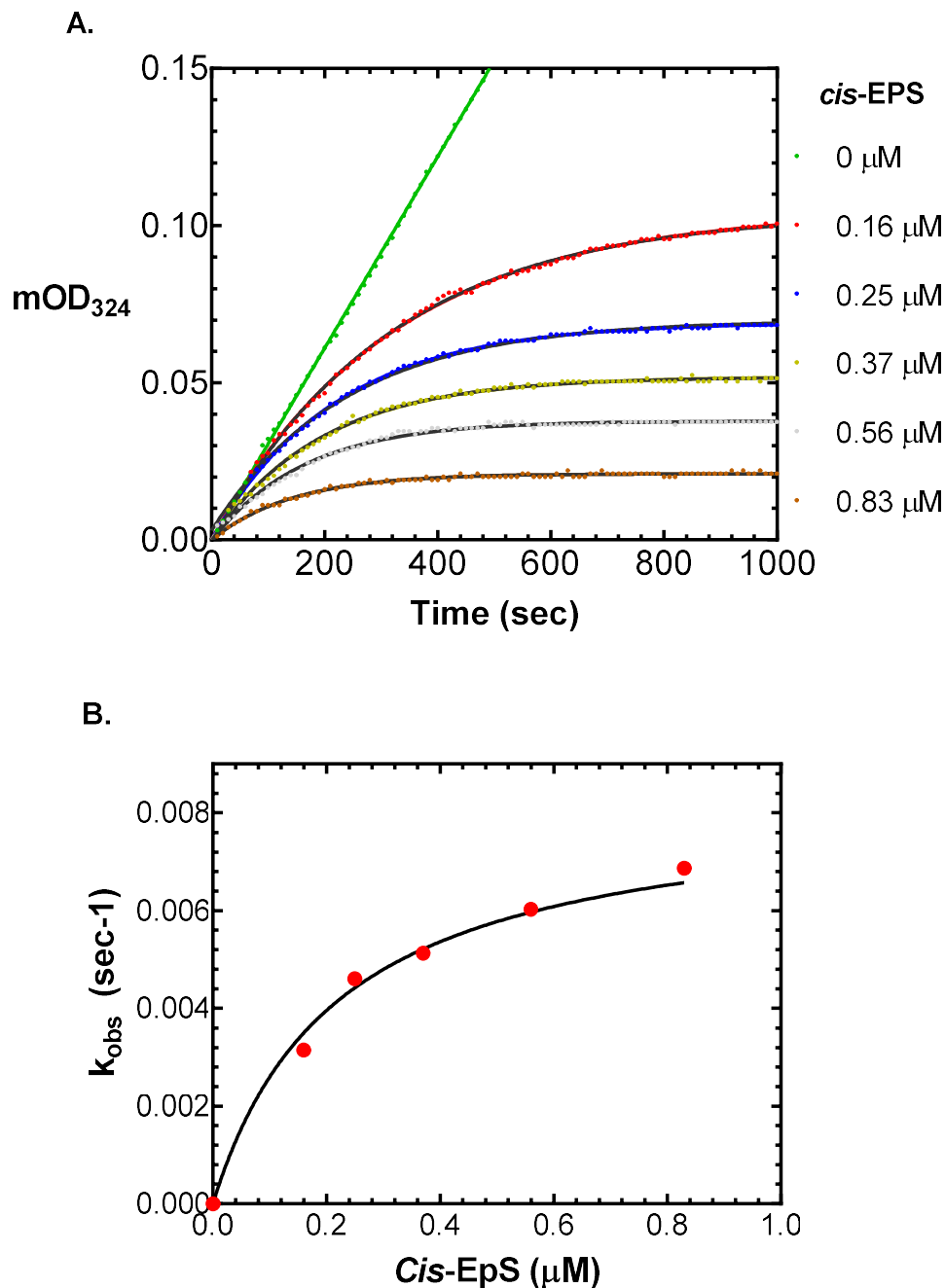
Figure 5-1 Inactivation kinetics of *cis*-EpS in the presence of (2*R*,3*S*)-isocitrate

A. Glyoxylate formation in the presence of 0-0.83 uM *cis*-EpS and 200 μM of substrate (2*R*,3*S*)-isocitrate was represented by absorbance changes (mOD) at 324 nm via reactions with phenyl-hydrazine. The lines drawn through the time course of glyoxylate formation from ICL catalysis were from global curve-fitting to equation (18) and (19) simultaneously, resulting into apparent k_{inact} and K_{inact} values of 0.33 ± 0.02 μM and 9.8 ± 0.3 x 10^{-3} s^{-1}. **B.** A replot of k_{obs} vs [*cis*-EpS] in which k_{obs} was an average result of values obtained from fitting glyoxylate formation data in Figure 5-1A to equation (18) independently and calculated values from the global fit of k_{inact} and K_{inact}. The line drawn through k_{obs} data points were from fitting to equation (19)

The time courses of glyoxylate formation were fitted to equation (18), from which replotting of the apparent rates of inactivation (k_{obs}) vs. *cis*-EpS concentrations showed saturation of inactivation rate at sub-micromolar concentrations of *cis*-EpS, a signature of 2-step inactivation kinetics (**Figure 5-1B**). Global nonlinear regression analysis of inactivation time courses was fitted with equation (18) and (19), modelling a 2-step irreversible inactivation, in which the apparent inactivation constant ($^{app}K_{inact}$) was 0.33 ± 0.02 µM and the apparent maximal rate of inactivation ($^{app}k_{inact}$) was $9.8 \pm 0.3 \times 10^{-3}$ s^{-1}.

Additionally, increasing concentrations of isocitrate led to a hyperbolic increase of the apparent rate of inactivation (k_{obs}) by 0.25 µM *cis*-EpS (**Figure 5-2A**). On the other hand, increasing succinate resulted into a hyperbolic decrease in k_{obs} (**Figure 5-2A**). Values of k_{obs} in **Figure 5-2A** were fitted to equation (21) and equation (22), which is consistent with an uncompetitive inactivation versus isocitrate, and competitive versus succinate, respectively. The inactivation mode of *cis*-EpS in the presence of isocitrate and succinate supported the preferential binding of *cis*-EpS to ICL1-glx or ICL1-glycolate complexes (binary-ICL1 complexes).

After determining the binding mode, we sought to evaluate inactivation kinetic values via fitting of the time-course data globally with various concentrations of *cis*-EpS in the presence of 25 to 200 µM of isocitrate. Describe the equations used for global fitting, In **Figure 5-2B**, apparent values of k_{inact} and K_{inact}, obtained from fitting inactivation time courses to equation (11) and (12), was replotted against various isocitrate concentrations (Figure 5-2). These apparent inactivation kinetic values were fitted into equation (15), describing an uncompetitive inactivation model vs. isocitrate, from which the inactivation

constant (K_{inact}) was 0.20 ± 0.05 µM and the maximal rate of inactivation (k_{inact}) was $1.0 \pm 0.1 \times 10^{-2}$ s^{-1} (**Figure 5-2B**).
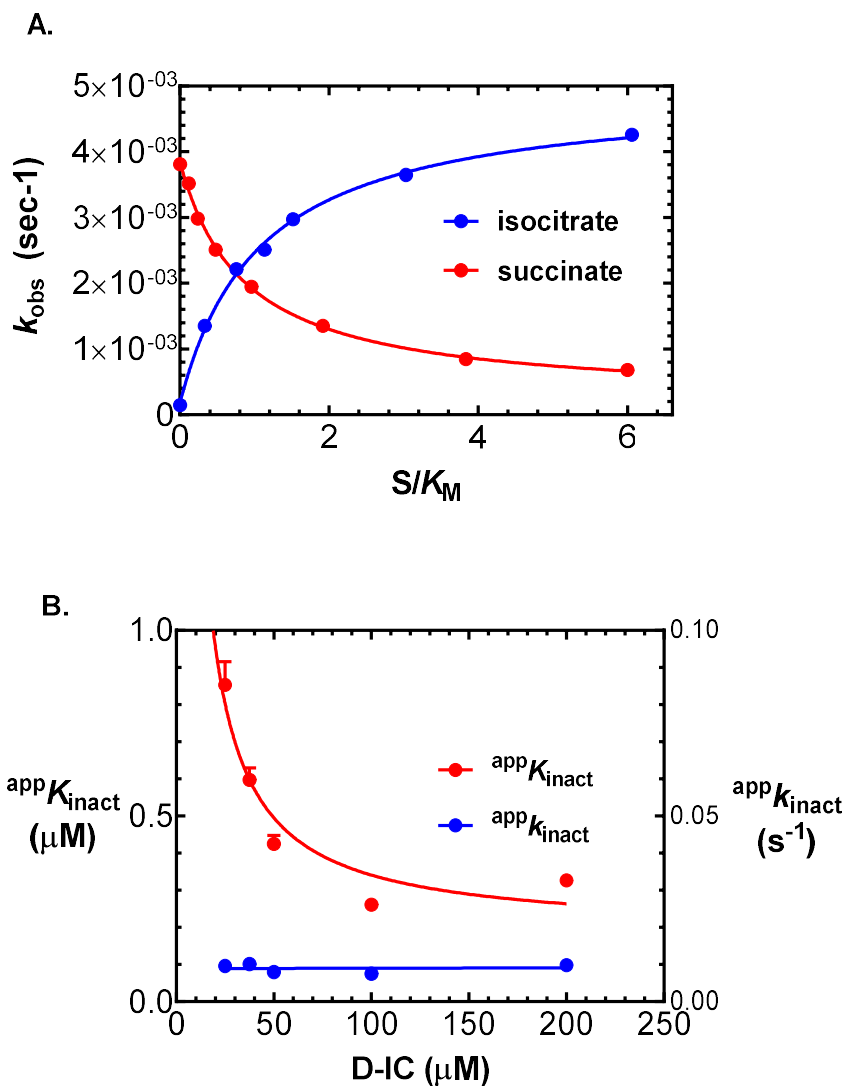
Figure 5-2 *Cis*-epoxy-succinate inactivation mode in the presence of ICL1 substrates

A. Apparent k_{obs} was from fitting inactivation time courses of 0.25 µM *cis*-EpS in the presence of various S/K_M level of substrate (succinate (in red) and isocitrate (in blue)) into equation (18) and lines drawn through k_{obs} data points were from fitting into equation (19) and (20), respectively. **B.** Apparent k_{inact} and K_{inact} values at various (2R,3S)-isocitrate concentrations was obtained from global fitting inactivation time courses to equation (18) and (19) simultaneously. Lines drawn through data points were from fitting $^{app}K_{inact}$ to equation (21) and from linear regression of k_{inact} values

In contrast, under the same reaction conditions, low micromolar concentrations of *trans*-2,3-epoxy-succinate did not exhibit time-dependent inhibition effects on ICL1. Overnight incubation of 100 µM of *trans*-2,3-epoxy-succinate with 0.5 µM of ICL1 had no effects on ICL1 catalytic activity. As expected, *trans*-EpS could afford ICL1 isocitrate-competitive inhibition ($K_{is} = 0.8 \pm 0.2$ mM) but not inactivation (**Figure 5-3**). A plot of 1/v and S/v vs. [*trans*-EpS] displayed both slope and intercept effects, which supported a competitive inhibition vs. isocitrate. Hence, in contrast to *cis*-EpS, *trans*-EpS binds preferentially to the apo-ICL1 form in which the epoxy ring likely coordinates the Mg^{2+} cation. In fact, the value of K_{is} of racemic *trans*-EpS was twice that of (2*R*)-malate, suggesting that only (*R,R)-trans*-EpS affords binding to apo-ICL1. That *Trans*-EpS acts as a competitive inhibitor vs. isocitrate was consistent with the earlier observation that the *cis*-form of EpS was a prerequisite for binding to E-glx complex.
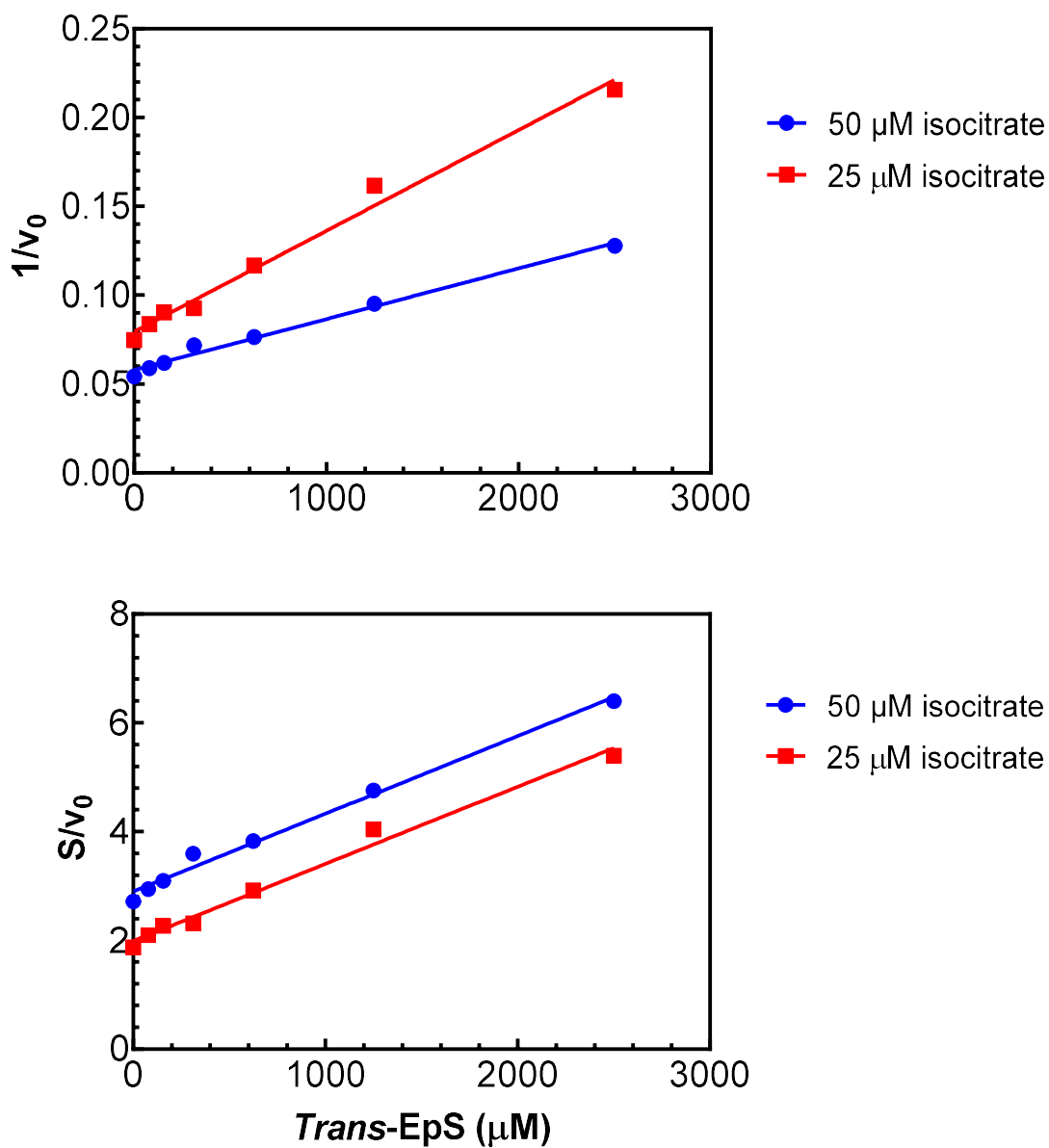
Figure 5-3 *Trans*-EpS inhibition is competitive vs. isocitrate

The lines drawn through reciprocal initial velocity data points (1/v) were from global-fitting of equation (8), which determines competitive inhibition constant K_{is}[104]. Lines drawn through S/v data were a result of linear regression analysis yielding straight lines whose slope is not significant different from each other.

ICL1 Inactivation Resulted from an Apparent Irreversible, Covalent Reaction of Cys191

to cis-EpS

Further analysis of inactivation mechanism was carried out to ascertain the irreversibility of ICL1 inactivation by *cis*-EpS. First, ICL1 (0.5 µM) was pre-incubated with sub-stoichiometric amounts of *cis*-EpS (0-2 µM) either in the absence or presence of substrate glyoxylate (100 µM) for 20 hours. Pre-incubation samples were then diluted 100-fold into assay buffer containing 1 mM D-IC in order to rescue reversible inhibition by *cis*-EpS. Assessment of residual ICL1 retro-aldol cleavage activity in *cis*-EpS pre-incubated samples showed that *cis*-EpS afforded a complete ICL1 inactivation in which the ratio of ICL1:*cis*-EpS was 1:1 (**Figure 5-4**). Spin-dialysis of inactivated enzyme to remove unbound cis-EpS did not lead to any appreciable recovery of enzyme activity. Therefore, the inactivation was apparently irreversible and one molecule of the inactivator was required for inactivation of every single ICL1 subunit. In contrast to the previous experiments, despite its preferred binding mode to binary-ICL1 complexes, *cis*-EpS could also inactivate the apo-ICL1 enzyme but perhaps the inactivation was not as potent as with ICL1-glx and ICL1-glycolate.
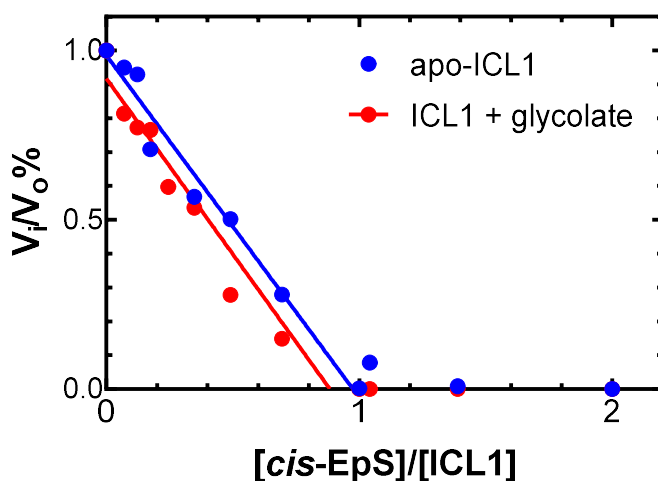
Figure 5-4 ICL1 active-site titration by epoxide in the presence or absence of glyoxylate

Twenty-hour pre-incubation mixture of 0.5 μM ICL1 with 0-1.0 μM cis-epoxide were diluted 50-fold into reaction buffer containing 1 mM (2R,3S)-isocitrate in order to estimate ICL1 remaining activity. Lines drawn through data points were from linear regression of data points that contains [*cis*-EpS]/[ICL1] < 1.0

Hence, we sought to compare *cis*-EpS inactivation of apo-ICL1 with that of ICL1-glycolate via a pre-incubation study in which residual ICL1 activity was examined at various time intervals for 10 min. *Cis*-EpS inactivation of apo-ICL1 was 10-fold less efficient than that of ICL1-glycolate (**Figure 5-5**). In the absence of glycolate, inactivation of apo-ICL1 by *cis*-EpS exhibited ime-dependent irreversible kinetics ($k_{inact} = 1.3 \pm 0.1 \times 10^{-3}$ sec^{-1} and $K_{inact} = 3.0 \pm 0.5$ μM). In the presence of glycolate (100 μM), inactivation kinetics was similar to *cis*-EpS inactivation of ICL1 in the presence of isocitrate, for which $k_{inact} = 1.1 \pm 0.1 \times 10^{-2}$ sec^{-1} and apparent $K_{inact} = 0.6 \pm 0.1$ μM. The similar k_{inact} implied that the rate limiting of the inactivation of apo-ICL1 and ICL1-glx is governed by the chemical reactivity between the epoxy-ring and the nucleophilic active site residue. The 5-fold increase of K_{inact} in the inactivation of apo-ICL1 supported that the ICL1 binary complex (ICL1-Glx or ICL1-glycolate) is more favored for *cis*-EpS binding.

We also conducted exhaustive dialysis of complexes of *cis*-EpS-ICL1 in order to ascertain that the inactivation is irreversible. After a day of extensive dialysis of treated and untreated ICL1 samples (0.4 mL) into buffer solution (2.0 L), less than 3.5% of ICL1 activity had been restored and there was no further re-activation of ICL1 after 2 and 3 days of dialysis. Therefore, the inactivation of ICL1 by *cis*-EpS is virtually irreversible.
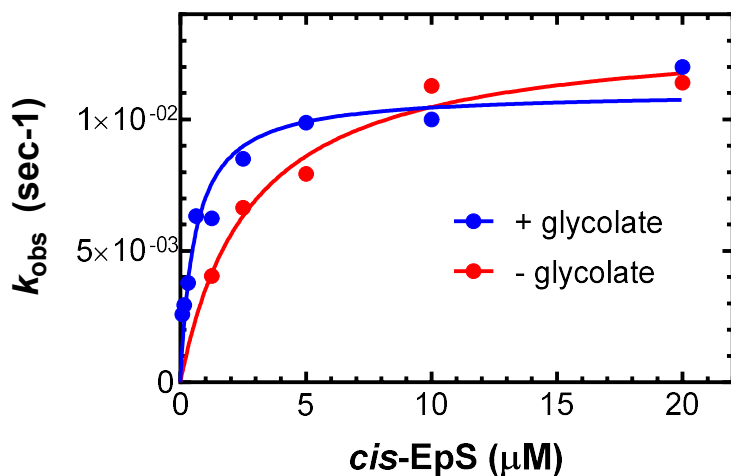
Figure 5-5 Irreversible, time-dependent and saturable inactivation kinetics exhibited by *cis*-epoxide was enhanced in the presence of glycolate.

Fifty nM ICL1 was preincubated with 0-20 µM of *cis*-EpS in the presence or absence of 100 µM glycolate. Samples were taken at 15-60 second intervals and diluted 50-fold into reaction buffer containing 1 mM (2R,3S)-isocitrate in order to measure residual activity of ICL1. k_{obs} were calculated by global fitting of residual activity data to equation (9). Lines drawn through k_{obs} data points was from fitting data to equation (10).

Crystallographic analysis of *cis*-EpS-inactivated ICL1 confirmed that inactivation by *cis*-EpS results from ring-opening of the epoxide accompanying the formation of a carbon-sulfur bond with Cys191. The *cis*-EpS inactivated ICL1 structure contained hydrated glyoxylate trapped near Mg^{2+} ions, and covalently modified Cys191 residues. The epoxy ring is open to form Cys191-(*S*)-malic, or (*S*)-malanoylyl-C191 adduct in all four subunits

of ICL1 (**Figure 5-6**). This is the first structure of ICL1 in complex with a hydrate form of glyoxylate. Prior to the ring-opening reaction, the epoxide might be protonated by either the same water molecule that participated in the hydration of glyoxylate or an active-site residue. This result suggested that binding of *cis*-EpS to E-glyoxylate is stereospecific and consistent with the uncompetitive inhibition mode of (2*S*)-malate. Malanoyl-C191 adduct (Mal-C191) occupied the succinate sub-site and formed similar hydrogen bonds with Thr347, Asn313, Ser315, Ser317, His193 and Arg228 residues. The hydroxyl group of Mal-C191 was in proximity for hydrogen bonding with Thr347 and the hydrated glyoxylate.
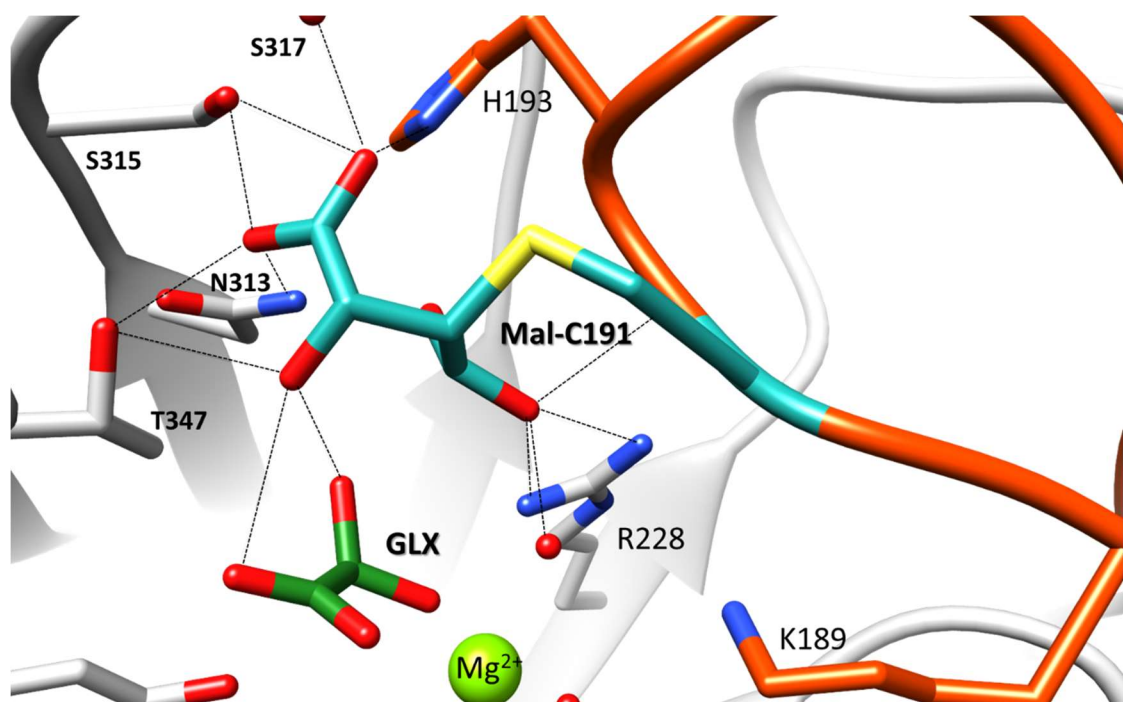
Figure 5-6 Crystal structure of *cis*-EpS covalently-inactivated ICL1

Cis-EpS treated ICL1 resulted in a malynoyl-C191 adduct (Mal-C191, sea green). The active-site loop containing K189KCGH193 (orange) assumed a close conformation. Hydrated glyoxylate (Glx) was shown in forest green. Dash-lines represent potential hydrogen bonds to the covalent adduct (Mal-C191).

Selective Inactivation of ICL by cis-EpS in vitro

Irreversible inactivation of ICL1 by 1 μM *cis*-EpS action was unaffected by the addition of either 1 mM DTT or 1 mM glutathione, suggesting that the di-carboxylate epoxide is stable to free thiols in the reaction mixtures. This could be accounted for by the fact that epoxide ring-opening reactions require either strong nucleophiles or protonation of the epoxy-ring prior to reaction with weak nucleophiles such as thiols[141]. Additionally, *cis*-epoxy-succinate (up to 1 mM) did not exert inhibition on either aconitase, isocitrate dehydrogenase or ATP-citrate lyase, possibly owing to its *cis*-conformation. Similarly, at 1 mM of *cis*-EpS there was no observable inhibition effect on other enzymes in the tricarboxylic acid cycle (TCA), and glyoxylate shunt, which includes α-keto-glutarate dehydrogenase, malate synthase, fumarase, citrate synthase, and succinyl CoA synthetase (**Table A-7**). Together with the untreated control, reaction mixtures containing 2.5 μg of each of these enzymes (**Table A-7**) and ICL1 was treated with 1 mM *cis*-EpS for one hour, and analyzed by 2-D Difference Gel Electrophoresis (DIGE). Protein spots representing a single protein at multiple pI values shown in **Figure 5-7** could arise from posttranslational modifications of protein residues (e.g. phosphorylation of lysine & cysteine). Covalent labeling with *cis*-EpS would increase the total negative charges on proteins, which cause the migration to lower pI region on the gel. There were no differential migration between untreated and *cis*-EpS treated of TCA cycle and ATP-citrate synthase enzymes. On the other hand, treated ICL1 migrated to a lower pI area than that of untreated ICL1 (**Figure 5-7**).
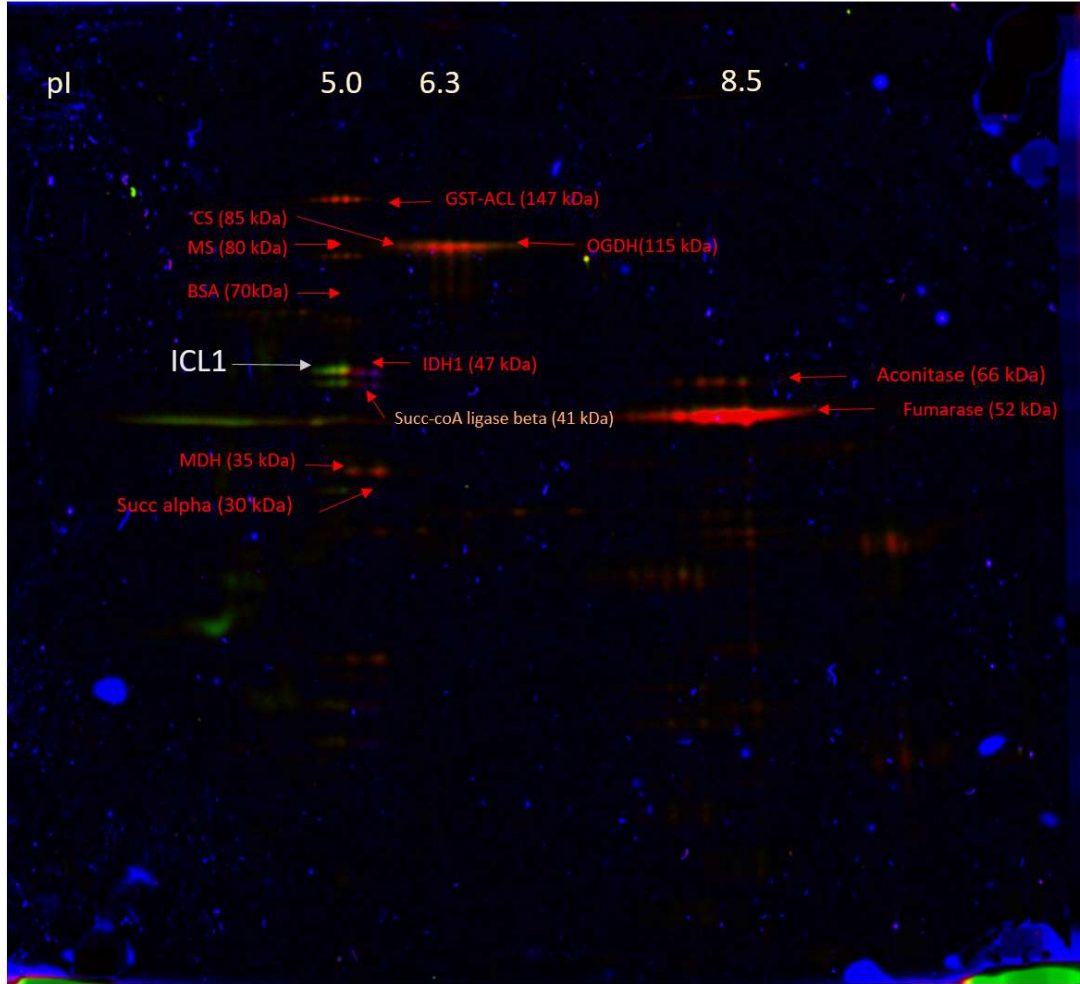
Figure 5-7 2-D DIGE analysis of TCA cycle enzymes

A mixture of TCA cycle enzymes (25 µg total) were treated with 1 mM *cis*-EpS for 1 hour and analyzed in a 2D gel together with a control sample. Untreated sample and treated sample were labeled with cy5 and cy2, respectively. Protein spots shown in red showed no differential migration between untreated and treated samples.

We examined whether *cis*-EpS covalently labeled other proteins in *E. coli* lysate using 2D DIGE. The technique provides a sensitive detection of up to 5,000 protein spots in a large 2D gel format[138]. Along with a control sample, *E. coli* lysate was treated with 1 mM of *cis*-EpS. All proteins in control and treated *E. coli* lysate samples migrated to the same position, indicating that *cis*-EpS did not react with these proteins (**Figure 5-8**). In recombinant *E. coli*, which was transformed with plasmids carrying *Mtb* ICL1 gene, some treated protein spots migrated to lower pI region compared to control sample (**Figure 5-8**). These spots were consistent with ICL1 spots in the cocktail mix (**Figure 5-7**). These results demonstrated that, among more than 1,000 proteins in *E. coli* lysate, the covalent addition of *cis*-EpS was selective to ICL1.

Treatment of *M. tuberculosis mc² 7000* with *cis*-EpS yielded a dose response inhibition of growth in M9-acetate medium ($IC_{50} = 100 \pm 10$ µM, or 13 µg/ml) but had no effect on *Mtb* grown in M9-glucose medium (**Figure A-12**). Since ICL1 and glyoxylate shunt are essential for growth in M9-acetate medium, *cis*-EpS mode of action on *Mtb* cell growth was pertaining to inactivation of glyoxylate cycle and ICL1. Consistently, *trans*-EpS had no effects on *M. tb* growth in either media (**Figure A-12**).
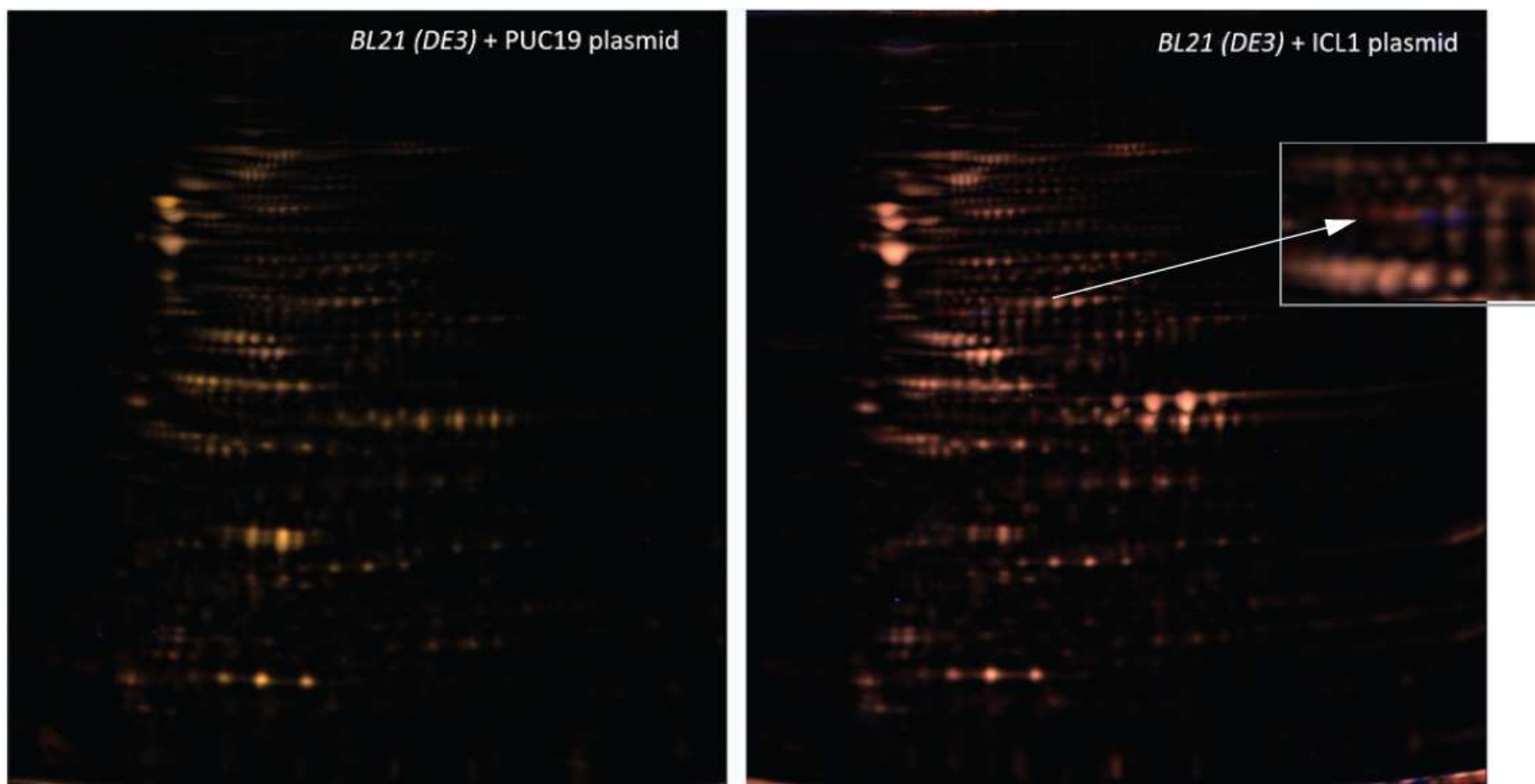
Figure 5-8 2-D DIGE analysis of *E. coli* lysate enzymes

E. coli lysate (0.2 mg/ml) were treated with 1 mM *cis*-EpS for 1 hour. Untreated sample and treated sample were labeled with cy5 and cy2, respectively. Protein spots shown in brown had no differential migration between untreated and treated samples

5.4. Conclusions

Here we incorporated epoxy-ring into a *cis*-succinate configuration to form a covalent, time-dependent inactivator of ICL1, *cis*-epoxy-succinate. As a succinate-analog, *cis*-EpS preferentially binds to E-glx complex and reacts with Cys191. The formation of (*S*)-malyl-Cys191 adduct was observed in the crystal structure of ICL1 treated with *cis*-EpS and isocitrate. On the other hand, *trans*-EpS is merely a competitive inhibitor vs. isocitrate. The competitive inhibition mode of *trans*-EpS is probably unproductive for the ring opening reaction between Cys191 and *trans*-EpS. The inactivation of apo-ICL1 by *cis*-EpS most likely occurs via initial binding to glyoxylate subsite from which *cis*-EpS migrates into succinate subsite and then reacts with Cys191. The migration of *cis*-EpS would be similar to that of 2-vinyl-glyoxylate.

(2*R*,3*S*)-epoxy-succinate (*cis*-EpS) was 35-fold more efficient than bromo-pyruvate and 750-fold better than 2-VIC. The inactivator also exhibited a remarkable selectivity for ICL1 in the presence of other TCA enzymes and >1,000 proteins in *E. coli* lysate. *Cis*-EpS also inhibited *Mtb* cell growth in M9-acetate media, albeit at much higher concentrations (IC$_{50}$ = 100 µM). Even though the di-anionic charges on *cis*-EpS probably lead to limited cellular uptake of the compound, exploration of *cis*-epoxy-succinate esters could yield better cellular permeability and anti-*Mtb* effects while maintaining inactivation specificity.

6. CONCLUSIONS

6.1. Summary

The first part of this thesis focused on uncovering ICL1 active-site residue roles during catalysis, especially the identity of the base that leads to the deprotonation of $(2R,3S)$-isocitrate (D-IC), resulting into C_2-C_3 cleavage. k_{cat} – pH profile provided a marker to follow the first proton abstraction step during the retro-aldol catalysis of ICL1. Mutagenesis studies suggested that Lys189 is the catalytic base acting in concert with Mg^{2+}-bound water to form hydroxide anion, which then abstracts the proton from isocitrate, initiating the retro-aldol cleavage reaction. Compilation of kinetic data from this research and previous literature also allows the preliminary assessment of the rate limiting step(s) in ICL1 catalysis.

The characterization of the mechanism-based inactivation of ICLs by 2-VIC reported a moderate maximal inactivation rate (k_{inact}) of 0.08 ± 0.006 min^{-1} and inactivation constant (K_{inact} of 22 ± 3 μM). Our results indicated that 2-vinyl glyoxylate (2-VG), the electrophilic species formed from ICL-catalyzed retro-aldol cleavage of 2-VIC, is a highly efficient Michael acceptor, poised for nucleophilic attack by the conserved cysteine in the active site of ICLs. However the covalent inactivation via Michael addition of ICL-generated 2-VG to the active-site cysteine sidechain is hindered in the presence of other competing thiols. The Michael addition adducts are also slowly reversible during extensive dialysis. Additionally, catalysis of 2-VIC to 2-VG and succinate by ICL is partially rate limiting during 2-VIC inactivation and at least 2-fold slower than the Michael addition step.

These results suggest that the next generation of mechanism-based inactivator should contain the following features: 1) a more efficient scaffold for better catalysis and 2) a less

reactive electrophilic species to elude capture by other thiols, especially glutathione. In order to improve the catalysis efficiency, we seek to uncover additional details of ICL1 active-site "chemical space".

Semi-quantitative structural activity relationship study (semi-qSAR) of ICL1 substrate analogs revealed the stringency of ICL1 active site and significant synergy between analogs of glyoxylate and succinate. Replacing carboxylic acid of succinate with nitro, cyano and aldehyde group is allowed. Moderate inhibition of (2*R*)-malate, (2*S*)-malate, oxaloacetate and potent inhibition from hydroxycitrate, itaconitate demonstrated that the succinate-binding site affords some spatial availability for a small, electron-withdrawing additional group (i.e. hydroxyl and keto groups).

On the other hand, binding to the binary E-glx complex requires a *cis*-isomer or *syn*-conformation of the dicarboxylic group. This observation has led to the discovery of *cis*-epoxy-succinate as a potent and selective inactivator of ICL. *Cis*-EpS irreversibly inactivated ICL1 and ICL2. The inactivation is much more potent for ICL1 in which k_{inact} approximates 1.0×10^{-2} s^{-1} and K_{inact} approaches 200 nM. In contrast, inactivation of ICL2 requires low mM of *cis*-EpS (K_{inact}). The mechanism of inactivation in ICL1 encompasses the ring-opening reaction of *cis*-EpS by Cys191. *Cis*-EpS-inactivation of ICL1-glx complex occurs 10-fold more favorably than that of apo-ICL1 ($^{apo-ICL}K_{inact} = 3.0 \pm 0.5$ μM) which partially account for its remarkable selectivity. Analysis of the proteomic 2-D gel electrophoresis of *E. coli* lysate and the effects of *cis*-EpS in cell cultures of *Mtb* showed that *cis*-EpS does not label other proteins nor does it affect *Mtb* growth in which conditions ICL activity is dispensable. Therefore, *cis*-EpS is a potential lead for development of compounds whose inactivation is selective for ICL *in vivo*.

6.2. Future Directions

This work suggested that Lys189 plays an important role in *Mtb* ICL1 catalytic mechanism. Further characterization of K189Q and K190Q would provide additional evidence for their roles in activating Mg^{2+}-bound water that initiates the first deprotonation step. pH-rate profiles of K190Q would reveal if the residue indeed modulate Lys189 pK_a value. Solvent kinetic isotope effects of K189Q would be essential to understand mutant's catalytic mechanism. Obtaining crystal structures of the mutants will allow an independent assessment of Lys189 pK_a value and structural comparisons to WT ICL1. It is also crucial to examine H180A and Glu182 mutation. His180 is also positioned favorably to act as the catalytic base and H180A mutation has detrimental effects on ICL1 activity. On the other hand, there has been little study on kinetic mechanisms of ICL2, which is an interesting area to be explored.

Mechanism-based inactivation by 2-VIC and survey of substrate analogs revealed subtle changes to constitute new ICL1 inhibitors. Installation of a smaller, electron-withdrawing group at C-2 of isocitrate could improve alternative substrate binding and catalysis rate. As alkynyl group exerts smaller steric hindrance, 2-alkynylisocitrate might be a better substrate for ICL1 than 2-VIC. 2-fluoroisocitrate is another potential 2-substitute-(2*R*,3*S*)-isocitrate for inhibiting ICL1 even though 2-fluoro-(2*R*,3*S*)-isocitrate is also a substrate of aconitase, and leads to oxaloacetate formation.

On the other hand, small and electron-withdrawing substituents on succinate fragment could yield a better leaving group for retro-aldol catalysis. NMR study of 2-mono-substituted-succinate analogs could reveal deuterium exchange kinetics during ICL1-catalyzed carbanion formation. 2-cyano-succinate could act as a succinate analog and a

potential inactivator. 2-halogen-3-nitropropionate and 2-halogen-3-cyanopropionate derivatives are other alternative succinate analogs, which comprise only one carboxylate group. 2,3-fluoro-3-nitro-propionate might improve specificity of 3-nitropropionate because there is no suitable hydrogen to initiate the mechanism-based inactivation of succinate dehydrogenase. 2-fluoro-maleate could activate maleate into a more electrophilic succinate analog, yielding a potential time-dependent inhibitor or inactivator. Lastly, the potent inactivation by *cis*-EpS encouraged further exploration of *cis*-epoxy-succinate derivatives to discover new ICL1 inactivators. *Cis*-EpS ester and amide conjugates are potential prodrug molecules to improve *in vivo* bioavailability and efficacy.

REFERENCES

[1] WHO. (2018) Global tuberculosis report 2018, Geneva: World Health Organization. https://www.who.int/tb/publications/global_report/en/

[2] Gomez, J. E., and McKinney, J. D. (2004) M. tuberculosis persistence, latency, and drug tolerance, *Tuberculosis 84*, 29-44.

[3] Smith, C. V., Sharma, V., and Sacchettini, J. C. (2004) TB drug discovery: addressing issues of persistence and resistance, *Tuberculosis 84*, 45-55.

[4] Bhusal, R. P., Bashiri, G., Kwai, B. X. C., Sperry, J., and Leung, I. K. H. (2017) Targeting isocitrate lyase for the treatment of latent tuberculosis, *Drug Discovery Today 22*, 1008-1016.

[5] Seung, K. J., Keshavjee, S., and Rich, M. L. (2015) Multidrug-Resistant Tuberculosis and Extensively Drug-Resistant Tuberculosis, *Cold Spring Harbor Perspectives in Medicine 5*, a017863.

[6] Selwyn, P. A., Alcabes, P., Hartel, D., Buono, D., Schoenbaum, E. E., Klein, R. S., Davenny, K., and Friedland, G. H. (1992) Clinical Manifestations and Predictors of Disease Progression in Drug Users with Human Immunodeficiency Virus Infection, *NEJM 327*, 1697-1703.

[7] Ferebee, S. H., and Mount, F. W. (1962) Tuberculosis Morbidity in a Controlled Trial of the Prophylactic Use of Isoniazid among Household Contacts, *American Review of Respiratory Disease 85*, 490-510.

[8] Fox, G. J., Oxlade, O., and Menzies, D. (2015) Fluoroquinolone Therapy for the Prevention of Multidrug-Resistant Tuberculosis in Contacts. A Cost-Effectiveness Analysis, *American Journal of Respiratory and Critical Care Medicine 192*, 229-237.

[9] Gumbo, T., Louie, A., Liu, W., Ambrose, Paul G., Bhavnani, Sujata M., Brown, D., and Drusano, George L. (2007) Isoniazid's Bactericidal Activity Ceases because of the Emergence of Resistance, Not Depletion of Mycobacterium tuberculosis in the Log Phase of Growth, *The Journal of Infectious Diseases 195*, 194-201.

[10] Calver, A. D., Falmer, A. A., Murray, M. B., Strauss, O. J., Streicher, E. M., Hanekom, M., Liversage, T., Masibi, M., Helden, P. D. v., Warren, R. M., and Victor, T. C. (2010) Emergence of Increased Resistance and Extensively Drug-Resistant Tuberculosis Despite Treatment Adherence, South Africa, *Emerg Infect Dis 16*, 264-271.

[11] Srivastava, S., Pasipanodya, J. G., Meek, C., Leff, R., and Gumbo, T. (2011) Multidrug-resistant tuberculosis not due to noncompliance but to between-patient pharmacokinetic variability, *J Infect Dis 204*, 1951-1959.

[12] Schnappinger, D., Ehrt, S., Voskuil, M. I., Liu, Y., Mangan, J. A., Monahan, I. M., Dolganov, G., Efron, B., Butcher, P. D., Nathan, C., and Schoolnik, G. K. (2003) Transcriptional Adaptation of *Mycobacterium tuberculosis* within Macrophages: Insights into the Phagosomal Environment, *The Journal of Experimental Medicine 198*, 693-704.

[13] McKinney, J. D., zu Bentrup, K. H., Muñoz-Elías, E. J., Miczak, A., Chen, B., Chan, W.-T., Swenson, D., Sacchettini, J. C., Jacobs Jr, W. R., and Russell, D. G. (2000) Persistence of *Mycobacterium tuberculosis* in macrophages and mice requires the glyoxylate shunt enzyme isocitrate lyase, *Nature 406*, 735.

[14] Gould, T. A., Van De Langemheen, H., Muñoz-Elías, E. J., McKinney, J. D., and Sacchettini, J. C. (2006) Dual role of isocitrate lyase 1 in the glyoxylate and methylcitrate cycles in *Mycobacterium tuberculosis*, *Molecular Microbiology 61*, 940-947.

[15] Eoh, H., and Rhee, K. Y. (2013) Multifunctional essentiality of succinate metabolism in adaptation to hypoxia in *Mycobacterium tuberculosis*, *Proc Natl Acad Sci 110*, 6554-6559.

[16] Muttucumaru, D. G. N., Roberts, G., Hinds, J., Stabler, R. A., and Parish, T. (2004) Gene expression profile of *Mycobacterium tuberculosis* in a non-replicating state, *Tuberculosis 84*, 239-246.

[17] Nandakumar, M., Nathan, C., and Rhee, K. Y. (2014) Isocitrate lyase mediates broad antibiotic tolerance in *Mycobacterium tuberculosis*, *Nat Commun 5*.

[18] Graham, J. E., and Clark-Curtiss, J. E. (1999) Identification of *Mycobacterium tuberculosis* RNAs synthesized in response to phagocytosis by human macrophages by selective capture of transcribed sequences (SCOTS), *Proc Natl Acad Sci 96*, 11554-11559.

[19] Höner Zu Bentrup, K., Miczak, A., Swenson, D. L., and Russell, D. G. (1999) Characterization of Activity and Expression of Isocitrate Lyase in *Mycobacterium avium* and *Mycobacterium tuberculosis*, *J Bacteriol 181*, 7161-7167.

[20] Eoh, H., and Rhee, K. Y. (2014) Methylcitrate cycle defines the bactericidal essentiality of isocitrate lyase for survival of *Mycobacterium tuberculosis* on fatty acids, *Proc Natl Acad Sci 111*, 4976-4981.

[21] Kannan, K. B., Katoch, V. M., Bharadwaj, V. P., Sharma, V. D., Datta, A. K., and Shivannavar, C. T. (1985) Metabolic studies on mycobacteria--II. Glyoxylate by-pass (TCA cycle) enzymes of slow and fast growing mycobacteria, *Indian Journal of Leprosy 57*, 542-548.

[22] Cozzone, A. J. (1998) Regulation of acetate metabolism by protein phosphorylation in enteric bacteria, *Annu Rev Microbiol 52*, 127-164.

[23] Fang, F. C., Libby, S. J., Castor, M. E., and Fung, A. M. (2005) Isocitrate Lyase (AceA) Is Required for Salmonella Persistence but Not for Acute Lethal Infection in Mice, *Infection and Immunity 73*, 2547-2549.

[24] Dolan, S. K., and Welch, M. (2018) The Glyoxylate Shunt, 60 Years On, *Annu Rev Microbiol 72*, 309-330.

[25] Puckett, S., Trujillo, C., Wang, Z., Eoh, H., Ioerger, T. R., Krieger, I., Sacchettini, J., Schnappinger, D., Rhee, K. Y., and Ehrt, S. (2017) Glyoxylate detoxification is an essential function of malate synthase required for carbon assimilation in *Mycobacterium tuberculosis*, *Proc Natl Acad Sci 114*, E2225-E2232.

[26] Smith, R. A., and Gunsalus, I. C. (1954) Isocitritase: a new tricarboxylic acid cleavage system *J Am Chem Soc 76*, 5002-5003.

[27] Clark, J. D., O'Keefe, S. J., and Knowles, J. R. (1988) Malate synthase: proof of a stepwise Claisen condensation using the double-isotope fractionation test, *Biochemistry 27*, 5961-5971.

[28] Quartararo, C. E., and Blanchard, J. S. (2011) Kinetic and Chemical Mechanism of Malate Synthase from *Mycobacterium tuberculosis*, *Biochemistry 50*, 6879-6887.

[29] Akram, M. (2014) Citric acid cycle and role of its intermediates in metabolism, *Cell biochemistry and biophysics 68*, 475-478.

[30] Dunn, M. F., Ramírez-Trujillo, J. A., and Hernández-Lucas, I. (2009) Major roles of isocitrate lyase and malate synthase in bacterial and fungal pathogenesis, *Microbiology 155*, 3166-3175.

[31] Singh, K. S., Sharma, R., Keshari, D., Singh, N., and Singh, S. K. (2017) Down-regulation of malate synthase in *Mycobacterium tuberculosis* H37Ra leads to reduced stress tolerance, persistence and survival in macrophages, *Tuberculosis (Edinburgh, Scotland) 106*, 73-81.

[32] Narayanan, B., Niu, W., Joosten, H. J., Li, Z., Kuipers, R. K., Schaap, P. J., Dunaway-Mariano, D., and Herzberg, O. (2009) Structure and function of 2,3-dimethylmalate lyase, a PEP mutase/isocitrate lyase superfamily member, *J Mol Biol 386*, 486-503.

[33] Jia, Y., Lu, Z., Huang, K., Herzberg, O., and Dunaway-Mariano, D. (1999) Insight into the mechanism of phosphoenolpyruvate mutase catalysis derived from site-directed mutagenesis studies of active site residues, *Biochemistry 38*, 14165-14173.

[34] Narayanan, B. C., Niu, W., Han, Y., Zou, J., Mariano, P. S., Dunaway-Mariano, D., and Herzberg, O. (2008) Structure and function of PA4872 from Pseudomonas aeruginosa, a novel class of oxaloacetate decarboxylase from the PEP mutase/isocitrate lyase superfamily, *Biochemistry 47*, 167-182.

[35] Brock, M., Darley, D., Textor, S., and Buckel, W. (2001) 2-Methylisocitrate lyases from the bacterium Escherichia coli and the filamentous fungus *Aspergillus nidulans*, *FEBS Letters*, *268*, 3577-3586.

[36] Liu, S., Lu, Z., Han, Y., Melamud, E., Dunaway-Mariano, D., and Herzberg, O. (2005) Crystal structures of 2-methylisocitrate lyase in complex with product and with isocitrate inhibitor provide insight into lyase substrate specificity, catalysis and evolution, *Biochemistry 44*, 2949-2962.

[37] Grimek, T. L., Holden, H., Rayment, I., and Escalante-Semerena, J. C. (2003) Residues C123 and D58 of the 2-Methylisocitrate Lyase (PrpB) Enzyme of Salmonella enterica Are Essential for Catalysis, *J Bacteriol 185*, 4837-4843.

[38] Grimm, C., Evers, A., Brock, M., Maerker, C., Klebe, G., Buckel, W., and Reuter, K. (2003) Crystal Structure of 2-Methylisocitrate Lyase (PrpB) from *Escherichia coli* and Modelling of its Ligand Bound Active Centre, *J Mol Biol 328*, 609-621.

[39] Sharma, V., Sharma, S., zu Bentrup, K. H., McKinney, J. D., Russell, D. G., Jacobs, W. R., and Sacchettini, J. C. (2000) Structure of isocitrate lyase, a persistence factor of *Mycobacterium tuberculosis*, *Nat Struct Mol Biol 7*, 663-668.

[40] Kinhikar, A. G., Vargas, D., Li, H., Mahaffey, S. B., Hinds, L., Belisle, J. T., and Laal, S. (2006) *Mycobacterium tuberculosis* malate synthase is a laminin-binding adhesin, *Molecular Microbiology*, *60*, 999-1013.

[41] Muñoz-Elías, E. J., and McKinney, J. D. (2005) Mycobacterium tuberculosis isocitrate lyases 1 and 2 are jointly required for in vivo growth and virulence, *Nat Med 11*, 638.

[42] Muñoz-Elías, E. J., Upton, A. M., Cherian, J., and McKinney, J. D. (2006) Role of the methylcitrate cycle in *Mycobacterium tuberculosis* metabolism, intracellular growth, and virulence, *Molecular Microbiology 60*, 1109-1122.

[43] Pham, T. V., Murkin, A. S., Moynihan, M. M., Harris, L., Tyler, P. C., Shetty, N., Sacchettini, J. C., Huang, H.-l., and Meek, T. D. (2017) Mechanism-based inactivator of isocitrate lyases 1 and 2 from *Mycobacterium tuberculosis*, *Proc Natl Acad Sci 114*, 7617-7622.

[44] Carey, A. F., Rock, J. M., Krieger, I. V., Chase, M. R., Fernandez-Suarez, M., Gagneux, S., Sacchettini, J. C., Ioerger, T. R., and Fortune, S. M. (2018) TnSeq of *Mycobacterium tuberculosis* clinical isolates reveals strain-specific antibiotic liabilities, *PLOS Pathogens 14*, e1006939.

[45] Cole, S. T., Brosch, R., Parkhill, J., Garnier, T., Churcher, C., Harris, D., Gordon, S. V., Eiglmeier, K., Gas, S., Barry, C. E., Tekaia, F., Badcock, K., Basham, D., Brown, D., Chillingworth, T., Connor, R., Davies, R., Devlin, K., Feltwell, T., Gentles, S., Hamlin, N., Holroyd, S., Hornsby, T., Jagels, K., Krogh, A., McLean, J., Moule, S., Murphy, L., Oliver, K., Osborne, J., Quail, M. A., Rajandream, M. A., Rogers, J., Rutter, S., Seeger, K., Skelton, J., Squares, R., Squares, S., Sulston, J. E., Taylor, K., Whitehead, S., and Barrell, B. G. (1998) Deciphering the biology of *Mycobacterium tuberculosis* from the complete genome sequence, *Nature 393*, 537-544.

[46] Upton, A. M., and McKinney, J. D. (2007) Role of the methylcitrate cycle in propionate metabolism and detoxification in *Mycobacterium smegmatis*, *Microbiol Res 153*, 3973-3982.

[47] Savvi, S., Warner, D. F., Kana, B. D., McKinney, J. D., Mizrahi, V., and Dawes, S. S. (2008) Functional Characterization of a Vitamin B_{12}-Dependent Methylmalonyl Pathway in *Mycobacterium tuberculosis*: Implications for Propionate Metabolism during Growth on Fatty Acids, *Journal of Bacteriology*, *190*, 3886-3895.

[48] Gengenbacher, M., Rao, S. P. S., Pethe, K., and Dick, T. (2010) Nutrient-starved, non-replicating *Mycobacterium tuberculosis* requires respiration, ATP synthase and isocitrate lyase for maintenance of ATP homeostasis and viability, *Microbiology 156*, 81-87.

[49] Wayne, L. G., and Lin, K. Y. (1982) Glyoxylate metabolism and adaptation of *Mycobacterium tuberculosis* to survival under anaerobic conditions, *Infection and Immunity 37*, 1042-1049.

[50] Rustad, T. R., Harrell, M. I., Liao, R., and Sherman, D. R. (2008) The Enduring Hypoxic Response of *Mycobacterium tuberculosis*, *PLOS ONE 3*, e1502.

[51] Schubert, Olga T., Ludwig, C., Kogadeeva, M., Zimmermann, M., Rosenberger, G., Gengenbacher, M., Gillet, Ludovic C., Collins, Ben C., Röst, Hannes L., Kaufmann, Stefan H. E., Sauer, U., and Aebersold, R. (2015) Absolute Proteome Composition and Dynamics during Dormancy and Resuscitation of *Mycobacterium tuberculosis*, *Cell Host & Microbe 18*, 96-108.

[52] Shi, L., Sohaskey, C. D., Pheiffer, C., Datta, P., Parks, M., McFadden, J., North, R. J., and Gennaro, M. L. (2010) Carbon flux rerouting during *Mycobacterium tuberculosis* growth arrest, *Molecular Microbiology 78*, 1199-1215.

[53] Baek, S.-H., Li, A. H., and Sassetti, C. M. (2011) Metabolic Regulation of Mycobacterial Growth and Antibiotic Sensitivity, *PLOS Biology 9*, e1001065.

[54] Kratky, M., and Vinsova, J. (2012) Advances in mycobacterial isocitrate lyase targeting and inhibitors, *Curr Med Chem 19*, 6126-6137.

[55] Schloss, J. V., and Cleland, W. W. (1982) Inhibition of isocitrate lyase by 3-nitropropionate, a reaction-intermediate analog, *Biochemistry 21*, 4420-4427.

[56] Ko, Y. H., and McFadden, B. A. (1990) Alkylation of isocitrate lyase from Escherichia coli by 3-bromopyruvate, *Arch Biochem Biophys 278*, 373-380.

[57] Porter, D. J., and Bright, H. J. (1980) 3-Carbanionic substrate analogues bind very tightly to fumarase and aspartase, *J Biol Chem 255*, 4772-4780.

[58] Huang, L.-s., Sun, G., Cobessi, D., Wang, A. C., Shen, J. T., Tung, E. Y., Anderson, V. E., and Berry, E. A. (2006) 3-Nitropropionic Acid Is a Suicide Inhibitor of Mitochondrial

Respiration That, upon Oxidation by Complex II, Forms a Covalent Adduct with a Catalytic Base Arginine in the Active Site of the Enzyme, *J Biol Chem 281*, 5965-5972.

[59] Coles, C. J., Edmondson, D. E., and Singer, T. P. (1979) Inactivation of succinate dehydrogenase by 3-nitropropionate, *J Biol Chem 254*, 5161-5167.

[60] Ganapathy-Kanniappan, S., Geschwind, J.-F. H., Kunjithapatham, R., Buijs, M., Vossen, J. A., Tchernyshyov, I., Cole, R. N., Syed, L. H., Rao, P. P., Ota, S., and Vali, M. (2009) Glyceraldehyde-3-phosphate Dehydrogenase (GAPDH) Is Pyruvylated during 3-Bromopyruvate Mediated Cancer Cell Death, *Anticancer Res 29*, 4909-4918.

[61] Alston, T. A., Mela, L., and Bright, H. J. (1977) 3-Nitropropionate, the toxic substance of *Indigofera*, is a suicide inactivator of succinate dehydrogenase, *Proc Natl Acad Sci 74*, 3767-3771.

[62] Ray, S., Kreitler, D. F., Gulick, A. M., and Murkin, A. S. (2018) The Nitro Group as a Masked Electrophile in Covalent Enzyme Inhibition, *ACS Chem Biol 13*, 1470-1473.

[63] Sun, F., Huo, X., Zhai, Y., Wang, A., Xu, J., Su, D., Bartlam, M., and Rao, Z. (2005) Crystal Structure of Mitochondrial Respiratory Membrane Protein Complex II, *Cell 121*, 1043-1057.

[64] Ho, N., Morrison, J., Silva, A., and Coomber, Brenda L. (2016) The effect of 3-bromopyruvate on human colorectal cancer cells is dependent on glucose concentration but not hexokinase II expression, *Biosci Rep 36*, e00299.

[65] Krátký, M., Vinšová, J., Novotná, E., Mandíková, J., Wsól, V., Trejtnar, F., Ulmann, V., Stolaříková, J., Fernandes, S., Bhat, S., and Liu, J. O. (2012) Salicylanilide derivatives block Mycobacterium tuberculosis through inhibition of isocitrate lyase and methionine aminopeptidase, *Tuberculosis 92*, 434-439.

[66] Sriram, D., Yogeeswari, P., Methuku, S., Vyas, D. R. K., Senthilkumar, P., Alvala, M., and Jeankumar, V. U. (2011) Synthesis of various 3-nitropropionamides as Mycobacterium tuberculosis isocitrate lyase inhibitor, *Bioorg Med Chem Lett 21*, 5149-5154.

[67] Shingnapurkar, D., Dandawate, P., Anson, C. E., Powell, A. K., Afrasiabi, Z., Sinn, E., Pandit, S., Venkateswara Swamy, K., Franzblau, S., and Padhye, S. (2012) Synthesis and characterization of pyruvate–isoniazid analogs and their copper complexes as potential ICL inhibitors, *Bioorg Med Chem Lett 22*, 3172-3176.

[68] Blondeau, J. M. (2004) Fluoroquinolones: mechanism of action, classification, and development of resistance, *Survey of Ophthalmology 49*, S73-S78.

[69] Khodursky, A. B., Zechiedrich, E. L., and Cozzarelli, N. R. (1995) Topoisomerase IV is a target of quinolones in Escherichia coli, *Proceedings of the National Academy of Sciences of the United States of America 92*, 11801-11805.

[70] Evans-Roberts, K. M., Mitchenall, L. A., Wall, M. K., Leroux, J., Mylne, J. S., and Maxwell, A. (2016) DNA Gyrase Is the Target for the Quinolone Drug Ciprofloxacin in Arabidopsis thaliana, *J Biol Chem 291*, 3136-3144.

[71] Silverman, R. B. (1995) Mechanism-based enzyme inactivators, In *Methods in Enzymology*, pp 240-283, Academic Press.

[72] ElAzzouny, M., Tom, C. T., Evans, C. R., Olson, L. L., Tanga, M. J., Gallagher, K. A., Martin, B. R., and Burant, C. F. (2017) Dimethyl Itaconate Is Not Metabolized into Itaconate Intracellularly, *J Biol Chem 292*, 4766-4769.

[73] Ehinger, J. K., Piel, S., Ford, R., Karlsson, M., Sjövall, F., Frostner, E. Å., Morota, S., Taylor, R. W., Turnbull, D. M., Cornell, C., Moss, S. J., Metzsch, C., Hansson, M. J., Fliri, H., and Elmér, E. (2016) Cell-permeable succinate prodrugs bypass mitochondrial complex I deficiency, *Nature Communications 7*, 12317.

[74] Krieger, Inna V., Freundlich, Joel S., Gawandi, Vijay B., Roberts, Justin P., Gawandi, Vidyadhar B., Sun, Q., Owen, Joshua L., Fraile, Maria T., Huss, Sofia I., Lavandera, J.-L., Ioerger, Thomas R., and Sacchettini, James C. (2015) Structure-Guided Discovery of Phenyl-diketo Acids as Potent Inhibitors of M. tuberculosis Malate Synthase, *Chem & Biol 19*, 1556-1567.

[75] May, E. E., Leitão, A., Tropsha, A., and Oprea, T. I. (2013) A systems chemical biology study of malate synthase and isocitrate lyase inhibition in Mycobacterium tuberculosis during active and NRP growth, *Computational Biology and Chemistry 47*, 167-180.

[76] Strittmatter, L., Li, Y., Nakatsuka, N. J., Calvo, S. E., Grabarek, Z., and Mootha, V. K. (2014) CLYBL is a polymorphic human enzyme with malate synthase and beta-methylmalate synthase activity, *Human molecular genetics 23*, 2313-2323.

[77] Chen, C., Sun, Q., Narayanan, B., Nuss, D. L., and Herzberg, O. (2010) Structure of oxalacetate acetylhydrolase, a virulence factor of the chestnut blight fungus, *The Journal of Biological Chemistry 285*, 26685-26696.

[78] Quartararo, C. E., Hadi, T., Cahill, S. M., and Blanchard, J. S. (2013) Solvent Isotope-induced Equilibrium Perturbation for Isocitrate Lyase, *Biochemistry 52*, 9286-9293.

[79] Moynihan, M. M., and Murkin, A. S. (2014) Cysteine Is the General Base That Serves in Catalysis by Isocitrate Lyase and in Mechanism-Based Inhibition by 3-Nitropropionate, *Biochemistry 53*, 178-187.

[80] Hoffmann, C., Gaietta, G., Bunemann, M., Adams, S. R., Oberdorff-Maass, S., Behr, B., Vilardaga, J.-P., Tsien, R. Y., Ellisman, M. H., and Lohse, M. J. (2005) A FlAsH-based FRET approach to determine G protein-coupled receptor activation in living cells, *Nat Meth 2*, 171-176.

[81] Kolb, H. C., Finn, M. G., and Sharpless, K. B. (2001) Click Chemistry: Diverse Chemical Function from a Few Good Reactions, *Angew Chem Int Ed Engl 40*, 2004-2021.

[82] Neubert, F., Beliu, G., Terpitz, U., Werner, C., Geis, C., Sauer, M., and Doose, S. (2018) Bioorthogonal click chemistry enables site-specific fluorescence labeling of functional NMDA receptors for super-resolution imaging, *Angew Chem Int Ed*.

[83] Hoffmann, C., Gaietta, G., Zurn, A., Adams, S. R., Terrillon, S., Ellisman, M. H., Tsien, R. Y., and Lohse, M. J. (2010) Fluorescent labeling of tetracysteine-tagged proteins in intact cells, *Nat Protocols 5*, 1666-1677.

[84] Wong, I. L. K., Zhu, X., Chan, K. F., Law, M. C., Lo, A. M. Y., Hu, X., Chow, L. M. C., and Chan, T. H. (2018) Discovery of novel flavonoid dimers to reverse multidrug resistance protein 1 (MRP1; ABCC1)-mediated drug resistance in cancers using a high throughput platform with "click chemistry", *J Med Chem 61*, 9931-9951.

[85] Bradshaw, J. M., McFarland, J. M., Paavilainen, V. O., Bisconte, A., Tam, D., Phan, V. T., Romanov, S., Finkle, D., Shu, J., Patel, V., Ton, T., Li, X., Loughhead, D. G., Nunn, P. A., Karr, D. E., Gerritsen, M. E., Funk, J. O., Owens, T. D., Verner, E., Brameld, K. A., Hill, R. J., Goldstein, D. M., and Taunton, J. (2015) Prolonged and tunable residence time using reversible covalent kinase inhibitors, *Nat Chem Biol 11*, 525-531.

[86] Krishnan, S., Miller, R. M., Tian, B., Mullins, R. D., Jacobson, M. P., and Taunton, J. (2014) Design of reversible, cysteine-targeted Michael acceptors guided by kinetic and computational analysis, *J Am Chem Soc 136*, 12624-12630.

[87] Serafimova, I. M., Pufall, M. A., Krishnan, S., Duda, K., Cohen, M. S., Maglathlin, R. L., McFarland, J. M., Miller, R. M., Frodin, M., and Taunton, J. (2012) Reversible targeting of noncatalytic cysteines with chemically tuned electrophiles, *Nat Chem Biol 8*, 471-476.

[88] Galibert, M., Wartenberg, M., Lecaille, F., Saidi, A., Mavel, S., Joulin-Giet, A., Korkmaz, B., Bromme, D., Aucagne, V., Delmas, A. F., and Lalmanach, G. (2018) Substrate-derived triazolo- and azapeptides as inhibitors of cathepsins K and S, *Eur J Med Chem 144*, 201-210.

[89] Gauthier, J. Y., Chauret, N., Cromlish, W., Desmarais, S., Duong, L. T., Falgueyret, J. P., Kimmel, D. B., Lamontagne, S., Leger, S., LeRiche, T., Li, C. S., Masse, F., McKay, D. J., Nicoll-Griffith, D. A., Oballa, R. M., Palmer, J. T., Percival, M. D., Riendeau, D., Robichaud, J., Rodan, G. A., Rodan, S. B., Seto, C., Therien, M., Truong, V. L., Venuti, M. C., Wesolowski, G., Young, R. N., Zamboni, R., and Black, W. C. (2008) The discovery of odanacatib (MK-0822), a selective inhibitor of cathepsin K, *Bioorg Med Chem Lett 18*, 923-928.

[90] Holdgate, G. A., Meek, T. D., and Grimley, R. L. (2018) Mechanistic enzymology in drug discovery: A fresh perspective, *Nature Reviews Drug Discovery 17*, 115-132.

[91] Wolff, D. J., and Lubeskie, A. (1995) Aminoguanidine Is an Isoform-Selective, Mechanism-Based Inactivator of Nitric Oxide Synthase, *Arch Biochem Biophys 316*, 290-301.

[92] Amorim Franco, T. M., Favrot, L., Vergnolle, O., and Blanchard, J. S. (2017) Mechanism-Based Inhibition of the *Mycobacterium tuberculosis* Branched-Chain Aminotransferase by d- and l-Cycloserine, *ACS Chem Biol 12*, 1235-1244.

[93] Tuley, A., and Fast, W. (2018) The Taxonomy of Covalent Inhibitors, *Biochemistry 57*, 3326-3337.

[94] Diehl, P., and McFadden, B. A. (1993) Site-directed mutagenesis of lysine 193 in Escherichia coli isocitrate lyase by use of unique restriction enzyme site elimination, *J Bacteriol 175*, 2263-2270.

[95] Diehl, P., and McFadden, B. A. (1994) The importance of four histidine residues in isocitrate lyase from *Escherichia coli*, *J Bacteriol 176*, 927-931.

[96] Rehman, A., and McFadden, B. A. J. C. M. (1997) Serine319 and 321 Are Functional in Isocitrate Lyase from Escherichia coli, *Curr Microbiol 34*, 205-211.

[97] Rehman, A., and McFadden, B. A. J. C. M. (1997) Cysteine 195 Has a Critical Functional Role in Catalysis by Isocitrate Lyase from *Escherichia coli*, *Curr Microbiol 35*, 267-269.

[98] Rehman, A., and McFadden, B. A. J. C. M. (1997) Lysine 194 Is Functional in Isocitrate Lyase from *Escherichia coli*, *Curr Microbiol 35*, 14-17.

[99] Shukla, H., Shukla, R., Sonkar, A., Pandey, T., and Tripathi, T. (2017) Distant Phe345 mutation compromises the stability and activity of Mycobacterium tuberculosis isocitrate lyase by modulating its structural flexibility, *Sci Rep 7*, 1058.

[100] Shukla, R., Shukla, H., and Tripathi, T. (2018) Activity loss by H46A mutation in Mycobacterium tuberculosis isocitrate lyase is due to decrease in structural plasticity and collective motions of the active site, *Tuberculosis 108*, 143-150.

[101] Lindskog, S. (1997) Structure and mechanism of carbonic anhydrase, *Pharm & Ther 74*, 1-20.

[102] Christianson, D. W., and Cox, J. D. (1999) Catalysis By Metal-Activated Hydroxide in Zinc and Manganese Metalloenzymes, *Annu Rev Biochem 68*, 33-57.

[103] Liu, H., and Naismith, J. H. J. B. B. (2008) An efficient one-step site-directed deletion, insertion, single and multiple-site plasmid mutagenesis protocol, *BMC Biotechnology 8*, 91.

[104] Cornish-Bowden, A. (1974) A simple graphical method for determining the inhibition constants of mixed, uncompetitive and non-competitive inhibitors (Short Communication), *Biochem J 137*, 143-144.

[105] Loudon, G. M. (1991) Mechanistic interpretation of pH-rate profiles, *J Chem Educ 68*, 973.

[106] Wallace Cleland, W. (1982) [22] The use of pH studies to determine chemical mechanisms of enzyme-catalyzed reactions, In *Methods in Enzymology* (Purich, D. L., Ed.), pp 390-405, Academic Press.

[107] Cleland, W. W. (2006) Determining the Chemical Mechanisms of Enzyme-Catalyzed Reactions by Kinetic Studies, In *Advances in Enzymology and Related Areas of Molecular Biology*, John Wiley & Sons, Inc.

[108] Pastra-Landis, S. C., Evans, D. R., and Lipscomb, W. N. (1978) The effect of pH on the cooperative behavior of aspartate transcarbamylase from Escherichia coli, *J Biol Chem 253*, 4624-4630.

[109] Brocklehurst, K., and Dixon, H. B. (1976) PH-dependence of the steady-state rate of a two-step enzymic reaction, *The Biochemical journal 155*, 61-70.

[110] Tu, C. K., Silverman, D. N., Forsman, C., Jonsson, B. H., and Lindskog, S. (1989) Role of histidine 64 in the catalytic mechanism of human carbonic anhydrase II studied with a site-specific mutant, *Biochemistry 28*, 7913-7918.

[111] Colleluori, D. M., Reczkowski, R. S., Emig, F. A., Cama, E., Cox, J. D., Scolnick, L. R., Compher, K., Jude, K., Han, S., Viola, R. E., Christianson, D. W., and Ash, D. E. (2005) Probing the role of the hyper-reactive histidine residue of arginase, *Arch Biochem Biophys 444*, 15-26.

[112] Cook, P. F., and Cleland, W. W. (2007) *Enzyme kinetics and mechanism*, 1 ed., Garland Science.

[113] Dumas, D. P., and Raushel, F. M. (1990) Chemical and kinetic evidence for an essential histidine in the phosphotriesterase from Pseudomonas diminuta, *J Biol Chem 265*, 21498-21503.

[114] Goldberg, R. N., Kishore, N., and Lennen, R. M. (2002) Thermodynamic Quantities for the Ionization Reactions of Buffers, *Journal of Physical and Chemical Reference Data*, *31*, 231-370.

[115] Kuramitsu, S., Ikeda, K., Hamaguchi, K., Fujio, H., Amano, T., Miwa, S., and Nishina, T. (1974) Ionization Constants of Glu 35 and Asp 52 in Hen, Turkey, and Human Lysozymes, *J Biochem 76*, 671-683.

[116] Inoue, M., Yamada, H., Yasukochi, T., Kuroki, R., Miki, T., Horiuchi, T., and Imoto, T. (1992) Multiple role of hydrophobicity of tryptophan-108 in chicken lysozyme: structural stability, saccharide binding ability, and abnormal pKa of glutamic acid-35, *Biochemistry 31*, 5545-5553.

[117] Davoodi, J., Wakarchuk, W. W., Campbell, R. L., Carey, P. R., and Surewicz, W. K. (1995) Abnormally High pKa of an Active-Site Glutamic Acid Residue in *Bacillus Circulans Xylanase*, *Eur J Biochem 232*, 839-843.

[118] Isom, D. G., Castañeda, C. A., Cannon, B. R., and García-Moreno E., B. (2011) Large shifts in pK$_a$ values of lysine residues buried inside a protein, *Proc Natl Acad Sci*.

[119] Quartararo, C. E., Hazra, S., Hadi, T., and Blanchard, J. S. (2013) Structural, Kinetic and Chemical Mechanism of Isocitrate Dehydrogenase-1 from *Mycobacterium tuberculosis*, *Biochemistry 52*, 1765-1775.

[120] Klenchin, V. A., Taylor Ringia, E. A., Gerlt, J. A., and Rayment, I. (2003) Evolution of Enzymatic Activity in the Enolase Superfamily: Structural and Mutagenic Studies of the Mechanism of the Reaction Catalyzed by o-Succinylbenzoate Synthase from Escherichia coli, *Biochemistry 42*, 14427-14433.

[121] Highbarger, L. A., Gerlt, J. A., and Kenyon, G. L. (1996) Mechanism of the Reaction Catalyzed by Acetoacetate Decarboxylase. Importance of Lysine 116 in Determining the pKa of Active-Site Lysine 115, *Biochemistry 35*, 41-46.

[122] Ahlstrom, L. S., Vorontsov, I. I., Shi, J., and Miyashita, O. (2017) Effect of the Crystal Environment on Side-Chain Conformational Dynamics in Cyanovirin-N Investigated through Crystal and Solution Molecular Dynamics Simulations, *PLOS ONE 12*, e0170337.

[123] Scouras, A. D., and Daggett, V. (2011) The dynameomics rotamer library: Amino acid side chain conformations and dynamics from comprehensive molecular dynamics simulations in water, *Protein Science : A Publication of the Protein Society 20*, 341-352.

[124] Harms, M. J., Castañeda, C. A., Schlessman, J. L., Sue, G. R., and Bertrand García-Moreno, E. (2009) The pK(a) values of acidic and basic residues buried at the same internal location in a protein are governed by different factors, *J Mol Biol 389*, 34-47.

[125] Kolappan, S., Zwahlen, J., Zhou, R., Truglio, J. J., Tonge, P. J., and Kisker, C. (2007) Lysine 190 Is the Catalytic Base in MenF, the Menaquinone-Specific Isochorismate Synthase from Escherichia coli: Implications for an Enzyme Family, *Biochemistry 46*, 946-953.

[126] Carlson, G. M., and Holyoak, T. (2009) Structural Insights into the Mechanism of Phosphoenolpyruvate Carboxykinase Catalysis, *J Biol Chem 284*, 27037-27041.

[127] Gerlt, J. A., Babbitt, P. C., and Rayment, I. (2005) Divergent evolution in the enolase superfamily: the interplay of mechanism and specificity, *Arch Biochem Biophys 433*, 59-70.

[128] Mitra, B., Kallarakal, A. T., Kozarich, J. W., Gerlt, J. A., Clifton, J. R., Petsko, G. A., and Kenyon, G. L. (1995) Mechanism of the Reaction Catalyzed by Mandelate Racemase: Importance of Electrophilic Catalysis by Glutamic Acid 317, *Biochemistry 34*, 2777-2787.

[129] Zhou, M., Xie, L., Yang, Z., Zhou, J., and Xie, J. (2017) Lysine succinylation of Mycobacterium tuberculosis isocitrate lyase (ICL) fine-tunes the microbial resistance to antibiotics, *J Biomol Struct Dyn 35*, 1030-1041.

[130] Kitagawa, M., Ara, T., Arifuzzaman, M., Ioka-Nakamichi, T., Inamoto, E., Toyonaga, H., and Mori, H. (2005) Complete set of ORF clones of Escherichia coli ASKA library (a complete set of E. coli K-12 ORF archive): unique resources for biological research, *DNA research : an international journal for rapid publication of reports on genes and genomes 12*, 291-299.

[131] Kitz, R., and Wilson, I. B. (1962) Esters of Methanesulfonic Acid as Irreversible Inhibitors of Acetylcholinesterase, *J Biol Chem 237*, 3245-3249.

[132] Trott, O., and Olson, A. J. (2010) AutoDock Vina: improving the speed and accuracy of docking with a new scoring function, efficient optimization, and multithreading, *Journal of computational chemistry 31*, 455-461.

[133] Batt, S. M., Jabeen, T., Bhowruth, V., Quill, L., Lund, P. A., Eggeling, L., Alderwick, L. J., Fütterer, K., and Besra, G. S. (2012) Structural basis of inhibition of *Mycobacterium tuberculosis* DprE1 by benzothiazinone inhibitors, *Proc Natl Acad Sci 109*, 11354-11359.

[134] Yonetani, T., and Theorell, H. (1964) Studies on liver alcohol hydrogenase complexes. 3. Multiple inhibition kinetics in the presence of two competitive inhibitors, *Archives of biochemistry and biophysics 106*, 243-251.

[135] Asante-Appiah, E., and Chan, W. W. (1996) Analysis of the interactions between an enzyme and multiple inhibitors using combination plots, *The Biochemical journal 320*, 17-26.

[136] Boiadjiev, S. E., and Lightner, D. A. (2000) Steric Size in Conformational Analysis. Steric Compression Analyzed by Circular Dichroism Spectroscopy, *J Am Chem Soc 122*, 11328-11339.

[137] Crousilles, A. L., Dolan, S. K., Brear, P., Chirgadze, D. Y., and Welch, M. (2018) Three enzymes and one substrate; regulation of flux through the glyoxylate shunt in the opportunistic pathogen, Pseudomonas aeruginosa, *Biorxic Preprint* https://www.biorxiv.org/content/biorxiv/early/2018/05/09/318345.full.pdf.

[138] Kondo, T., and Hirohashi, S. (2007) Application of highly sensitive fluorescent dyes (CyDye DIGE Fluor saturation dyes) to laser microdissection and two-dimensional difference gel electrophoresis (2D-DIGE) for cancer proteomics, *Nature Protocols 1*, 2940.

[139] Rueden, C. T., Schindelin, J., Hiner, M. C., DeZonia, B. E., Walter, A. E., Arena, E. T., and Eliceiri, K. W. (2017) ImageJ2: ImageJ for the next generation of scientific image data, *J BMC Bioinformatics 18*, 529.

[140] Morrison, J. F., and Wash, C. T. (2006) The Behavior and Significance of Slow-Binding Enzyme Inhibitors, In *Advances in Enzymology and Related Areas of Molecular Biology*, John Wiley & Sons, Inc.

[141] Parker, R. E., and Isaacs, N. S. (1959) Mechanisms Of Epoxide Reactions, *Chem Rev 59*, 737-799.

APPENDIX
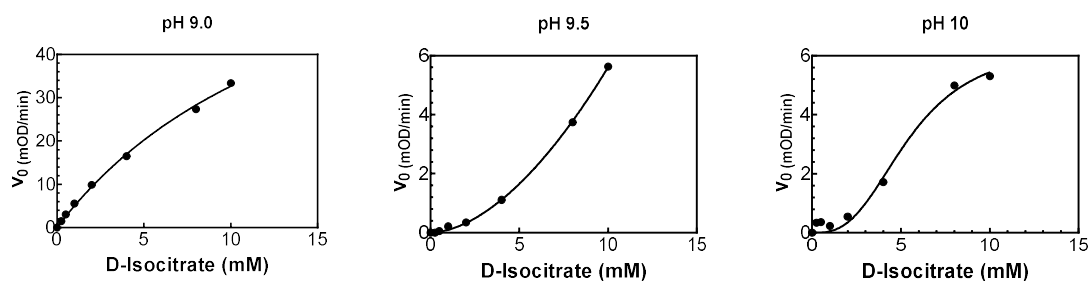
Figure A-1 ICL1 exhibited non-saturable kinetic rate at pH 9.0 and significant cooperativity at pH 9.5 and pH 10

Initial velocity of glyoxylate formation (V_0) was determined by extrapolating the early linear region of A_{324} changes (mOD/min). The line drawn through initial velocity data points in pH 9.0 plot was the fitted curve from equation (1). Lines drawn in pH 9.5 and pH 10 were from fitting initial velocity data to equation (2)
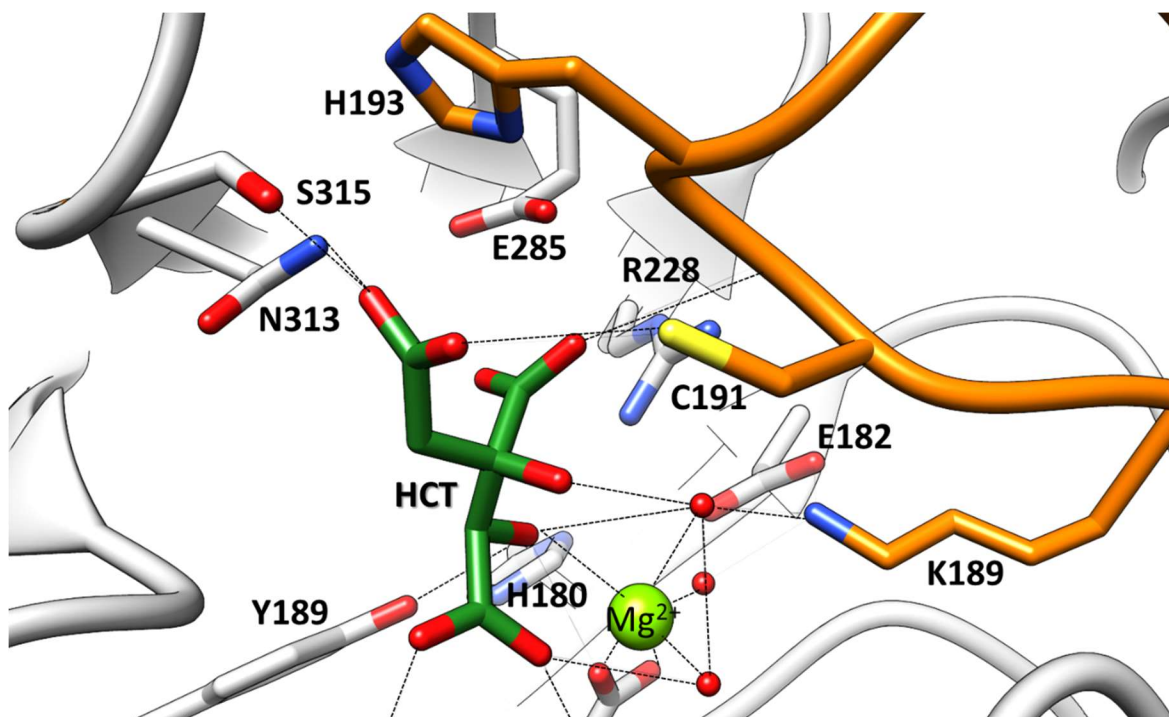
Figure A-2 Hydroxycitrate-bound ICL1 crystal structure

Above ICL1 structure was from cocrystalization with 10 mM hydroxycitrate (HCT), shown in forest green. The active site loop containing K189KGCH193 is shown in orange. Dash-lines are potential hydrogen interactions between hydroxycitrate and ICL1 active-site residues.
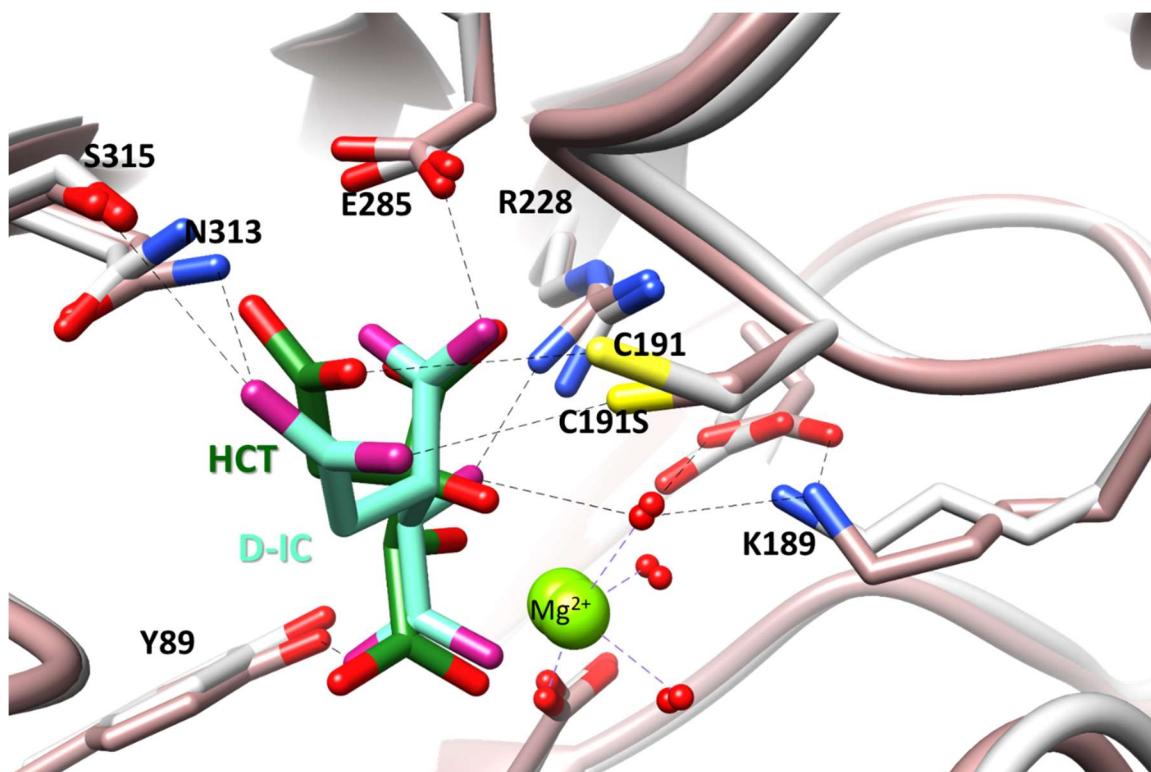
Figure A-3 Overlay of ICL1 structure in complex with hydroxycitrate and the docking model of (2*R*,3*S*)-isocitrate in ICL1 active site

Hydroxycitrate (HCT) is shown in forest green and (2*R*,3*S*)-isocitrate is shown in cyan. Dash-lines are potential hydrogen interactions between hydroxycitrate and ICL1 active-site residues.
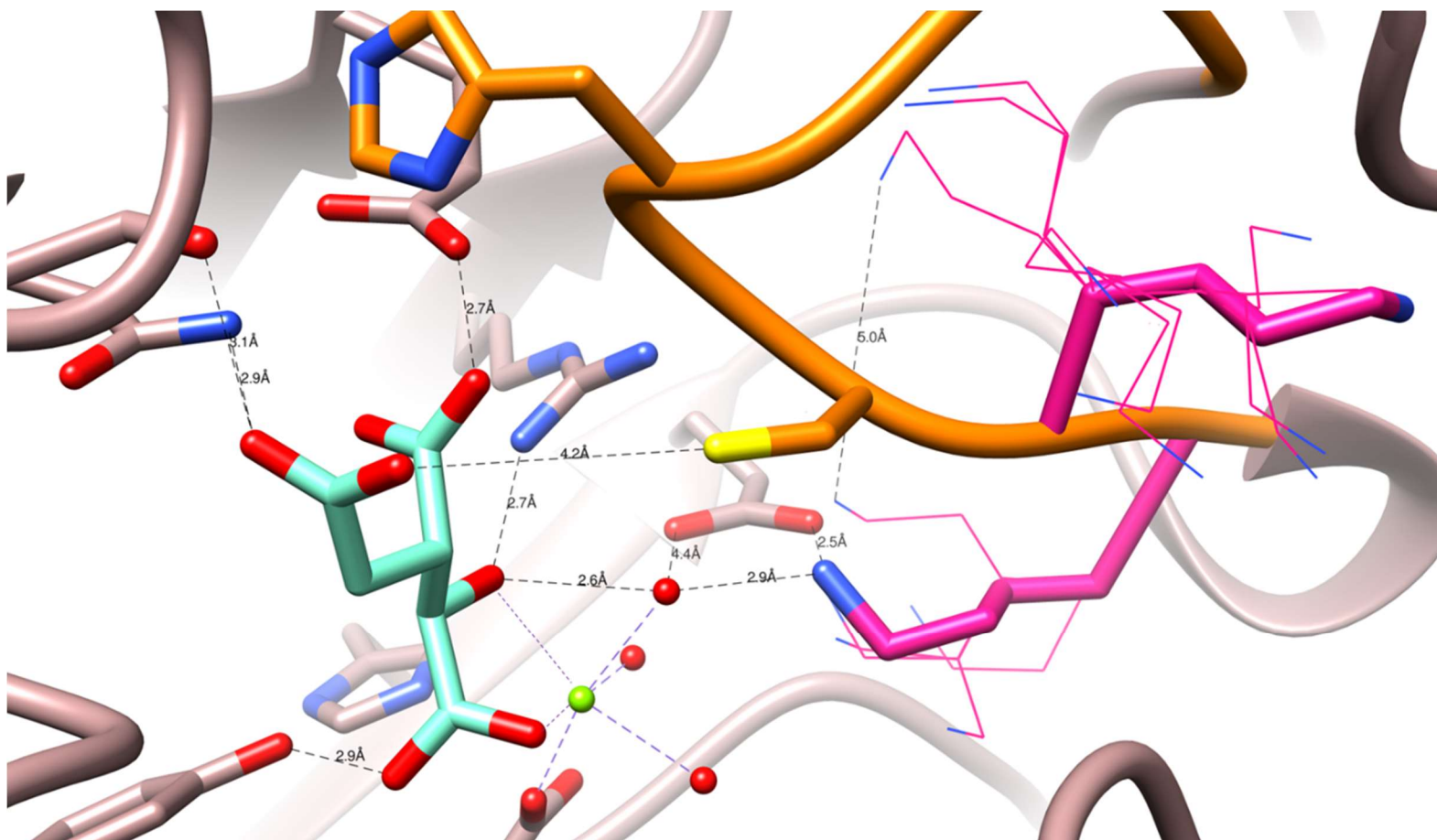
Figure A-4 Potential rotamers of K189 and K190 in solution

Above ICL1 structure was a model of ICL1 active site with D-IC (cyan). The active site loop containing K189KGCH193 is shown in orange. Dash-lines are potential hydrogen interactions among ICL1 active-site residues and with D-IC. Potential rotamers of K189 and K190 (shown as pink wires) were selected from the built-in "dynameomics rotamer library"[123] from Chimera which exhibited no "clashed" contacts with other atoms in the model.
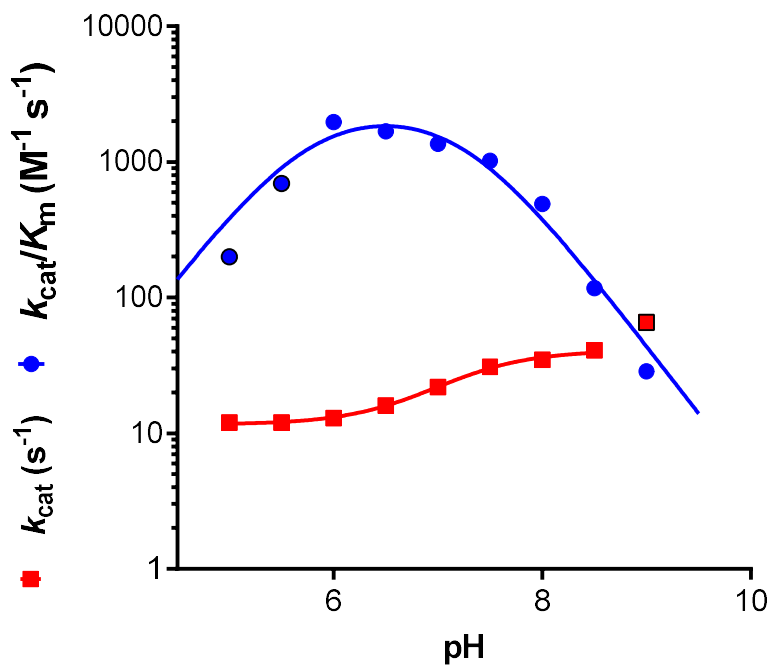
	k_{cat}/K_m (M^{-1} sec^{-1})	k_{cat} (sec^{-1})
pKa	5.7 ± 0.2	
pKb	7.3 ± 0.2	
pK1		7.3 ± 0.1

Figure A-5 pH-rate profiles of ICL1-catalyzed isocitrate cleavage

Initial velocities of ICL1 catalysis at different concentration of (2*R*,3*S*)-isocitrate were fitted into equation (1) to obtain k_{cat}/K_m and k$_{cat}$ data points. Continuous-lines were drawn from fitting k_{cat}/K_m and k_{cat} data points to equation (3) and (6), respectively.
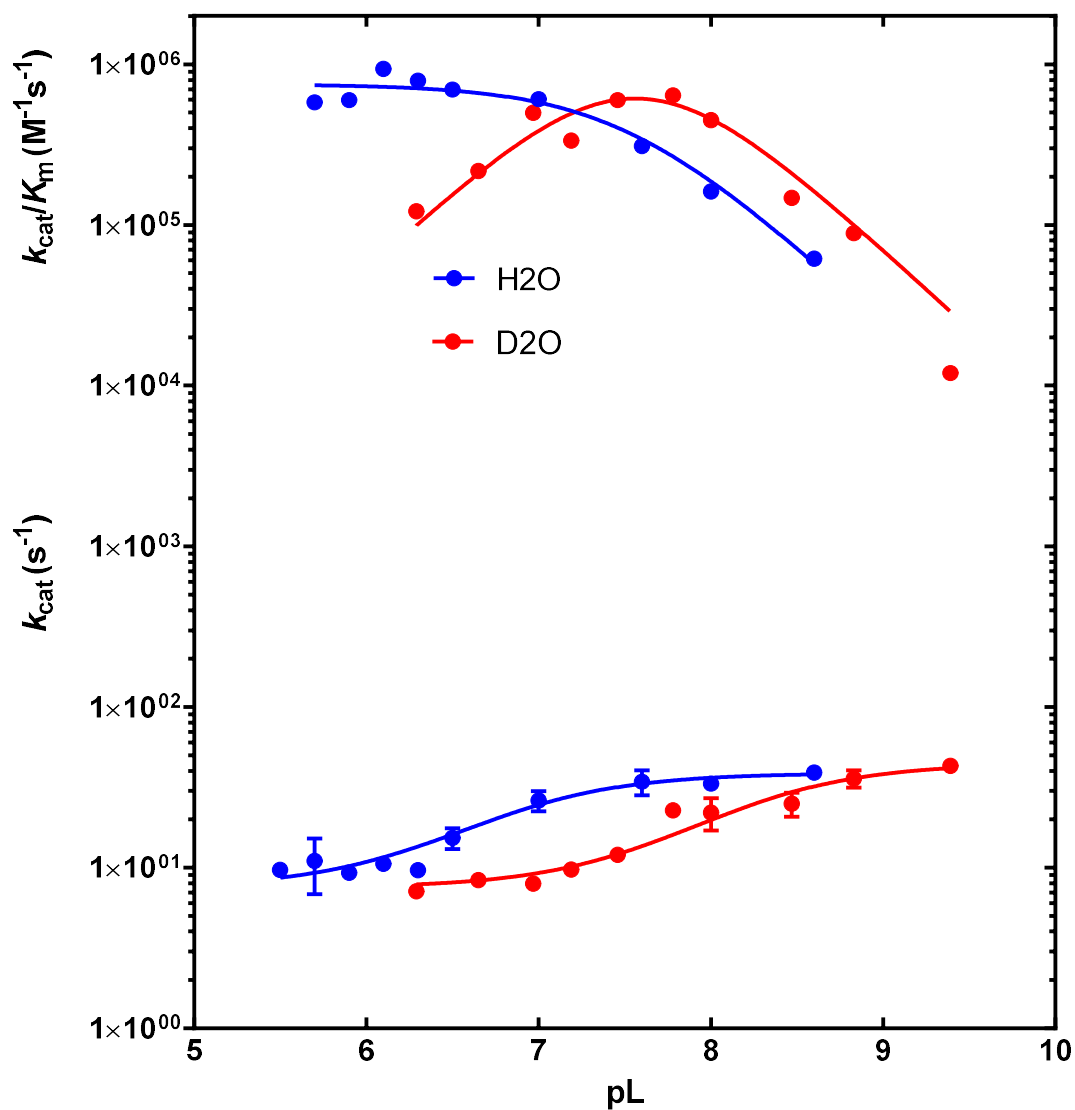
Figure A-6 Solvent kinetic isotope effects of ICL1 retro-aldol catalysis

ICL1 catalysis was measured in the isocitrate cleavage direction at varying pL in D_2O (red) and H_2O (blue). Initial velocities of ICL1 catalysis at different concentration of $(2R,3S)$-isocitrate were fitted into equation (1) to obtain k_{cat}/K_m and k_{cat} data points. Continuous-lines were drawn from fitting k_{cat}/K_m and k_{cat} data points to equation (5) and (6), respectively. sKIE values were 1.3 ± 0.2 for k_{cat} and 1.0 ± 0.2 at the low and high limit of k_{cat}, respectively. sKIE for k_{cat}/K_m was 1.7 ± 0.2
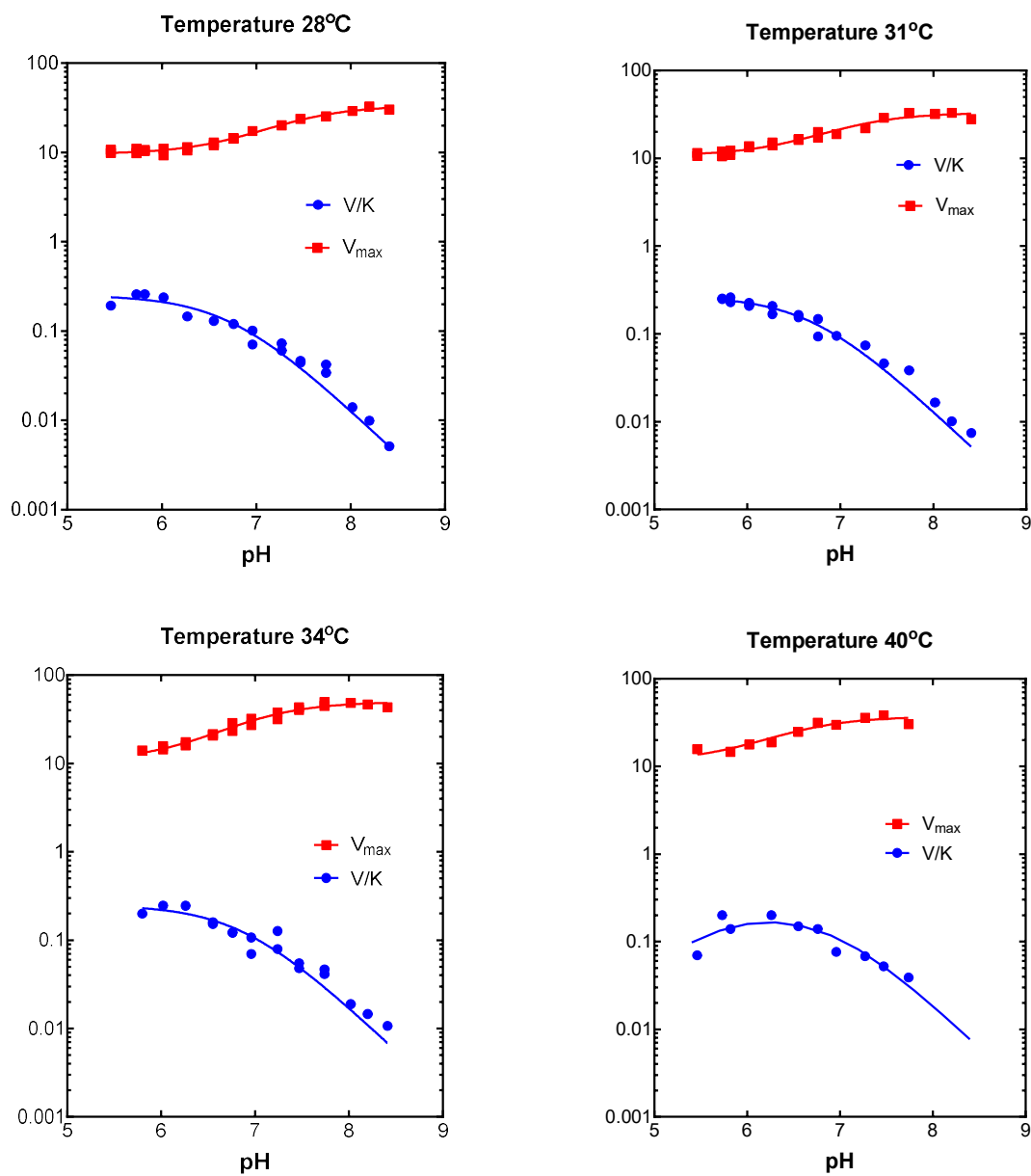
Figure A-7 pH-rate profiles of ICL1 retro-aldol catalysis at 28 – 40 ºC

Initial velocities of ICL1 catalysis at different concentration of (2*R*,3*S*)-isocitrate were fitted into equation (1) to obtain k_{cat}/K_m and k_{cat} data points. Continuous-lines were drawn from fitting k_{cat}/K_m and k_{cat} data points to equation (5) and (6), respectively. The exception is the line drawn though k_{cat}/K_m at 40 ºC which was obtained from fitting data to equation (3).
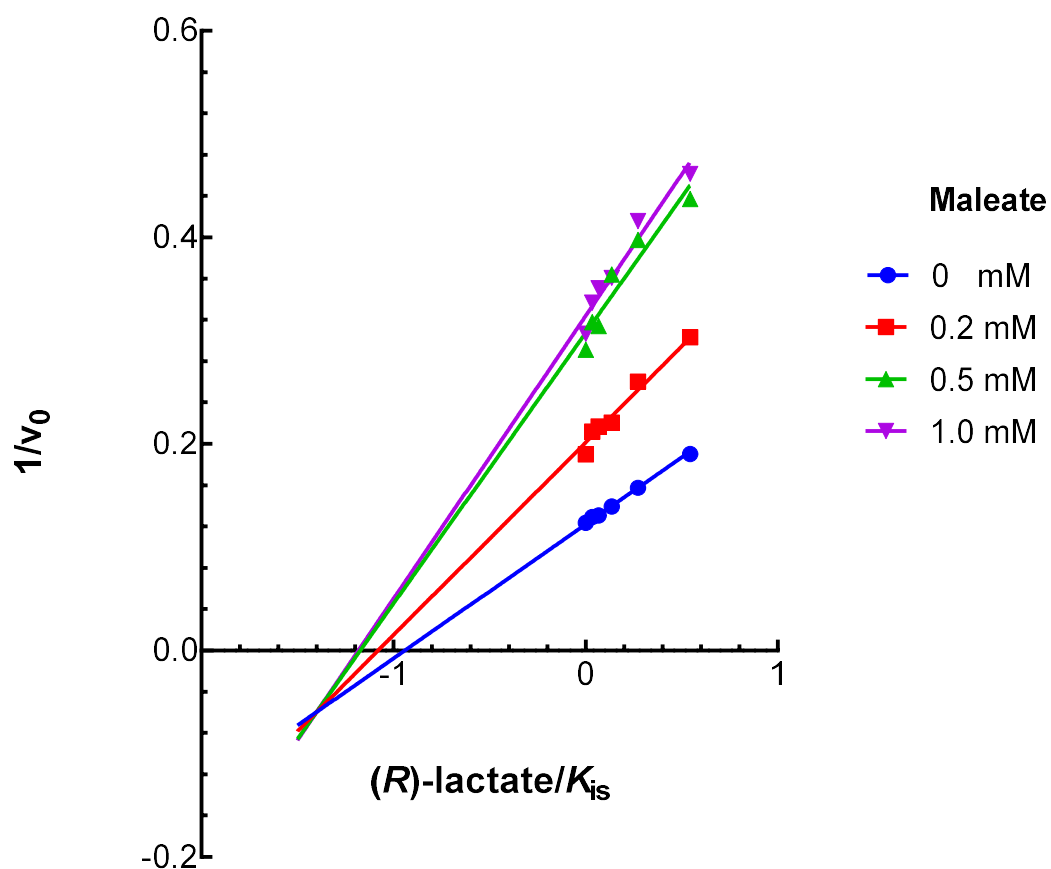
Figure A-8 Yonetani-Theorell analysis of agonistic interactions between maleate and (*R*)-lactate inhibition

Reciprocal of initial velocity of ICL1 catalysis in the presence of varying (R)-lactate at fixed concentration of maleate (0, 0.2, 0.5 and 1.0 mM) was plotted against the ratio of (*R*)-lactate and its competitive inhibition constant ($K_{is} = 2.3 \pm 0.3$ mM). Lines were drawn from linear regression analysis and the synergistic value α was calculated by equation α = "x-axis intercept" x K_m/S
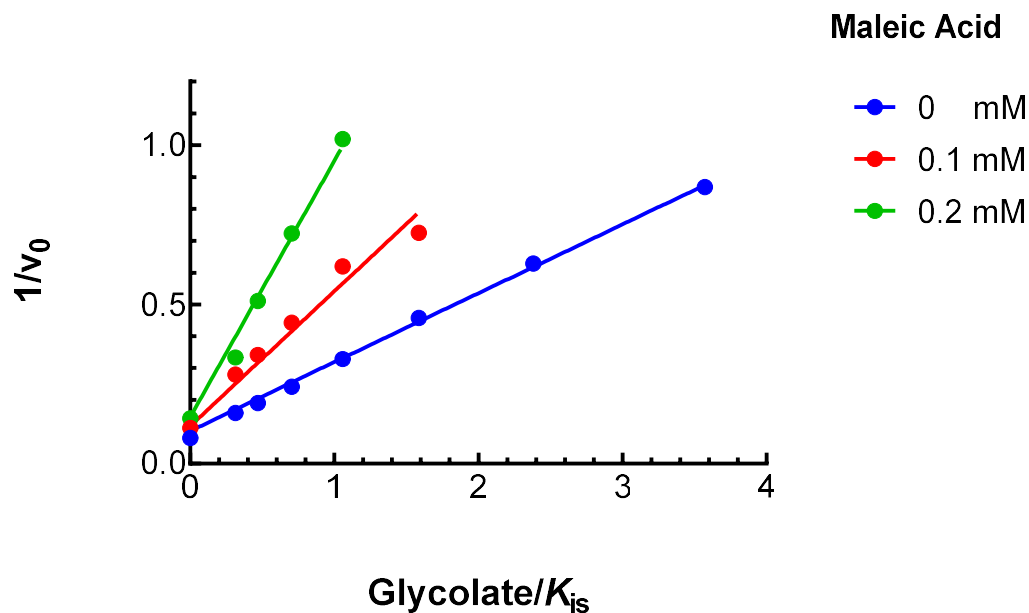
Figure A-9 Yonetani-Theorell analysis of agonistic interactions between maleate and (*R*)-glycolate inhibition

Reciprocal of initial velocity of ICL1 catalysis in the presence of varying (*R*)-lactate at fixed concentration of maleate (0, 0.1 and 0.2 mM) was plotted against the ratio of glycolate concentration and its competitive inhibition constant (K_{is} = 70 ± µM). Lines were drawn from linear regression analysis and the synergistic value α was calculated by equation α = "x-axis intercept" x K_m/S.
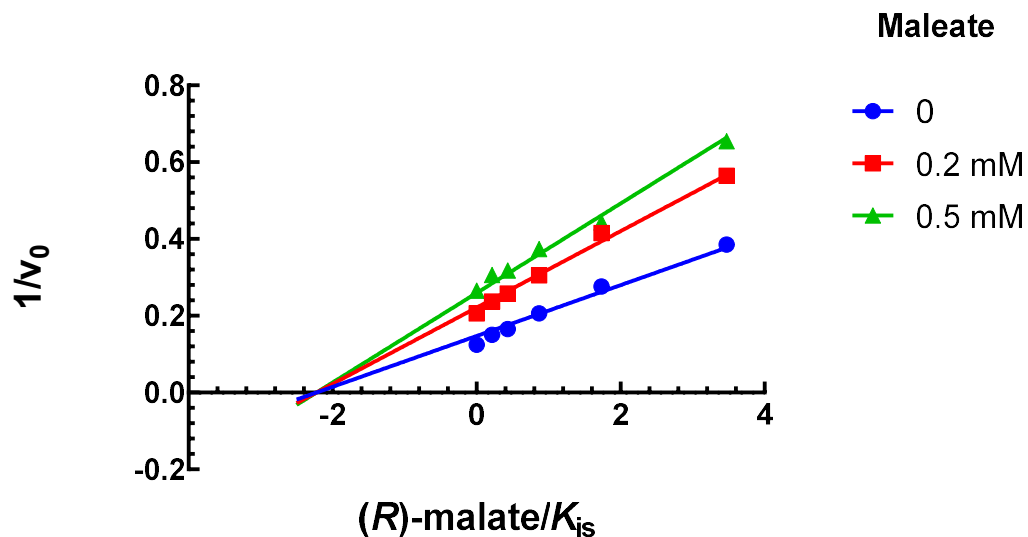
Figure A-10 Yonetani-Theorell analysis of independent interactions between maleate and (*R*)-malate inhibition

Reciprocal of initial velocity of ICL1 catalysis in the presence of varying (*R*)-malate at fixed concentration of maleate (0, 0.2, and 0.5 mM) was plotted against the ratio of (*R*)-malate and its competitive inhibition constant ($K_{is} = 0.3 \pm 0.1$ mM). Lines were drawn from linear regression analysis and the synergistic value α was calculated by equation α = "x-axis intercept" x K_m/S.
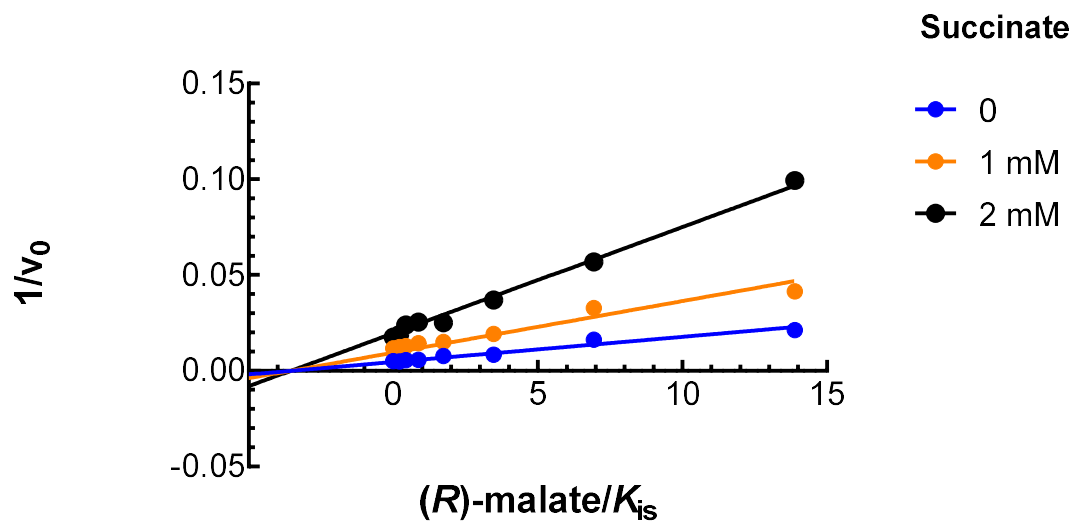
Figure A-11 Yonetani-Theorell analysis of independent interactions between succinate and (*R*)-malate inhibition

Reciprocal of initial velocity of ICL1 catalysis in the presence of varying (*R*)-malate at fixed concentration of succinate (0, 1.0 , and 2.0 mM) was plotted against (*R*)-malate concentration. Lines were drawn from linear regression analysis and the synergistic value α was calculated by equation α = "x-axis intercept" x K_m/S.
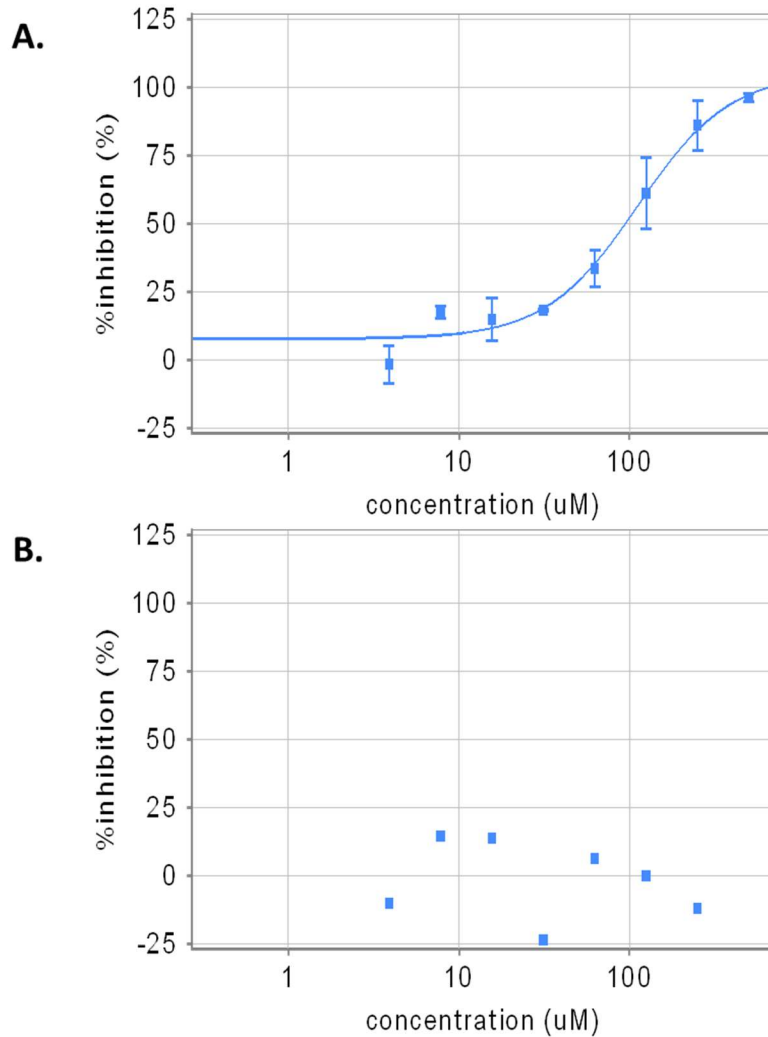
Figure A-12 Inhibition of *Mtb mc2 7000* growth by *cis*-EpS and *trans*-EpS

Effects of (A) *cis*-EpS and (B) *trans*-EpS on *Mtb mc2 7000* grown on acetate carbon source. Dose response curve from c*is*-EpS inhibition was fitted to equation $y = 100 - 100/(1+ [I]/IC_{50})$ where y is normalized inhibition (%) and [I] is the concentration of *cis*-EpS in the x-axis and IC_{50} represents the concentration of *cis*-EpS to achieve 50% inhibition ($IC_{50} = 100 \pm 10$ μM).

149

Table A-1 Thermodynamic constants of pK_1 and pK_b

	ΔH (kcal/mol)	ΔS (cal/mol)
pK_1	30 ± 3 (21 – 39)	60 ± 9 (38 – 96)
pK_b	3.0 ± 0.4 (1.8 – 4.2)	-21 ± 1 (-17 – -25)

() denotes a range of pK_a values defined by 95% confidence intervals

Table A-2 Comparisons of binding penalty (kcal/mol) and A-values as an indicator for functional group steric size

R group	$K_i/^{Glx}K_d$	Penalty Energy (kcal/mol)	A-values[136]
H	3.5	0.8	-
Methyl	115	2.9	1.7
Ethyl	450	3.8	$1.8^{\alpha}/2.6^{\beta}$
Oxet-2-yl	125	3.0	-
Benzyl	50/1000	2.4/4.3	$2.8^{\alpha}/2.6^{\beta}$
Phenyl	250	3.4	$1.7^{\alpha}/2.3^{\beta}$

$^{\alpha}$ Classical conformational A-values; $^{\beta}$ Exciton chirality A-values, which was used to plot Figure 4-2

Table A-3 Summary of pH-rate profiles and solvent kinetic isotope effects (sKIE) on 2-VIC inactivation of ICL1

	k_{inact}/K_{inact}[α]	k_{inact}[α]
pK_a	5.9 ± 0.2	5.6 ± 0.2
pK_b	7.6 ± 0.2	8.2 ± 0.2
sKIE	0.5	1.8

[α] Inactivation kinetic values from pH-dependent 2-VIC mechanism-based inactivation of ICL1 described in Chapter 3

Table A-4 Inactivation kinetic parameters of 2-vinyl-(2R,3S)-Isocitrate

Enzyme	2-Vinyl-D-Isocitrate		
	k_{inact}/K_{inact} ($\mu M^{-1} min^{-1}$)	k_{inact} (min^{-1})	K_{inact} (μM)
ICL1	$(3.5 \pm 0.7) \times 10^{-3}$	0.08 ± 0.006	22 ± 3
ICL2	$(4.6 \pm 0.7) \times 10^{-5}$	0.019 ± 0.001	420 ± 70
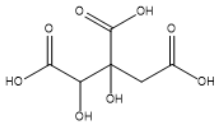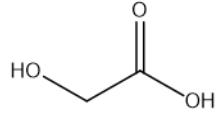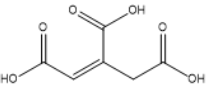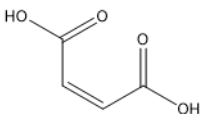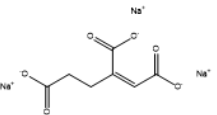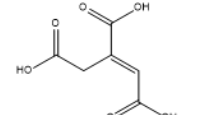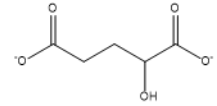
Inactivation kinetic values from 2-VIC mechanism-based inactivation of ICL1 described in Chapter 3.
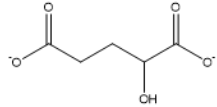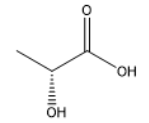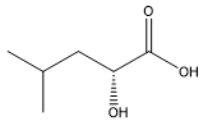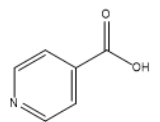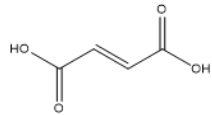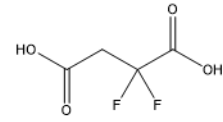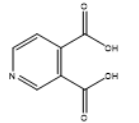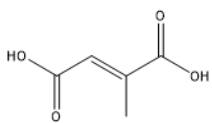
Table A-5 Synergistic constant (α) between multiple inhibitor of ICL1
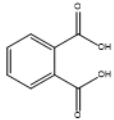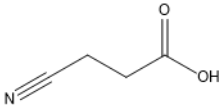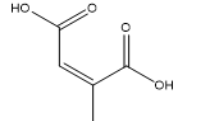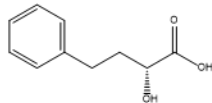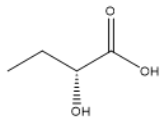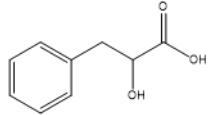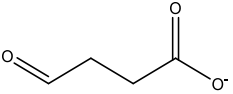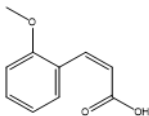
Inhibitor 1	Inhibitor 2	Synergistic constant (α)
(R)-malate	Maleate	1.1 ± 0.1
	Succinate	0.9 ± 0.2
Glycolate	Maleate	0.36 ± 0.05
(R)-lactate	Maleate	0.7 ± 0.1
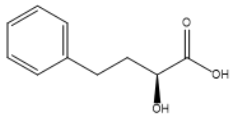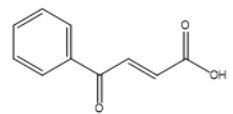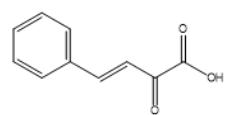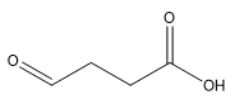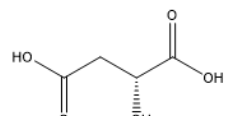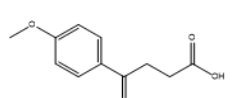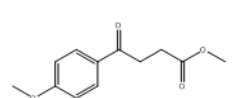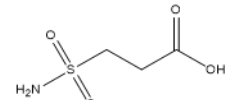
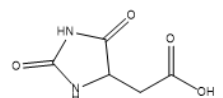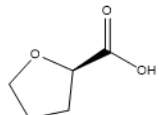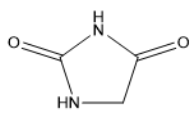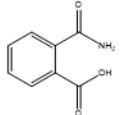α values were determined from Yonetani-Theorell plots as described in Chapter 4
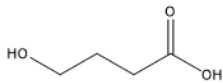
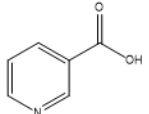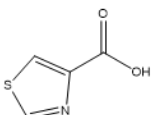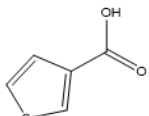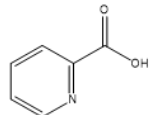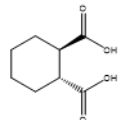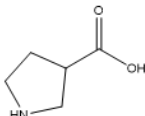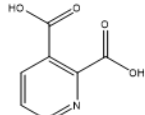**Table A-6** List of substrate analogs and their corresponding inhibition constants
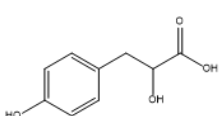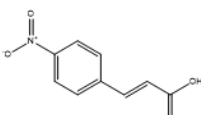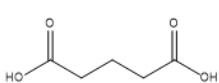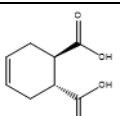
Compound	Structure	Inhibition Mode	h	$\pm\Delta h$	IC_{50} (mM)	$\pm\Delta IC_{50}$ (mM)	K_{is} (mM)	$\pm\Delta K_{is}$ (mM)	K_{ii} (mM)	$\pm\Delta K_{ii}$ (mM)
Hydroxycitrate		C	0.80	0.03	0.012	0.001	0.008	0.001		
Glycolic Acid		C	1.1	0.1	0.18	0.016	0.065	0.006		
cis-aconitic acid		C/B	0.86	0.03	0.37	0.02	0.22/0.5	0.01/0.1		
Maleic acid		U	0.90	0.05	0.45	0.02			0.30	0.02
Sodium cis-homoaconitate tribasic		C/B	0.66	0.04	0.9	0.09	0.4/2.3	0.1/0.3		
trans-aconitic acid		M	1.0	0.1	1.3	0.08	5	1	0.8	0.1
D-α -hydroxyglutarate		C	0.6	0.04	1.5	0.2	0.70	0.05		
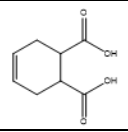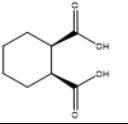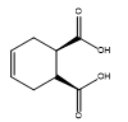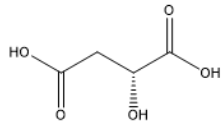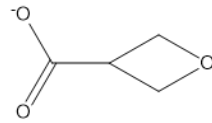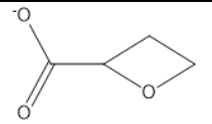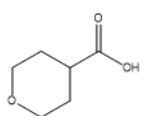
Compound	Structure	Inhibition Mode	h	$\pm\Delta h$	IC_{50} (mM)	$\pm\Delta IC_{50}$ (mM)	K_{is} (mM)	$\pm\Delta K_{is}$ (mM)	K_{ii} (mM)	$\pm\Delta K_{ii}$ (mM)
L-α-hydroxyglutarate		C	0.8	0.1	1.7	0.2	0.6	0.2		
D-lactic acid		C	0.70	0.04	2	0.1	2.3	0.3		
(R)-2-hydroxy-4-methylpentanoic acid		ND			> 100					
Pyridine-4-carboxylic acid		ND	1.0	0.1	2.15	0.2	4	0.3	20	5
Fumaric acid		C	0.74	0.02	2.4	0.1	1.9	0.4		
2,2-Difluorosuccinic acid		M	0.68	0.04	2.5	0.1	2.35	0.4	9.3	1.4
Pyridine-3,4-dicarboxylic acid		C	0.71	0.02	2.7	0.2	1.2	0.4		
Mesaconic acid		C/NC/B	0.7	0.04	3.3	0.3	1.1/4	0.1/3	4	3

Compound	Structure	Inhibition Mode	h	$\pm\Delta h$	IC_{50} (mM)	$\pm\Delta IC_{50}$ (mM)	K_{is} (mM)	$\pm\Delta K_{is}$ (mM)	K_{ii} (mM)	$\pm\Delta K_{ii}$ (mM)
Phthalic acid		C	0.8	0.1	4	0.7	2.4	0.3		
3-cyanopropanoic acid		M	1.00	0.04	6.6	0.3	20	6	3.4	0.7
Citraconic acid		U	0.6	0.1	12	4			5.2	0.8
(R)-2-hydroxy-4-phenylbutyric acid		ND	1		16	1				
(R)-2-hydroxybutyric acid		M	0.4	0.1	17	6	9	5	13	5
DL-3-phenyllactic acid		U	0.5	0.1	25					
Succinic semialdehyde solution		M					1	0.2	0.47	0.06
cis-2-methoxycinnamic acid		FA			> 10					

Compound	Structure	Inhibition Mode	h	$\pm\Delta h$	IC_{50} (mM)	$\pm\Delta IC_{50}$ (mM)	K_{is} (mM)	$\pm\Delta K_{is}$ (mM)	K_{ii} (mM)	$\pm\Delta K_{ii}$ (mM)
(S)-2-hydroxy-4-phenylbutyric acid		ND			> 10					
(2E)-4-oxo-4-phenylbut-2-enoic acid		ND			> 10					
(3E)-2-oxo-4-phenylbut-3-enoic acid		FA			> 10					
Succinic semialdehyde solution		S/FA					10	1		
D-(+)-Malic acid		C					0.3	0.06		
3-(4-methoxybenzoyl)propanoic acid		TD			> 10					
methyl 4-(4-methoxyphenyl)-4-oxobutanoate		TD			> 10					
3-(aminosulfonyl)propanoic acid		ND			> 10					

Compound	Structure	Inhibition Mode	h	$\pm\Delta h$	IC$_{50}$ (mM)	$\pm\Delta$IC$_{50}$ (mM)	K_{is} (mM)	$\pm\Delta K_{is}$ (mM)	K_{ii} (mM)	$\pm\Delta K_{ii}$ (mM)
GHB sodium salt solution		ND			> 10					
Hydantoin-5-acetic acid		ND	0.5	0.1	> 10		50			
(R)-(+)-tetrahydro-2-furoic acid		ND			> 10					
Hydantoin		ND			> 10					
Phthalamic acid		ND			> 10					
Pyridine-3-carboxylic		ND			> 5					
1,3-thiazole-4-carboxylic acid		ND			> 10					
Pyridine-2-carboxylic acid		ND			> 10					

Compound	Structure	Inhibition Mode	h	$\pm\Delta h$	IC_{50} (mM)	$\pm\Delta IC_{50}$ (mM)	K_{is} (mM)	$\pm\Delta K_{is}$ (mM)	K_{ii} (mM)	$\pm\Delta K_{ii}$ (mM)
Thiophene-3-carboxylic acid		ND			> 10					
trans-cyclohexane -1,2-dicarboxylic acid		C	0.6	0.1	> 10		15	3		
Pyrrolidine-3-carboxylic acid		ND	0.5	0.1	> 10		12	3		
Quinolinic acid		C	0.8	0.1	> 10		12	1		
DL-p-hydroxyphenyllactic acid		B			> 10		0.9/21	0.1/6		
4-nitrocinnamic acid, trans		TD			> 10					
Glutaric acid		ND			> 10					
(+/-)-*trans*-4-cyclohexene-1,2-dicarboxylate		C	0.27	0.05	> 10		11.6	2.8		

Compound	Structure	Inhibition Mode	h	$\pm\Delta h$	IC_{50} (mM)	$\pm\Delta IC_{50}$ (mM)	K_{is} (mM)	$\pm\Delta K_{is}$ (mM)	K_{ii} (mM)	$\pm\Delta K_{ii}$ (mM)
cis-4-cyclohexene-1,2-dicarboxylic acid		ND			> 10					
cis-1,2-Cyclohexanedicarboxylic acid		ND			> 10					
(1*R*,2*R*)-cyclohexane -1,2-dicarboxylic acid		ND			> 10					
L-(−)-malic acid		M/B			1.9	0.1	1.4/13	0.3/8	7	3
Oxetane-3-carboxylic acid		ND			> 10					
Oxetane-2-carboxylic Acid		C			6	0.4	2.3	0.25		
Tetrahydro-2H-pyran-4-carboxylic acid		ND			> 10					

ND – Not determined; C – Competitive inhibition; UC – Uncompetitive; M – Mix/ Noncompetitive inhibition; h – Hill coefficient; B – Biphasic Inhibition ; TD – Time-dependent inhibition. All inhibition constants and IC_{50} values were determined by equation (8) in Chapter 4.

Table A-7 List of TCA cycle and other enzymes tested

Enzyme Name	MW	pI	Sources	Stock Buffer Conditions
Succinyl coA synthetase	29.8 kDa (α), 41.4 kDa (β)	6.3 & 5.4	*E. coli*	50 mM HEPES, pH 8.0, 150 mM sodium chloride, 20% glycerol
GST-ATP-citrate lyase (ACL)	147 kDa	6.9	Human	25 mM Tris-HCl, pH 8.0, 100 mM NaCl, 0.05% Tween-20 and 10% glycerol
Citrate Synthase (CS)	85 kDa	6.1 - 6.6	Porcine Heart	Water
Malic dehydrogenase (MDH)	36 kDa	6.2	Porcine Heart	2.8 M $(NH_4)_2SO_4$ solution, pH 6.0
Fumarase	50.2 kDa		Human	20 mM Tris-HCl buffer (pH 8.0)
α-ketoglutarate dehydrogenase (OGDH)	120 kDa	6.28	Porcine Heart	50% glycerol solution containing ~9 mg per mL bovine serum albumin (BSA), 30% sucrose, 1.5 mM EDTA, 1.5 mM 2-mercaptoethanol, 0.3% Triton™ X-100, 0.003% sodium azide, and 15 mM potassium phosphate, pH 6.8
Aconitase	66 kDa	8.1 - 8.5	Porcine Heart	Water
Isocitrate dehydrogenase 1 (IDH1)	47 kDa	6.5	Human	Tris-HCl pH 8.0, trehalose, ammonium sulfate and DTT
Isocitrate lyase (ICL1)	47.8 kDa	5.3	*M. tb*	50 mM HEPES, pH7.5, 10 mM MgCl2
Bovine Serum Albumine (BSA)	69 kDa	5.8	*Bos taurus*	see OGDH
Malate synthase (MS)	80 kDa	5	*M. tb*	50 mM Tris, pH 7.5

Table A-8 Data collection and refinement statistics for crystallographic analysis 2-VIC-treated ICL1[43]

Resolution range (Å)	42.31 - 1.78 (1.81 - 1.78)
Space group	$P2_12_12_1$
Unit cell dimension	
a, b, c (Å)	75.086, 129.236, 167.952
α, β, γ (°)	90, 90, 90
Total reflections	1204296
Unique reflections	155553
Multiplicity	7.7 (4.1)
Completeness (%)	99.61 (96.85)
$I/\sigma I$	14.01 (0.53)
Wilson B-factor	34.52
R_{merge}	0.095 (0.167)
R_{work}	0.203 (0.371)
R_{free}	0.246 (0.400)
Refinement	
Resolution (Å)	34.28 - 1.78
Number of atoms	14521
Macromolecules	13248
Ligands	33
Water	1240
Protein residues	1708
RMS(bonds)	0.008
RMS(angles)	1.13
Ramachandran favored (%)	96.9
Ramachandran outliers (%)	0.3
Clashscore	3.2
Average B-factor	32.2
Macromolecules	32.0
Ligands	30.8
Solvent	35.1

Table A-9 Preliminary data collection and refinement statistics for crystallographic analysis *cis*-EpS-treated ICL1

Data collection		
Space group	P 2_1 2_1 2_1	
Cell dimensions		
	75.065	129.065
a, b, c (Å)	167.825	
α, β, γ (°)	90, 90, 90	
Resolution (Å)	1.88	
R_{merge}	0.211(2.279)	
$I/\sigma I$	2.2	
Completeness (%)	90.7(53.1)	
Redundancy	9 (4.9)	

Refinement	
Resolution (Å)	48.935-1.88
No. reflections	119322
R_{work}/ R_{free}	0.1848/0.2331
No. atoms	
Protein	13323
Water	717
Metal/ligand	73
B-factors	
Protein	25
All atoms	26
R.m.s deviations	
Bond lengths (Å)	0.007
Bond angles (°)	0.849